Dynamics of the Southern Annular Mode during Austral Spring and Summer: Stratospheric and Tropospheric Interactions

Evgenia Titova

A thesis submitted in fulfillment of the requirements for the degree of

Doctor of Philosophy in Environment and Geography

Department of Environment and Geography

Faculty of Science

Macquarie University, Sydney, Australia

February, 2014

Statement of Candidate

I certify that the work in this thesis entitled “Dynamics of the Southern Annular Mode during Austral Spring and Summer: Stratospheric and Tropospheric Interactions” has not previously been submitted for a degree, nor has it been submitted as part of requirements for a degree, to any other university or institution other than Macquarie University.

I also certify that the thesis is an original piece of research, and it has been written by me. Any help and assistance that I have received in my research work and the preparation of the thesis itself have been appropriately acknowledged.

In addition, I certify that all information sources and literature used are indicated in the thesis.

……..
Evgenia Titova
February 2014

TABLE OF CONTENTS

Abstract

The study has examined the mechanisms of the Southern Annular Mode (SAM) during austral spring and summer. The focus has been on the dynamical processes which operate on the seasonal time scales enabling predictability of the SAM. By employing concepts of wave-mean flow interactions, an observational analysis of the interconnections between tropical, extratropical and stratospheric circulations relevant for the dynamics of the SAM has been performed.

Firstly, it has been shown that from mid-October until late December the persistence of the SAM is dominated by its downward coupling with the stratospheric polar vortex. Most of the year-to-year changes in the strength of this coupling are determined by the seasonal peak in the upward heat fluxes across the tropopause observed from August to mid-October and, hence, can be estimated in advance. Additional predictability of the springtime SAM arises from the pre-conditioning of the polar vortex during late autumn – early winter when its background state is conductive to upward propagating waves. Dynamical processes which underlie the stratospheric impact on the SAM have been further investigated.

Secondly, it has been shown that starting from January the variability of the SAM is dominated by the impact of tropical convective systems over South America, Africa and Indonesia. Persistent variability in the latter is present throughout austral winter and spring and is related to long-lived ENSO-like variability in the Pacific Ocean. However, only upon the solstitial poleward shift of the thermal equator does it begin to affect the SAM. The sensitivity can be understood in terms of the impact of the poleward intruding subtropical highs on the propagation pathways of extratropical waves. It is then argued that the location of the subtropical boundary plays a regulating role in the summer climate system whereby the expanding tropics have enabled a stronger impact of tropical variations on the circulation of the midlatitudes.

The results contribute to the growing body of evidence that tropical and stratospheric circulations can have a significant impact on midlatitude weather patterns and suggest that eliminating the model biases would help to achieve improved seasonal forecasts of the SAM.

Acknowledgements

This thesis would not have been possible without the generous help of others. I wish to thank my supervisors: Professor Murry Salby, for encouraging me to undertake this thesis and for his support in the first stages of this thesis, and A/Professor Ian Goodwin and Dr Kevin Cheung for their guidance in the final stages of the completion and submission of this thesis.

I also wish to thank Macquarie University for awarding me the international Macquarie University scholarship, for the travel funding and for the technical support. I am also grateful to Dr. Steven Phipps from the University of New South Wales and Stuart Browning for willingly providing data from their modeling experiments.

A special thanks goes to my fellow postgraduate students and to my family who had to endure my extended candidature.

Chapter 1: Introduction

1.1 Research problem

Currently, there is an increasing demand for improved long-range weather forecasts and projections of interannual and decadal variability in climate from the perspectives of infrastructure, agriculture and energy use planning and better adaptation to a changing climate. At regional spatial scales and short to medium term time scales, achieving reliable projections requires, however, a better understanding of natural unforced climate variability and the way it can interact with the long-term trends.

In this respect, there is a particular interest in the dominant modes of extratropical variability, the so-called Northern and Southern Annular Modes (NAM and SAM) alternatively known as the Arctic and Antarctic Oscillations or zonal index. Annular modes regulate the location of large-scale weather systems which develop in the midlatitude westerlies and, hence, contribute to the temperature and precipitation anomalies over much of the extratropics [Thompson and Wallace, 2000 (part 1)], including Australia [Hendon at al., 2007]. Besides, up to 50 % of regional surface temperature and precipitation changes over the last few decades project on the observed positive trends in the SAM and NAM [Thompson and Wallace, 2000 (part 2)].

Defined as the leading empirical orthogonal functions (EOF) of sea level pressure variability poleward of 20° N/S [Thompson and Wallace, 1998-2000], annular modes capture internal variability of the atmosphere which dominates the extratropics. They manifest themselves primarily as the north-south migration of the midlatitude jet stream accompanied by the see-saw of pressure between midlatitudes and polar cap. Their temporal behavior can be characterized as persistent fluctuations with a maximum variance on time scales longer than a month. Although the existence of such variability in atmospheric jet streams has been well known back from the early XX century [Rossby at al, 1939; Namias, 1950] and was later reproduced in laboratory experiments [Hide, 1953], the temporal evolution of a zonal index was first believed to have limited predictability [Lorenz, 1986]. To a first approximation, changes in the jet stream are maintained by “stochastic” fluctuations in the poleward transport of angular momentum accomplished by atmospheric eddies [Lorenz, 1952]. That is, in order to predict NAM/SAM’s impact on the weather systems it would be necessary first to predict the weather patterns themselves. More recent studies have shown, however, that annular modes are susceptible to changes in variety of external natural and anthropogenic forcings such as changes in spatial temperature gradients associated with the enhanced amount of greenhouse gases or ozone depletion [Hartmann et al., 2000; Butler at al.,

2010; Son et al., 2010; Lu at al., 2008], variability in the tropical oceans [Seager et al., 2003; Fogt and Bromwich, 2006; Ding at al., 2012; Lim at al., 2013], sea ice extent [Petouhkov and Semenov, 2010; Orsolini at al., 2011; Kidson at al., 2011] or in stratospheric flow [Baldwin and Dunkerton, 1999-2001; Christiansen, 2001-2005; Chartlon at al., 2003; Thompson at al., 2005] as well as be maintained by positive internal feedbacks within the atmosphere [Feldstein and Lee, 1998; Lorenz and Hartmann, 2001-2003]. Understanding the controlling mechanisms behind these forcings provides an opportunity to improve representation of internally generated natural variability in modeling systems and their predictive skill.

A particularly interesting aspect of annular modes dynamics is that sometimes their variations appear to originate in the middle atmosphere and to descend over the course of several months down to the surface [Baldwin and Dunkerton, 2001; Christiansen, 2001; Graversen and Christiansen, 2003]. This downward coupling with the slowly varying stratospheric flow is arguably one of the dominant causes behind persistent anomalies in the annular modes during winter-spring seasons and provides potential for improved seasonal and daily forecasts on lead times beyond 5 days and beyond intrinsic timescales of annular modes (~10-14 days). Besides, an increasing number of studies has been suggesting that through the SAM/NAM, stratospheric variations might affect a wide range of tropospheric processes, spanning from the polar regions into the tropical belt as well as at different time scales, daily, seasonal and long term [Scientific Assessment of ozone depletion, 2010].

Generally, hypotheses about stratospheric impact rely on two broad lines of evidence. Firstly, observational analyses indicate that at times anomalous synoptic situations at the surface, and in particular synoptic blocking events [Woollings at al., 2010; Nishii at al., 2011; Anstey at al., 2013], have precursors in the stratosphere. Qualitatively, this link projects on the descending downward (from the middle atmosphere to the surface) zonal wind anomalies along 60° N/S accompanied by the change in polarity of the annular modes in the troposphere [Christiansen, 2001-2005; Graversen and Christiansen, 2003; Baldwin and Dunkerton, 2001; Thompson at al., 2005]. Secondly, increasing vertical resolution into the stratosphere and including heterogeneous chemistry modules in global circulation models help to improve simulations of seasonal climate variations and long-term circulation trends. According to a number of studies, stratosphere resolving models are able to reproduce teleconnections of ENSO [Ineson and Scaife, 2009; Bell at al., 2009], impact of Pinatubo eruption [Kirchner, 1999; Stenchikov at al., 2002, Charlton-Perez at al., 2013], solar forcing of winter climate variability in the Northern Hemisphere [Ineson at al., 2011] and as a result persistence of the SAM and NAM much better compared to the models with a low top. In the Southern Hemisphere, radiative and dynamical effects associated with the springtime development of

the ozone hole and lower stratospheric cooling have been shown to be responsible for an unexpectedly fast poleward migration of the jet stream and rapid circulation changes during austral summer [Thompson at al., 2011 and references therein]. In fact, the impact of the combined effect of global warming and ozone depletion on the SAM is one of the most consistent changes projected by the CMIP5 models [AR5] with uncertainty remaining as to which of the opposing impacts of ozone recovery and global warming will be dominant in the second half of the century.

Although there exists a number of theoretical concepts which potentially can explain the mechanisms behind the stratospheric impact the current level of scientific understanding of the stratospheric influence on the SAM is not sufficient. E.g., the relative role of different physical mechanisms, the predictive value of the stratospheric links, the origin of a 3 month lag between spring time development of the ozone hole and its proposed impact on climate are yet to be established. Additionally, analysis of CMIP5 models showed that despite a reasonably good reproduction of observed trends most of them show weak interannual and decadal variability. This results in a lack of persistent anomalies at the surface even in the high top stratosphere resolving models [Charlton-Perez at al., 2013]. Hence, reducing uncertainty in simulations of future ozone recovery and its canceling impact on current surface trends also requires better representation of stratospheric dynamical variability and its future evolution.

While the descent of zonal wind anomalies in daily datasets and influence of ozone depletion on summer climate trends in the Southern Hemisphere has received much attention in the recent literature, another interesting aspect of stratosphere-troposphere coupling has not been addressed extensively enough. That is, by taking advantage of the slow “pre-conditioned evolution” of the stratospheric flow it might be possible to improve seasonal forecasts over the extended winter-spring season. The feasibility of such forecasts has been highlighted in two recent studies of the Southern Hemisphere. Salby at al. (2012) showed that most of the interannual variability in the ozone hole could be accounted for by upward wave fluxes during August-September, while Son at al. (in press) found strong correlation between September total column ozone and October SAM.

The physical basis for understanding these lags is the so-called pre-conditioning effect. In both hemispheres, interannual variability in the total column ozone, polar lower stratospheric temperatures and the strength of the polar vortex during spring are to some degree controlled by dynamical processes which span the entire late autumn to late spring season [Fusco and Salby, 1999; Weber at al., 2003; Newman and Nash, 2005; Salby at al., 2012]. Excessive wave forcing of the stratosphere during winter drives anomalous equator to

pole transport of heat and ozone, contributes to adiabatic heating over the polar cap associated with the downwelling branch of the Brewer Dobson circulation and results into early close-down of the ozone hole and break-down of the polar vortex.

In the Southern Hemisphere, this wave driven evolution of the polar vortex is slow, locked to the annual cycle and involves nonlinear interactions between vertically propagating waves and the basic state of the polar night jet. These interactions result in the downward and poleward propagation of the polar night jet anomalies from the middle into lower stratosphere over a course of 6 months from May until October [Kuroda and Kodera, 1998]. Culminating in the final stratospheric warming during late spring, the descent of polar vortex anomalies is also accompanied by strong perturbations of the stratospheric flow during final warming events which are followed by anomalies in the NAM/SAM at the surface which tend to persist for up to 3 months [Baldwin and Dunkerton, 2001]. Similar though weaker lagged relationships have also been observed in the Northern Hemisphere during late winter-early spring which suggests the dynamical nature of the downward connection [Panteleeva (phd thesis), 2009].

The feedbacks between the stratosphere and surface climate and, in particular, the annular modes, are, however, two-fold whereby tropospheric processes strongly influence the stratospheric variability during this season as well. Annular modes strongly influence the direction and intensity of upward propagating wave activity in the troposphere, and through that modulate wave-driven Brewer-Dobson circulation, transport of trace gases and heat above the tropopause. The latter complicates estimating the ratio of downward and upward signals in the springtime coupling between annular mode and stratospheric polar night jet.

Despite a number of uncertainties, the slow evolution of the stratospheric vortex and its downward coupling with the SAM during late spring-early summer suggests an opportunity to improve seasonal forecasts over an extended season which starts during the austral winter when upward propagating planetary waves pre-condition the stratospheric vortex and extends through the spring when the stratospheric vortex is coupled to the position of jet stream well into the summer when springtime ozone hole affects the climate trends most.

1.1.1 Aims and dissertation structure

The aim of this study is to improve our understanding of the processes which govern variability of the SAM during austral spring and summer and the role of the stratosphere in enabling its seasonal predictability. Given that Global Circulation Models have deficiencies in the reproduction of the seasonal cycle of the strength, variability of the polar vortex and its planetary wave forcing [Hurwitz at al., 2010], the study will rely on the analysis of observational data.

The first part of the thesis attempts to identify the strength of the downward signal in help to identify biases in models the stratosphere-troposphere coupling, its timing and controlling mechanisms an understanding of which can lead to improving seasonal predictions and simulations of the interannual and decadal variability in the annular modes. While the dynamical coupling between the polar vortex and annular modes is usually expected to be stronger in the Northern Hemisphere, the Southern Hemisphere and the Southern Annular Mode example is more illustrative. Firstly, the dynamical processes in the Southern Hemisphere evolve in the "slow motion regime" and are locked to the annual cycle [Kuroda and Kodera, 1998] allowing us to isolate a significant downward signal on the background of daily noise. Secondly, the distinct radiative and dynamical processes which lead to the phenomenon of the ozone hole have been alleged to have a strong impact on the austral summer climate trends with a 3 month delay which suggests that there is an opportunity to improve summer forecasts of the SAM as well.

Furthermore, different aspects of tropospheric dynamics relevant for variations of the stratosphere will be addressed. Given the interplay between the Brewer-Dobson circulation, radiative processes and the strength of the polar vortex and, as a result, the long stratospheric memory, the springtime stratosphere and its impact on the SAM are expected to depend on anomalous dynamical processes during the entire previous winter season. The study will address the tropospheric processes relevant for driving upward propagation events and pre-conditioning the vortex as well as the role of the polar vortex itself in modulating the amount of wave activity to be absorbed.

Additionally, the origin of the coherent changes observed between the SAM, the Brewer Dobson circulation and the Hadley circulation during winter and spring season [Salby and Callaghan, 2004-2005] will be addressed. Similar connections have been also observed between tropical clouds and the Northern Hemisphere branch of the Brewer Dobson circulation during boreal winter [Liu and Thompson, 2013]. The origin of these links is currently not well understood and the available evidence is rather sporadic. For instance, Salby (2008) noticed that the spatial structure of coherent anomalies during boreal winter

resembles the mass exchange between the stratosphere and troposphere whereby the stratospheric pump pushes the air across the tropopause driving upwelling in the deep tropics and downwelling over the pole. However, other mechanisms cannot be discarded as well such as the role of the subtropical jet in modulating the propagation and growth of the extratropical planetary waves which will ultimately lead to the upward propagation events. For instance, Newman and Nash (2005) notice that subtropical variability might have played a role in driving the anomalous ozone hole of 2002.

The final part of the thesis will address the mechanisms behind the summertime persistence of the SAM which need to be represented for improved seasonal predictions.

The thesis is structured as follows.

Chapter 2 describes dynamical concepts and statistical methods used in the study. The analysis begins with considering the wave driven daily evolution of the stratospheric polar vortex (Chapter 3) and estimating the pre-conditioned downward component of the coupling the springtime polar vortex and the SAM. The origin of the springtime long-lived SAM anomalies and the lagged downward coupling with the stratospheric polar vortex is then addressed in Chapter 4 by tracking circulation changes that accompany a single upward propagating planetary wave disturbance. Chapter 5 includes a description of the winter-time dynamics of the upward propagating waves and tropospheric processes relevant for the pre-conditioning of the springtime stratospheric polar vortex and its downward coupling with the SAM at the surface. Climatological description of the anomalous processes in the troposphere which led to the early breakdown of the 2000 ozone hole and exceptionally low SAM anomalies at the surface is given. Chapter 6 addresses the stratospheric and tropospheric aspects of variability and predictability of the SAM during summer months. The thesis concludes with a summary and discussion.

1.2 Definition of the Southern Annular Mode (SAM) and its role in the Southern Hemisphere climate system

The changes of the extratropical climate system associated with the Southern Annular Mode have been a topic of active research over a long period. The SAM manifests itself primarily as north-south shifts in the position of the midlatitude jet associated with a seesaw of atmospheric mass between between the Antarctica and midlatitudes. One of the first accounts of the SAM belongs to Kidson (1975) and Rogers and Van Loon (1982). Subsequently, this phenomenon was addressed by [Kidson 1988, Karoly, 1990; Nigam, 1990; Hartmann and Lo, 1998; Feldstein and Lee, 1998; Thompson and Wallace, 1998-2000] and has been shown to represent essentially the same phenomenon as the zonal index or “index

cycle" [Rossby at al., 1939; Namias, 1950]. This variability is also captured by the leading modes of the lower tropospheric geopotential height fields or sea level pressure in the extratropics which are remarkably similar between the Northern and Southern Hemispheres [Thompson and Wallace, 1998-2000].

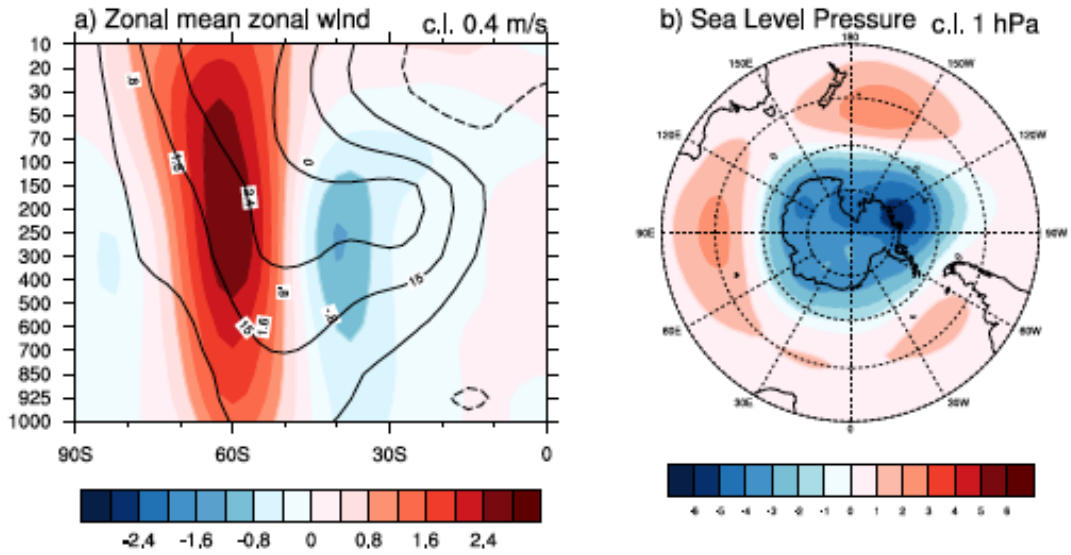

Figure 1.1 Regression of the Southern Annular Mode index on (a) the zonal mean zonal wind (black contour indicates climatology of zonal mean zonal wind) and (b) sea level pressure. Based on all months, 1979-2012. Based on NCEP/NCAR reanalysis.

Defined as the first empirical orthogonal function of the 850 mb geopotential height field poleward of 20°S, the SAM represents ~25% of the extratropical climate variability [Thompson and Wallace, 2000]. Figure 1.1 shows the standardized monthly SAM index regressed on the deseasonalized sea level pressure and zonal mean zonal wind. The positive phase of the SAM (also called the "higher index polarity" of the atmospheric flow) corresponds to strengthened westerlies poleward of 45°S and low pressure over the Antarctic polar cap. The opposite occurs during its negative phase or "lower index polarity". The dipole signature is robust on different time-scales and shows little variability between the seasons. The variance of the SAM index maximizes at periods longer than 1 month [Hartmann and Lo, 1998].

The SAM has been shown to affect different processes in the Southern Hemisphere climate system, including variability in the storm track [Kidson and Sinclair, 1996], sea ice extent [Liu et al. 2004; Lefebre at al., 2004; Pezza at al., 2008; Yuan and Li, 2008; Goosse et al., 2009], Southern Ocean Carbon cycle [Butler at al., 2007], sea surface temperatures [Fyfe et al., 2007; Ciasto and Thompson, 2008], the size and extent of the ozone hole [Scientific

Assessment of ozone depletion, 2006-2010], precipitation patterns [Hendon at al., 2007], surface Antarctic temperatures [Marshall, 2006]. Although the SAM is known to be an internal mode of climate variability, it might also show important dynamical linkages to the past century shifts in the climate system both due to enhanced amounts of greenhouse gases and ozone depletion. Thompson and Solomon (2002), Marshall et al. (2006) showed that observed temperature and circulation trends in the Southern Hemisphere project onto the SAM pattern, in particular the summer warming over the Western Antarctic Peninsula and cooling over the Eastern Antarctica.

The poleward shift of the SAM arguably results from nonlinear responses due to temperatures changes associated with different forcings. Basic dynamics suggests that location of jet streams, and so the annular modes, should be sensitive to the spatial temperature gradients, as confirmed by experiments with numerical models [Son and Lee, 2005; Eichelberg and Hartmann, 2005; Lim and Simmonds (2008)], while different thermal forcings provide a different response. Butler at al. (2010) find that both polar stratospheric cooling and tropical warming in the upper troposphere result in a poleward contraction of the storm tracks, while polar surface warming results in an equatorward shift of jet stream.

1.3 Wave-mean flow dynamics of the SAM

SAM-related variability encompasses a wide range of processes which accompany the latitudinal migration of the so-called “eddy-driven” jet (in contrast to the thermally driven subtropical jet) in the midlatitudes. Generally, understanding the dynamics behind the annular modes involves understanding the inter-dependencies between the extra-tropical macroturbulence, atmospheric jet streams and the thermally driven tropical Hadley circulation in the presence of orography and land-sea temperature contrasts. An idealized thermally driven Hadley circulation, such as an axisymmetric one cell circulation driven by differential heating varying only with latitude, even though mathematically possible [Schneider, 1977; Held and Hou, 1980; Lindzen and Hou, 1988] differs a lot from the real Earth’s atmosphere. At some point it becomes baroclinically unstable and contains fully developed eddies. Forced at the surface, baroclinic waves can propagate upward and meridionally in the upper troposphere where they drive a poleward flux of westerly momentum and establish a secondary, eddy-driven jet. At the same time extratropical waves transport heat and water vapor poleward reducing the meridional temperature gradients, strength of the subtropical jets. However, pre-existence of the thermally driven subtropical jet is not a pre-requisite for the establishment of the eddy-driven jet. Spontaneous growth of baroclinic waves is capable

of generating a jet, as shown in a number of simplified models, such as of Lee (1977), Williams (1979), Panetta and Held (1988), which assume no pre-existing jet [Lee and Kim, 2003].

Following its establishment, the eddy-driven jet can show spontaneous unforced migration which is believed to be a result of the interaction between zonal mean basic state and atmospheric wave-like disturbances. The study of the nature of such interactions usually involves two complementary theoretical concepts: first, the effect of the atmospheric wave activity on the mean flow, and second, the back-effect of the mean flow on the propagation and growth of the waves. The primary effect of the eddies on the zonal mean zonal wind averaged over the troposphere, and, hence the annular modes, is through the horizontal convergence of the eddy momentum flux [Hoskins, 1983]:

$$\frac{\partial\langle[u]\rangle}{\partial t} = -\frac{1}{\cos^2\phi}\frac{\partial\left(\langle[u'v']\rangle\cos^2\varphi\right)}{a\partial\varphi} - F \qquad (1.1)$$

where u is zonal wind, v – meridional wind, square brackets denote averaging along latitude circle, primes – deviation from zonal mean and $\langle\ \rangle$ brackets denote vertical averaging. F is residual forcing, a – radius of the Earth, φ – latitude.

In the annual mean, the secondary jet maximum in the upper troposphere centered at ~50° S as shown in Figure 1.2 where it clearly collocates with the maximum convergence of eddy flux of westerly momentum. At the surface, zonal wind anomalies of this eddy-driven jet are then maintained against friction by Coriolis force of the mean meridional circulation which is in turn induced by the eddies.

Lorenz (1952), in his study of the zonal index, showed zonal wind to lag changes in the poleward transport of the angular momentum, proportional to $-\frac{d[u'v']}{d\varphi}$ accomplished by the atmospheric eddies. Studies by Enger (1957) and Lorenz (1964) found that the Northern Hemisphere zonal index resemble irregular oscillations which can be closely approximated by a first order Markov process driven by “random” momentum forcing. Hence, zonal index could be interpreted

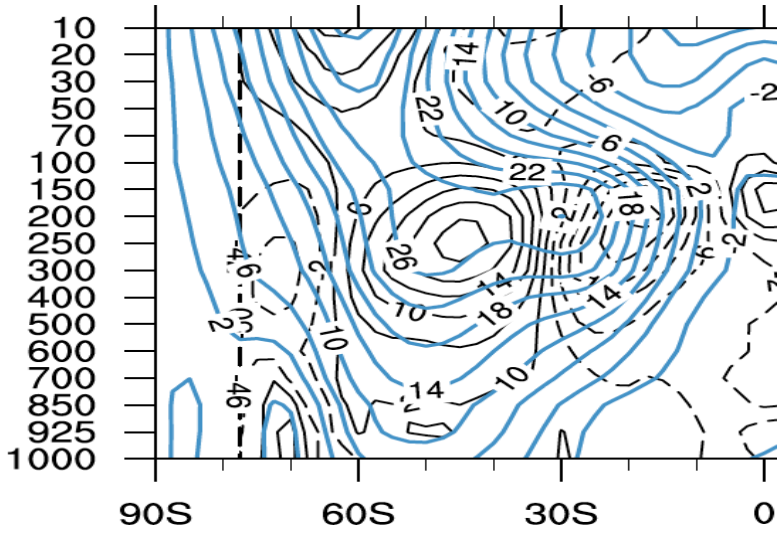

Figure 1.2. Annual mean zonal mean zonal wind (blue, c.i. 4 m/s) and horizontal convergence of momentum flux (black, c.i. 4.e-5 ms^{-2}). Based on NCEP/NCAR reanalysis (1979-2012).

as a slow integrated response of the midlatitude jet to the fast "stochastic" eddy momentum forcing of the high-frequency transients. Subsequent studies further demonstrated the existence of a positive feedback between the eddies and the mean structure of the jet which adds to the persistence of the zonal index or an annular mode [Robinson, 1991; Yu and Hartmann, 1993; Feldstein and Lee, 1998; Lorenz and Hartmann, 2001; Mudryk and Kushner, 2012; Geber et al., 2008]. The main processes responsible for the self-maintaining feedback include changes in the wave propagation in the upper troposphere and changes in the growth of wave activity, which precede and follow shifts of the tropospheric jet. A jet displaced poleward (positive SAM) favors equatorward propagation of wave activity, while a jet displaced equatorward (negative SAM) favours poleward propagation of wave activity [Hartmann and Lo, 1998]. An equatorward/poleward refraction of the tropospheric waves and changes in the baroclinic stability of the westerly jet and growth of the waves would then result into re-direction of momentum fluxes into or out of the midlatitude jet, reinforcing zonal wind anomalies poleward of 45°S and pushing the jet further poleward [Limpasuvan and Hartmann, 2000; Lorenz and Hartmann, 2001]. The relative role of the barotropic and baroclinic feedbacks in the maintenance of the annular modes is currently a topic of an active research [Barnes, 2010-2013; J.Kidston [phd thesis]; Robinson, 2006; Mudryk and Kushner, 2012; Gerber and Vallis, 2007; Baldwin at al., 2003]. Overall, this line of research shows that SAM represents an internal low-frequency variation of the extratropical atmosphere with a characteristic "red" variance spectrum and does not need an external forcing to exist.

1.4 Factors which control interannual variability of the SAM

1.4.1 Tropical circulation

The Southern Hemisphere climate system is quite distinct from the Northern Hemisphere. In the annual mean it features a strong Hadley cell bounded by a strong subtropical jet which is in turn driven by angular momentum transport from the deep tropics by the mean meridional circulation. Poleward of it is located a secondary jet maximum, often referred to as the "eddy-driven" jet in relation to the wave-mean flow feedbacks of the SAM. Evidence of the tropical influence on the Southern Annular Mode can be found in a number of studies which describe links of the SAM to the tropical circulation. In particular, the SAM has been shown to be related to:

1. Southern boundary of the Hadley circulation [Kang and Polvani, 2011; Ceppi and Hartmann, 2012];
2. SST changes in the tropical Pacific [Ding at al., 2012], including ENSO [Seager et al., 2003; Fogt and Bromwich, 2005; L'Heureux and Thompson, 2006; Lim at al., 2013]
3. Coherent changes between the upwelling branch of the Hadley circulation and the Brewer Dobson circulation [Salby, 2004-2005];

It, however, remains an open question whether the observed links between variability in the SAM and tropics reflect organization of the large-scale eddies and eddy-driven jets by the Hadley circulation or whether they imply the influence of the extratropical disturbances on the tropics.

Subject to the season, the daily index of the SAM leads changes of different parameters of the tropical circulation, such as zonal wind or temperature, by 20 days [Thompson and Lorenz, 2004]. The latter is consistent with the fact that the observed tropical circulation represents an intermediate regime where its variability is associated both with eddies and with thermal driving [Schneider, 2006]. The strength of annular-mode related influence on the tropics is also controlled by the tropical mean state, such as variability in the Walker circulation and the westerly equatorial duct in the Pacific which allows for the wave activity to reach poleward [Webster and Holton, 1982]. As a result, the Hadley circulation is more susceptible to the influence of the extratropical eddies during summer when it is close to the eddy-driven limit [Schneider, 2006; Caballero, 2007] and under La Niña-like conditions with stronger equatorial westerlies [Thompson and Lorenz, 2004].

At the same time the tropical circulation affects extratropical variability, by modulating growth and propagation of the eddies, and hence, the eddy-driven jet. Examples

of different model approaches to study the dynamical relationship between tropics and extratropics include effects of the strength of subtropical jet on the latitude of baroclinic wave growth [Sun and Lindzen, 1994; Lee and Kim, 2003] or sensitivity of the extratopical waves to the position of subtropical jet [Nigam and Lindzen, 1989]. Thus, Nigam and Lindzen (1989) hypothesized a relationship between extratropical stationary waves and the subtropical jet in the Northern Hemisphere. They argued that the stationary waves in the NH are stronger in the winter than in the summer due to the seasonal shifts of the subtropical jet and explained that in terms of refractive index changes. Seager et al. (2003) used a similar approach to explain the extratropical impact of ENSO in December-February by considering changes in the critical latitudes and in the direction of wave propagation in the meridional plane, while L'Heureux and Thompson (2006) stressed the importance of the rate of equatorward propagation. Webster and Holton (1982), Robinson (2002) emphasized the importance of the critical (zero-wind) line on the location of eddy absorption. Recently it was also noticed that the subtropical jet in the winter Southern Hemisphere is unstable and contains a source region of the eddies over Australia which apparently has some impact on the SAM [Ding et al., 2012].

1.4.2 Sea ice extent and Southern Ocean SST

The spatial distribution of temperatures in the Southern Hemisphere is marked by strong temperature contrasts between Antarctica and the Southern Ocean. In the climatological mean, the area of the largest baroclinicity associated with sharp temperature gradients is collocated with the westerly eddy-driven jet stream. The midlatitude SST anomalies affect, at least theoretically, the baroclinicity of the lower troposphere and can have an impact on the westerly jet stream by controlling the generation of the baroclinic waves, e.g. changes in their latitude and intensity [Kushnir at al., 2002; Nakamura at al., 2008]. At the same time, variability in sea ice extent regulates surface heat fluxes from the ocean into the atmosphere and can play a role in the variations of the eddy-driven jet and, hence, the SAM, subject to the location and seasonality of sea ice extent [Simmonds and Budd, 1991; Kidson at al., 2011].

At the same time, through the changes in the surface winds [Oke and England, 2004; Cai and Cowan, 2007] the SAM modifies both sea ice extent [Lefebre at al., 2004; Goosse et al., 2009] and the Southern Ocean SST, the latter with a several month e-folding time [Fyfe et al., 2007; Ciasto and Thompson, 2008]. Hence, the linkages between SST, sea ice extent and the SAM represent an example of the "Hasselmann's problem" [Frankignoul, C. and Hasselmann, K., 1977] whereby the coupled "atmosphere-ocean-sea ice system" integrates

the daily stochastic weather fluctuations and through the feedbacks generates internal low frequency variability. The intercomparison of CMIP5 models has shown that the coupling between the SAM, sea ice extent and the SST is underestimated by models [Karpechko at al., 2009].

1.4.3 The stratospheric polar vortex and its coupling with the SAM

The thermal regime above the tropopause is to a large extent controlled by radiative processes and the existence of a "heating surface" associated with the ozone layer. During winter, in the absence of solar heating, the polar stratosphere cools, which leads to a strong meridional temperature gradient. By thermal wind balance this leads to establishment of the polar night jet with maximum wind speeds peaking at 60° S. During summer, in the presence of strong heating associated with the polar ozone the equator to pole temperature gradient reverses which results into the summer stratospheric flow being dominated by the easterlies.

During the winter-spring season, when the stratospheric zonal flow is westerly, stratospheric climate cannot be, however, considered in isolation from the rest of the atmosphere. A bulk of the stratospheric variability comes from planetary-scale disturbances which are known to be vertically propagating Rossby waves forced at the surface [Charney and Drazin, 1961]. Under certain conditions this up-floating wave activity can reach the stratosphere driving poleward transport of heat and trace gases and the equator-to-pole mean meridional circulation (Brewer-Dobson circulation). The adiabatic warming associated with the descending branch of the Brewer Dobson circulation partly compensates for the cooling of the polar stratosphere and drives the mean temperature away from radiative equilibrium [Andrews at al., 1987]. Apart from planetary wave forcing, other factors such as seasonal transience play a role in driving residual mean transport in the stratosphere [Salby and Callaghan, 2006].

The cold and strong polar vortex together with a weaker wave activity in the Southern Hemisphere implies both reduced transport of ozone-rich air from the tropics towards the pole and enhanced potential for its chemical destruction during spring-time. When the polar stratospheric temperatures drop beyond certain thresholds, the likelihood of formation of the Polar Stratospheric Clouds (PSC) is enhanced. The PSCs represent precursors of chemical ozone loss. During spring-time in the presence of ultra-violet radiation catalytic reactions on the boundaries of the PSCs begin to occur which lead to spring-time development of the ozone hole over the Antarctica.

The interannual variability in the strength of the polar vortex is mostly associated with the anomalies in the forcing of the planetary scale waves [Weber at al., 2003; Fusco and

Salby, 1999]. Reduced planetary wave forcing implies weaker Brewer Dobson circulation, weaker adiabatic warming over the polar cap, cooler polar stratospheric temperatures, reduced transport of ozone-rich air, enhanced chemical destruction of ozone which would amplify the lower stratospheric cooling and strengthen the polar vortex further during spring-time. The propagation of planetary scale waves into the stratosphere depends on both the thermodynamic structure of the troposphere and on the zonal mean zonal wind in the polar vortex itself. Some configurations of the polar vortex impede the propagation of planetary waves, while other encourage it. In the Southern Hemisphere, the non-linear interaction between upward propagating waves and the stratospheric basic state results in the emergence of higher annular harmonics and downward propagation of polar vortex anomalies that are closely locked to the annual cycle [Kuroda and Kodea, 1998].

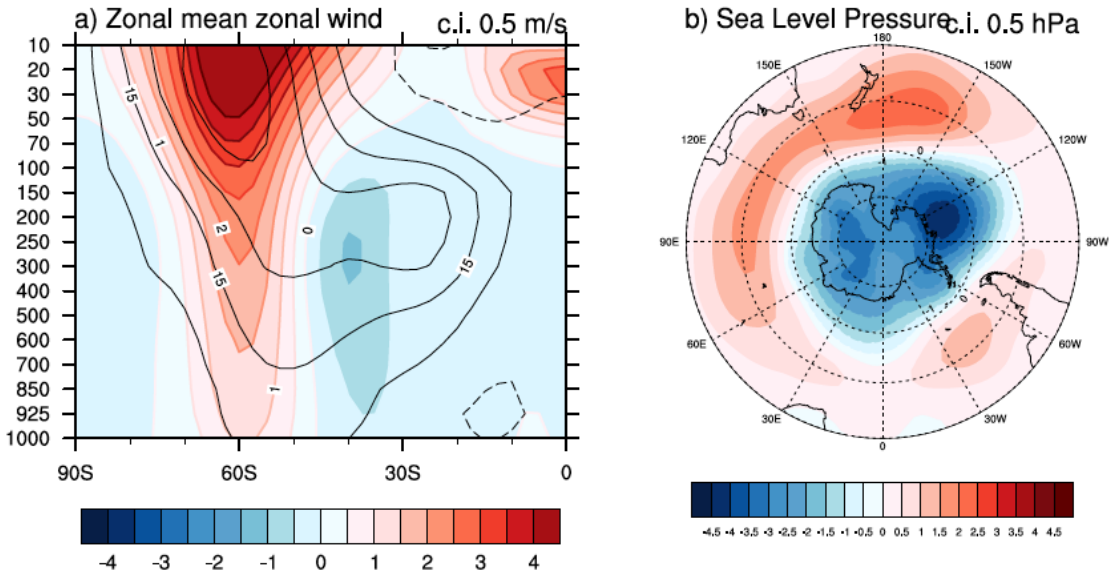

Figure 1.3 Regression of the Southern Annular Mode index on the (a) zonal mean zonal wind (black contour indicates climatology of zonal mean zonal wind) and (b) sea level pressure. September-November, 1979-2012. Based on NCEP-NCAR reanalysis.

During spring and early summer variability in the strength of the stratospheric vortex is strongly connected with variability in the position of the westerly eddy-driven jet [Thompson and Wallace, 2000]. Figure 1.3 shows anomalous zonal mean zonal wind and sea level pressure during September-November which correspond to 1 std increase in the SAM index. The SAM-related variability shows a barotopic signature with a dipole pattern in the troposphere coupled to the changes in the strength of the polar vortex. That is, positive SAM implies a simultaneous shift of the eddy-driven jet poleward and strengthening of the stratospheric vortex.

The nature of this coupling is likely to be two-fold. The tropospheric component of the SAM affects the propagation pathways of the waves. During positive SAM vertically propagating waves are refracted equatorward where they encounter the dynamical barrier of the tropical easterlies and, hence, are less likely to reach the stratosphere and to decelerate the stratospheric vortex [Limpasuvan and Hartmann, 2004]. The opposite occurs during negative SAM. The changes in the lower tropospheric baroclinicity and migration of the source regions of the wave activity which accompany the SAM can also impact the stratosphere with the waves originating in the midlatitudes being more likely to propagate into the stratosphere than those originating closer to the subtropics [Randel and Stanford, 1985].

Observational evidence, however, suggests that at times the changes in the polar vortex strength descend from the top of the atmosphere down to the surface in a series of downward propagating events followed by persistent anomalies in the SAM [Graversen and Christiansen, 2003; Thompson and Solomon, 2000]. Arguably, stratospheric impact on surface climate is mostly limited to the springtime and early summer circulations. Additional evidence of the stratospheric impact on the SAM can be found in the context of recent trends in the Southern Hemisphere which are reproduced by GCMs only when ozone depletion is included [Gillet and Thompson, 2003].

The mechanisms by which changes in the stratospheric climate can reach the surface, can be both radiative and dynamical. Having impact on both UV and IR parts of the radiation spectrum, ozone changes (subject to altitude and spatial distribution) can result into both radiative heating or cooling of climate. Lower stratospheric ozone losses, which occur through the catalytic cycles involving mostly chlorine and bromine species, are associated with an increase in the short-wave radiation fluxes and reduction in the long wave fluxes at the surface [WMO, 1987-2010; Aleksandrov at al., 1992]. This reduction in downwelling longwave radiation associated with the springtime ozone depletion can by itself reproduce the observed surface trends in the Southern Hemisphere as shown in a modeling study by [Grise at al., 2009]. On the other hand, the connection between variations in the position of the westerly eddy driven jet and variability in the strength of the polar night stratospheric vortex during respective “active’ season [Thompson and Wallace, 2000] creates a dynamical pathway for stratospheric perturbations to affect surface climate variability and trends.

Proposed dynamical mechanisms include:

1) The principle of the “downward control” [Haynes et al. 1991] suggests that stratospheric perturbations can reach the surface through the wave-induced mean meridional circulation. However, the momentum forcing in the stratosphere is arguably too weak to generate strong anomalies in the troposphere [Egger, 1996; Shepferd and Shaw, 2004]. The

observed downward coupling has been found to be incompatible with the "downward control" under which stratospheric perturbations results in more short-lived and weaker anomalies without obvious descent of the wave-induced circulation to the ground [Egger and Hoinka, 2005]. However, hypothetically the response can be amplified the eddy feedbacks in the troposphere [Song, Y., and W. Robinson, 2004]. Another version of this principle involves remote responses to the re-distribution of potential vorticity [Black, 2002; Ambaum and Hoskins, 2002].

2) Changes in the intensity of Brewer Dobson circulation triggering anomalous vertical motion across the tropopause over the pole/equator. Salby and Callaghan [2004-2006], Salby [2008] observed that amplification of heat and momentum transport in the stratosphere is accompanied by the cooling over equator in the upper branches of the Hadley circulation with intensification of organized convection and with warming over the polar cap. They hypothesized that driving mechanism could involve the cross-tropopause mass exchange driven by the Brewer-Dobson circulation. Downwelling motion over the polar cap associated with the descending branch of the Brewer Dobson circulation transfers air into the troposphere and is accompanied by adiabatic warming. A compensating motion must then occur with upwelling and adiabatic cooling which brings air back into the stratosphere.

3) Reflection of upward propagating waves. Theoretical considerations show that vertically propagating waves can be overreflected in the vertical plane from the stratospheric vortex and potentially can interfere with tropospheric waves [Bates, 1977; Schmitz and Grieger, 1980; Harnik and Lindzen, 2001; Harnik, 2009]. Downward wave fluxes are indeed often observed at the decaying stage of the Stratospheric Sudden Stratospheric Warmings events [Randel, 1985].

4) Impact of the wind shear at the tropopause levels on the propagation of wave activity from below. Chen and Robinson (1992) found in a series of numerical experiments that changes in wind shear and the static stability across the tropopause and in the lower stratosphere can have a significant impact on the refractive properties of the flow and affect propagation of tropospheric waves. The latter was later found to coherent with the changes of annular modes [Hartmann at al., 2000]. A strong polar vortex in the lower stratosphere would deflect the upward propagating wave activity equatorward contributing to the positive SAM, while a weak polar vortex would contribute to the poleward refraction of wave activity and negative SAM.

However, the relative role and prevalence of different mechanisms is yet to be quantified.

Chapter 2: Data and Methodology

2.1 Introduction

The dynamics of the SAM is believed to involve different aspects of the interactions between the atmospheric waves and the mean flow. Theoretical studies which focus on such interactions identified a number of diagnostics which describe influential attributes of the basic state, such as curvature and shear of the zonal mean zonal wind. Useful tools in the analysis of zonally-averaged flows and eddy disturbances include Eliassen Palm Flux (EP Flux), residual mass stream function and index of refraction [Eliassen and Palm, 1961; Edmon et al., 1980; Andrews et al., 1983; Andrews at al., 1987; Matsuno, 1970]. The EP flux can be used for both the description of wave propagation in the mean zonal shear flows and for the analysis of the zonal force exerted on the zonally-averaged flow by the waves. The refractive index describes the properties of the background mean flow which inhibit or favour wave propagation, for wave propagation is expected to follow the gradient in the refractive index defined for each wave speed and zonal wave number. The residual mass stream function can be used to approximate the wave-induced mean meridional circulation and the Brewer Dobson circulation. Combined in the Transformed Eulerian Mean formulation of the momentum equation, these diagnostics represent a powerful tool to identify the wave-driven evolution of the polar vortex and its coupling with the SAM.

While the underlying dynamics of SAM-related feedbacks is often complex and involves numerous physical mechanisms, stochastic models can be used to approximate the behavior of interest in a simpler way. Particularly useful in that respect are the autoregressive models representing approximations of discretized ordinary linear differential equations driven by stochastic forcing. Identifying and fitting such models involves estimation of time series parameters such as auto-/cross-correlation and spectrum.

The chapter outlines the main dynamical concepts, the calculations and statistical methods used throughout the thesis.

2.2 Diagnostics of the wave-mean flow interaction

To diagnose the wave forcing of the zonal mean flow, the Transformed Eulerian Mean (TEM) formulation of the momentum equation can be used. In log-pressure and spherical coordinates the TEM momentum equation (based on Equation 3.5.2a from Andrews et al., 1987) is:

$$\underbrace{\frac{\partial \bar{u}}{\partial t}}_{\substack{\text{Momentum}\\ \text{tendency}}} = \underbrace{f\bar{v}^*}_{\substack{\text{Coriolis force of}\\ \text{residual circulation}}} \underbrace{-\frac{\bar{v}^*}{a\cos\phi}\frac{\partial}{\partial\phi}(\bar{u}\cos\phi) - \bar{w}^*\bar{u}_z}_{\substack{\text{Advective}\\ \text{terms}}} + \underbrace{\frac{1}{\rho_0 a\cos\phi}\nabla\cdot F}_{\substack{\text{EP flux}\\ \text{divergence}}} + \underbrace{\bar{X}}_{\text{Residual Term}} \qquad (2.1)$$

In Eq. (2.1) and in the following equations, u is the zonal mean zonal wind, the TEM residual velocities $\bar{v}^*, \bar{w}^*$ are defined as in Andrews et al. (1987):

$$\bar{v}^* = \bar{v} - \frac{1}{\rho_0}\frac{\partial}{\partial z}\left(\rho_0 \frac{\overline{v'\theta'}}{\bar{\theta}_z}\right) \qquad (2.2)$$

$$\bar{w}^* = \bar{w} + \frac{1}{a\cos\varphi}\frac{\partial}{\partial\varphi}\left(\cos\varphi \frac{\overline{v'\theta'}}{\bar{\theta}_z}\right) \qquad (2.3)$$

where an overbar represents the zonal mean and primes indicate departures from the zonal mean. θ is potential temperature, v is the meridional wind and w is the vertical wind, F is the Eliassen Palm flux, a is the radius of the Earth, φ is the latitude, z is the log-pressure.

The vertical F_z and horizontal F_φ components of the EP flux are defined by (according to equations 3.5.3a and 3.5.3b in Andrews at al. (1987)):

$$F_\phi = \rho_0 a\cos\phi\left(\bar{u}_z\frac{\overline{v'\theta'}}{\bar{\theta}_z} - \overline{v'u'}\right) \qquad (2.4)$$

$$F_z = \rho_0 a\cos\phi\left[\left(f - \frac{1}{a\cos\phi}\frac{\partial}{\partial\phi}(\bar{u}\cos\phi)\right)\frac{\overline{v'\theta'}}{\bar{\theta}_z} - \overline{w'u'}\right] \qquad (2.5)$$

Under quasigeostrophic assumptions and in the absence of dissipation, equation (2.1) reduces to a balance between divergence of EP flux and Coriolis force of the residual mean motion:

$$\underbrace{\frac{\partial \bar{u}}{\partial t}}_{\substack{\text{Momentum}\\ \text{tendency}}} = \underbrace{f\bar{v}^*}_{\substack{\text{Coriolis}\\ \text{force}}} + \underbrace{\frac{1}{\rho_0 a\cos\phi}\nabla\cdot F}_{\substack{\text{EP flux}\\ \text{divergence}}} \qquad (2.6)$$

and the Eliassen Palm Flux are given by

$$F_\phi = -\rho_0 a\cos\phi\,\overline{v'u'} \qquad (2.7)$$

$$F_z = \rho_0 a\cos\phi f\frac{\overline{v'\theta'}}{\bar{\theta}_z} \qquad (2.8)$$

The TEM transformation offers a convenient approach to diagnose the eddy – mean flow interactions since the eddy forcing of the mean state is described by the single term $\nabla\cdot F$. According to the Eliassen Palm theorem, the equation permits a steady state under non-acceleration conditions, that is when the waves are linear, steady, conservative and $\nabla\cdot F$

vanishes [Eliassen and Palm, 1961]. Under these conditions, the full evolution of the zonal flow is independent of the eddies, otherwise the only internal forcing of the zonal mean flow by eddy disturbances is *F*. Later, Andrews and McIntyre (1976-1978) formulated the so-called generalized Eliassen-Palm theorem to describe a dependence of $\nabla \cdot F$ on properties of time varying wave amplitudes (the so-called "wave transience") and non-conservative wave effects. The theorem is given by:

$$\underbrace{\frac{\partial A}{\partial t}}_{\substack{Momentum \\ tendency}} + \nabla \cdot F = D + O(\alpha^3) \tag{2.9}$$

where A is "wave activity density", D is wave dissipation associated with the frictional and diabatic effects and $O(\alpha^3)$ term is a function of wave amplitude α and represents nonlinear wave effects. When terms on the right hand side of equation (2.9) are zero, it takes the law of conservation law for wave properties.

The eddy forcing of the zonal-mean flow can be displayed by mapping the Eliassen Palm cross-sections, which show the EP flux by vectors and isolines of its divergence by contours. The contours of $\nabla \cdot F$ represent zonal force per unit mass exerted on the mean state which represents the total effect of the eddies.

The direction of *F* vectors indicates the relative importance of the eddy fluxes of heat and momentum and the direction of the net propagation of wave activity in height and latitude if the dynamics of the flow is Rossby wavelike. Generally, the propagation of wave activity can be described in terms of the local refractive properties of the background basic state. The analytical solutions of equations which give the propagation rays of the way activity can be obtained only under idealized conditions, e.g. when the refractive properties of the medium vary slowly compared to the phase of oscillations, and are called the Wentzel–Kramers–Brillouin (WKB) approximation. It has been established that there is connection between F and transfer of wave activity [Edmon at al., 1980]. For planetary waves of small enough latitudinal and vertical wavelength, so that conditions of the WKB approximation are satisfied, F is parallel to the group velocity of a wave packet:

$$F = c\mathrm{A} \tag{2.10}$$

where ***c*** is the group velocity projected on the meridional plane and **A** is a measure of the local wave activity.

The residual circulation (v^*, w^*) induced by the eddies is necessary to maintain geostrophic balance in the presence of $\nabla \cdot F$, frictional and diabatic effects. It can be considered as an analogue of the Lagrangian mean motion as discussed by Dunkerton (1978),

even though it is not equivalent to it. The structure of the residual mean motion can be obtained by defining the residual mass stream function [Rosenlof and Holton, 1993]:

$$v^* = -\frac{1}{\rho_0 \cos\varphi}\frac{\partial \Psi}{\partial z}, \quad w^* = \frac{1}{\rho_0 \cos\varphi}\frac{\partial \Psi}{\partial \varphi} \tag{2.11}$$

The residual mean motion is particularly useful in the studies of the stratospheric circulation where it can serve as an approximation of the Brewer-Dobson circulation and a diagnostic of the ozone transport.

The quasi-geostrophic refractive index η_k^2 is a useful tool in the investigation of the propagation of the planetary waves [Matsuno, 1970; Chen and Robinson, 1991; Li and Graf, 2007]. For a traveling wave with a frequency σ and zonal wave number k it is defined as

$$\eta_k^2 = \frac{\bar{q}_y}{\bar{u} - (a\sigma\cos\varphi)/k} - \left(\frac{k}{a\cos\varphi}\right)^2 - \left(\frac{f}{2NH}\right)^2, \tag{2.12}$$

where

$$\bar{q}_y = \frac{2\Omega}{a}\cos\varphi - \frac{1}{a^2}\left[\frac{(\bar{u}\cos\varphi)_\varphi}{\cos\varphi}\right]_\varphi - \frac{f^2}{\rho_0}(\rho_0 \frac{\bar{u}_z}{N^2})_z \tag{2.13}$$

is the meridional gradient of zonal mean potential vorticity. Here $a, f, N, H, \Omega, \varphi$ stand for the radius of the Earth, the Coriolis parameter, the Brunt Vaisala frequency, the scale height, the Earth rotation frequency and the latitude respectively.

Refractive index conveys impact of the basic state on the pathways of wave propagation whereby the wave activity tends to propagate towards the regions of large positive η_k^2 and to avoid regions of negative η_k^2. If η_k^2 reaches zero, the vertical propagation becomes prohibited and reflection takes place. The heights and latitudes with $\eta_k^2 = 0$ are referred to as turning levels. Contrary, when the $\bar{u} - (a\sigma\cos\varphi)/k$ is reduced to zero, the η_k^2 approaches infinity, the propagation stalls and such conditions lead to the absorption of wave activity. The heights and latitudes with $\bar{u} = (a\sigma\cos\varphi)/k$ are referred to as critical levels.

The climatology of refractive index suggests that atmospheric waves tend to get refracted equatorward towards the higher refractive index values. However, the tropical easterlies inhibit their propagation. Waves encounter the critical (zero-wind) line and the wave activity becomes absorbed. On the contrary, in the stratosphere, subject to the season, upward propagating waves often get refracted equatorward from the strong westerlies of the polar-night jet to be absorbed later in the vicinity of the tropical easterlies.

Finally, given the quasigeostrophic relationship between the northward eddy flux of potential vorticity and the divergence of the Eliassen-Palm Flux:

$$\overline{v'q'} = \rho_0^{-1}\nabla \cdot F \tag{2.14}$$

the influence of the eddies on the zonal mean flow can be summarized by the zonal mean quasigeostropic potential vorticity equation:

$$\frac{\partial \overline{q}}{\partial t} + \frac{\partial \overline{v'q'}}{dy} = \frac{\partial \overline{q}}{\partial t} + \rho_0^{-1}\nabla \cdot F = D \tag{2.15}$$

where q is potential vorticity (PV), D represents zonal mean PV sources and sinks. The equation (2.15) illustrates that the flux of wave activity in and out of region which alternatively accelerates and decelerates the flow.

2.3 Indices of the Southern Annular Mode

Unless otherwise specified, the first empirical orthogonal function (EOF) of the geopotential height field poleward of 20°S at 700 mb level is used as an index of the SAM. Prior to computing data has been weighted by the squared root of cosine of latitude to account for the convergence of meridians towards the pole.

EOF analysis is a mathematical technique which allows identifying patterns of simultaneous variation and ordering them according to the percentages of the total variance they represent [Von Storch and Zwiers, 2000]. Intrinsically, they do not have to have a physical interpretation. However, the variability represented by the first EOFs of the lower tropospheric sea level pressure in the extratropics of both hemispheres captures a number of related circulation shifts associated with the north-south migration of the jet stream. Hence, given the prevalence of zonally symmetric variations in the Southern Hemisphere, SAM can be defined using other, more "physical" indices, such as, for example, the gradient of sea level pressure between 40°S and 65°S [Gong and Wang, 1999], the mean sea level pressure over the Antarctica or the latitude of the eddy driven jet [Ceppi and Hartmann, 2012]. A comparison of these indices shows little difference in the interannual variability, however, and so for the most of this study we use the 700hPa SAM index.

At times, the SAM also shows stronger and weaker connection to the tropical circulation [Fogt and Bromwich, 2006; Fogt et al, 2011]. Ding at al. (2012) found that SAM index defined as the first EOF of the 200 mb geopotential height field poleward of 20°S shows stronger connection to the tropical SST since the subtropical jet is present at these levels. In the NCEP/NCAR reanalysis I found, however, little difference in tropical-extratropical connection when defining A SAM index based on upper troposphere fields. Instead, in parts of this study a mass stream function index is used to identify coherent

patterns associated with a common tropical source. Such an index gives equal weight to perturbations in the tropics and extratropics and is preferable to using normalized variations in the geopotential height since geostrophic relationships break down in the tropics.

Following Oort and Yienger (1996), the Eulerian mean mass streamfunction Φ is defined by:

$$[\bar{v}] = g\frac{\partial \Phi}{2\pi R \cos\varphi \partial p} \tag{2.16}$$

$$[\bar{\omega}] = -g\frac{\partial \Phi}{2\pi R^2 \cos\varphi \partial \varphi} \quad , \tag{2.17}$$

where v is the meridional velocity, ω is the vertical velocity, R – the radius of the Earth, p is the pressure, square brackets stand for temporal averaging, overbars for zonal averaging. The field of mass streamfunction is obtained by integrating (2.11) downward to the surface. Prior to that the $[\bar{v}]$ field was corrected by removing its mass-weighted vertical mean value to ensure the vertical-mean mass balance. The seasonal mean mass streamfunction fields taken between 30°N and 90°S were then used to calculate main EOF's. Subject to the season the SAM related variability could be associated either with first, second or third EOF.

The quality of the reanalysis prior to the introduction of satellites is questionable due to insufficient data coverage. Hence, in the last part of the thesis, an observation based Marshall's SAM index will be used [Marshall, 2003]. The index is based on the ground-based sea level pressure measurements from 12 stations in the Southern Hemisphere. It is defined as the mean difference in the mean sea level pressure between the stations located in two latitude bands, in the vicinity of 40° and 65°S. The stations have been chosen so that they equally represent the two latitude bands centered at 40°S and 65°S and different longitudinal sectors within each band. Despite that the Pacific sector remains underrepresented in the index due to a lack of island locations and inaccessibility of coastal Antarctic stations. The index covers the time period since the International Geophysical Year of 1957/1958 when most of the stations became operational. The missing values in the records were imputed using multiple linear regression with mean sea level pressure from neighboring stations taken as a predictor.

2.4 Time series analysis

2.4.1 Simple mathematical models of stochastic processes

The climate variations owe their existence to the stochastic dynamics of the climate system. Hence, the time evolution of dynamical fields of the atmosphere usually can not be

described by deterministic components alone. Generally, they undergo irregular variations, the description of which involves the concept of a “stochastic” or “random” process.

Given a phase space T, the stochastic process X(t) can be defined as a function of time, a value of which at each $t \in T$ represents a random variable. The realization or a finite sample of a stochastic process is then called “time series”. To fully describe a probabilistic structure of a stochastic process X(t) it is necessary to specify for an arbitrary number of $t_1, t_2, ..., t_n$ from T an *n*-dimensional joint density function $F_{t_1,t_2,...,t_n}(x_1, x_2, ..., x_n)$ of a variable $(X(t_1), X(t_2)..., X(t_n))$:

$$F_{t_1,t_2,...,t_n}(x_1, x_2, ..., x_n) = P(X(t_1) \le x_1, X(t_2) \le x_2, ..., X(t_n) \le x_n) \qquad (2.18)$$

Under such definition, a complete statistical description of a random process would consist in stating all the finite-dimensional probability distributions for the values of all random fields that describe it. In practice, this general definition is rarely used. Instead, stochastic processes are given by mathematical models which rely on a number of assumptions. The simplest mathematical model of a random process is white noise, which is defined as a sequence of identically distributed independent random variables with a zero mean. Such process by construction does not have memory in time and, for every t, X(t) is independent of any other variable in the stochastic process. However, the white noise process does not typically adequately describe the behaviour of a time series.

Many processes possess the so-called Markov property: the future evolution of the process depends on the past through the present, that is it does not depend on how did the system arrived at the present state [Ventsel, 1958]. Mathematically, this can be expressed by defining a conditional probability of two events, with the first event *A* belonging to the past and representing a realization of a random variable $X(t_1)$ for $t_1 \le t-1$ and the second *B* belonging to the future and representing a realization of a random variable $X(t_2)$ for $t_2 \le t+1$. The stochastic process X(t) is said to possess Markov property, if for any given *A*, *B*, t:

$$P(AB \mid X(t)) = P(A \mid X(t))P(B \mid X(t)). \qquad (2.19)$$

. Among the models of time series which will be used here the first order autoregressive processes do possess Markov property. The autoregressive process of order p>0 can be represented as Markov as well by defining its state at the moment t to be the sequence of

($X(t)$, $X(t-1),...,X(t-p-1)$). Autoregressive processes can be viewed as approximations of discretized ordinary linear differential equations driven by stochastic forcing [Jenkins and Watts, 1968]. According to the equations 10.3.1 in [von Storch and Zwiers, 2000], the first order linear differential equation

$$\alpha_1 \frac{dX(t)}{dt} + \alpha_0 X(t) = \varepsilon_t \tag{2.20}$$

where ε_t is the forcing term, can be represented in discrete time as:

$$X(t) = \phi_1 X(t-1) + \varepsilon'_t, \tag{2.21}$$

where

$$\phi_1 = \frac{\alpha_1}{\alpha_0 + \alpha_1} \tag{2.22}$$

$$\varepsilon'_t = \frac{1}{\alpha_0 + \alpha_1} \varepsilon_t . \tag{2.23}$$

Analogously, a second-order linear differential equation

$$\alpha_2 \frac{d^2 X(t)}{dt^2} + \alpha_1 \frac{dX(t)}{dt} + \alpha_0 X(t) = \varepsilon_t \tag{2.24}$$

can be represented in discrete time as:

$$X(t) = \phi_1 X(t-1) + \phi_1 X(t-2) + \varepsilon'_t, \tag{2.25}$$

where

$$\phi_1 = \frac{\alpha_1 + 2\alpha_2}{\alpha_0 + \alpha_1 + \alpha_2} \tag{2.26}$$

$$\phi_2 = -\frac{\alpha_2}{\alpha_0 + \alpha_1 + \alpha_2} \tag{2.27}$$

$$\varepsilon'_t = \frac{1}{\alpha_0 + \alpha_1 + \alpha_2} \varepsilon_t . \tag{2.28}$$

When the stochastic forcing term ε_t is a white noise process, the random processes X(t) are called first- and second-order autoregressive processes.

2.4.2 Parameters of the time series

An important class of stochastic processes are the Gaussian processes. All the probability distributions of these processes are normal. This has important practical implications as their properties are entirely given by their bivariate density functions and the analysis of their properties can be limited to the mathematical expectation $\mu(t) = MX(t)$ and covariance function $\mathrm{cov}(X(t), X(s)) = M[(X(t) - \mu(t))(X(s) - \mu(s))]$. For t = s covariance gives the variance of the stochastic process $DX(t) = \mathrm{cov}(X(t), X(s))$.

For a stationary process, that is a process whose joint probability density functions (eq. 2.13) do not change with a time lag, $MX(t)$ and variance $DX(t)$ do not change with time for any s,t and a lag $\tau = s - t$. The covariance function is then simply function of a lag $\tau = s - t$.

The covariance of a variable against a time-shifted version of itself, for a stationary stochastic process X(t) with the mean μ and for a lag τ can be then written as

$$\gamma_{XX}(\tau) = M((X(t) - \mu)(X(t + \tau) - \mu)) \tag{2.29}$$

and is called auto-covariance function , and the normalized function

$$\rho_{XX}(\tau) = \frac{\gamma(\tau)}{\gamma(0)} \tag{2.30}$$

is called the auto-correlation function. The autocovariance function is one by one related to the power spectrum of X(t) which is defined as Fourier transform of the auto-covariance function:

$$\Gamma_{XX}(\omega) = \sum_{\tau=-\infty}^{\infty} \gamma_{XX}(\tau) e^{-2\pi i \tau \omega} \tag{2.31}$$

or

$$\Gamma(\omega) = \gamma(0) + 2\sum_{\tau=1}^{\infty} \gamma_{XX}(\tau) \cos(2\pi\tau\omega) \tag{2.32}$$

for all frequencies ω in the domain [-½, ½].

Thus, for a stationary Gaussian process, its probabilistic structure can be given entirely by the expectation and covariance function or equivalently its spectrum. While the autocovariance function describes distribution of variance in the time domain, the spectrum describes the distribution of variance as a function of time scale, that is in the frequency domain. The theoretical formulas of the auto-correlation function and spectra of the first- and second-order autoregressive processes are given in Table 2.1.

The first and second moments for a stationary bivariate stochastic process (X_t, Y_t) are given analogously, by expectation and autocovariance functions, but the second moment includes the cross-covariance function:

$$\gamma_{XY}(\tau) = M((X(t) - \mu_x)(Y(t+\tau) - \mu_y)) \tag{2.33}$$

where μ_X is the mean of X(t) and μ_Y is the mean of Y(t).

The Fourier transform of the cross-covariance function defines the cross-spectrum:

$$\Gamma_{XY}(\omega) = \sum_{\tau=-\infty}^{\infty} \gamma_{XY}(\tau) e^{-2\pi i \tau \omega} \tag{2.34}$$

for all frequencies ω in the domain [-½, ½].

The cross-spectrum can be then decomposed into co-spectrum, quadrature, amplitude and phase spectra. Of practical importance are the coherence squared spectrum which shows the correlation between X(t) and Y(t) as a function of frequency and phase spectrum showing the phase shift for each frequency.

Table 2.2 summarizes formulas for estimating power spectra and cross-spectra for discrete time series (based on Jenkins and Watts, 1968).

Table 2.1. Auto-correlation function and spectrum of the first and second order autoregressive processes

	Auto-correlation function	Spectrum
AR(1)	$\rho_{XX}(\tau) = \phi_1^{\lvert\tau\rvert}$, $\rho_{XX}(1) = \phi_1$	$\Gamma(\omega) = \dfrac{\sigma_{\varepsilon_t}^2}{1 + \phi_1^2 - 2\phi_1 \cos(2\pi\omega)}$
AR(2)	$\rho_{XX}(\tau) = \phi_1 \rho_{XX}(\tau - 1) + \phi_2 \rho_{XX}(\tau - 2)$, $\phi_1 = \dfrac{\rho(1) - \rho(1)\rho(2)}{1 - \rho(1)^2}; \phi_2 = \dfrac{\rho(2) - \rho(1)^2}{1 - \rho(1)^2}$	$\Gamma(\omega) = \dfrac{\sigma_{\varepsilon_t}^2}{1 + \phi_1^2 + \phi_2^2 - 2g(\omega)}$, where $g(\omega) = \phi_1(1 - \phi_2)\cos(2\pi\omega) + \phi_2 \cos(4\pi\omega)$

2.5 Data sources

The principal data used in this chapter are daily and monthly average values of the NCEP/NCAR reanalysis dataset [Kalnay at al., 1996] available on 2.5 degree grid and 17 pressure levels. Given poor quality of data in the Southern Hemisphere prior to introduction of satellites the analysis is limited to the satellite era covering the time period from 1979 up to 2009. At the beginning of this study a comparison of stratospheric variability in the ERA40, ERA Interim and NCEP/NCAR reanalyses has been performed. Significant differences in the stratospheric and tropospheric variability has been found only in the trends. However, since the focus of this study is on the interannual variability and most of the analysis is based on detrended data, only results from NCEP/NCAR reanalysis are provided for the purpose of conciseness.

To analyze the sea surface temperature fields, the study uses the NOAA Extended Reconstructed Sea Surface Temperature analysis, version ERSST V3b, which is constructed based on the surface marine observations from ships and buoys available on 2 degree grid

Table 2.2 Formulas for the estimation of cross-covariance and cross-spectra in discrete time[1]

Sample estimates of	
Auto-covariance function	$r_{xx}(\tau) = \frac{1}{N}\sum_{t=1}^{N-k}(x_t - \bar{x})(x_{t+\tau} - \bar{x}), \quad 0 \le \tau \le L-1,$ where $\bar{x} = \frac{1}{N}\sum_{t=1}^{N} x_t$
Smoothed estimate of the spectrum	$\hat{\Gamma}_{xx}(\omega) = 2\left[r_{xx}(0) + 2\sum_{\tau=1}^{L-1} r_{xx}(\tau) w(\tau) \cos(\frac{\pi\tau\omega}{F}) \right], \quad 0 \le \omega \le F$
Cross-covariance estimate	$r_{xy}(\tau) = \frac{1}{N}\sum_{t=1}^{N-k}(x_t - \bar{x})(y_{t+\tau} - \bar{y}), \quad 0 \le \tau \le L-1$ $r_{xy}(-\tau) = \frac{1}{N}\sum_{t=1}^{N-k}(x_{t+\tau} - \bar{x})(y_t - \bar{y}), \quad 0 \le \tau \le L-1$
Symmetric and anti-symmetric covariance functions	$l_{xy}(\tau) = \frac{1}{2}[r_{xy}(\tau) + r_{xy}(-\tau)], \quad 0 \le \tau \le L-1$ $q_{xy}(\tau) = \frac{1}{2}[r_{xy}(\tau) - r_{xy}(-\tau)], \quad 0 \le \tau \le L-1$
Smoothed estimate of co-spectrum	$\hat{L}_{xy}(\omega) = 2\left[l_{xy}(0) + 2\sum_{\tau=1}^{L-1} l_{xy}(\tau) w(\tau) \cos\frac{\pi\omega\tau}{F} \right], \quad 0 \le \omega \le F$

[1] where L denotes the number of lags used and F – frequency, w(r) – the spectral window. In the analysis Daniell spectral window is used.

Smoothed estimate of quadrature spectrum	$\hat{Q}_{xy}(\omega) = 4\sum_{\tau=1}^{L-1} q_{xy}(\tau) w(\tau) \sin\frac{\pi\omega\tau}{F}, \quad 1 \le \omega \le F-1$ $\hat{Q}_{xy}(0) = \hat{Q}_{xy}(F) = 0$
Smoothed estimate of the amplitude spectrum	$\hat{A}_{12}(\omega) = \sqrt{\hat{L}_{xy}^2(\omega) + \hat{Q}_{xy}^2(\omega)}, \qquad 0 \le \omega \le F$
Smoothed estimate of the phase spectrum	$\hat{F}_{xy}(\omega) = arctg[-\frac{\hat{Q}_{xy}(\omega)}{\hat{L}_{xy}(\omega)}], \qquad 0 \le \omega \le F$
Smoothed estimate of the coherence spectrum	$\hat{K}_{xy}^2 = \frac{\hat{A}_{xy}^2(\omega)}{\hat{\Gamma}_{xx}(\omega)\hat{\Gamma}_{yy}(\omega)}, \qquad 0 \le \omega \le F$

[Smith at al., 2008]. It is based on the International Comprehensive Ocean-Atmosphere Dataset (ICOADS) and incorporates the sea-ice concentration data in the high latitudes.

When specified, the results based on observational datasets are compared with the internal variability typical of the present-day climate in the coupled atmosphere –ocean – sea ice- land surface system as simulated by CSIRO Mk3L climate system model, version 1.2 [Phipps, 2011]. The Mk3L is a fully coupled general circulation model which includes modules describing atmosphere, sea ice, ocean and land surface. The atmospheric component of the model is the low-resolution version of CSIRO Mk3 model and is spectral in design. It is defined on 18 vertical levels from 1000mb to 5mb and has a horizontal resolution of R21 (zonal and meridional resolution of 5.625 and ~3.18 respectively). The 10000 year simulation run used in this study is the one used in [Goodwin et al., 2013]. It has constant boundary conditions with CO_2 equal to 280 ppm, solar irradiance set to 1365 W m^{-2} and 1950 CE orbital parameters.

In some parts of the study, a comparison with historical (1850-2005) and RCP4.5 scenario (2006-2100) integrations of the global circulation models which are a part of the fifth Coupled Model Intercomparison Project (CMIP5) is performed [Taylor at al., 2012]. The simulations are forced with changing concentrations of greenhouse gases, aerosols, stratospheric ozone and with the natural forcings. For the stratospheric comparison, only models with interactive chemistry modules have been included.

In all calculations based on daily data a smoothed annual cycle has been removed prior to analysis. The smoothing was performed by taking first 4 Fourier harmonics of the daily climatology. Derivatives are approximated by centered 1 day differences when computing diagnostics based on equations 2.1-2.10. The terms including the vertical wind are not calculated, since the quality of vertical wind data in the analyses is not sufficient.

Quasigeostrophic version of EP Flux based on equations was used in the study. For plotting purposes EP Flux vectors are scaled as in Edmon at al. (1980). Additionally, above 100mb vectors are multiplied by a scale factor equal to 3 for better visibility.

Chapter 3: Downward coupling between the stratospheric polar vortex and the SAM

3.1 Introduction

The spring-time circulation in the Southern Hemisphere is characterized by strong dynamical coupling between the stratosphere and the troposphere. This is evident in the vertically coherent anomaly in the zonal wind (Fig.1.3) associated with the September-November SAM. There is some debate on the nature of this coupling with certain studies [Baldwin and Dunkerton, 1999-2001; Graverson and Christiansen, 2003; Thompson et al., 2005] suggesting that middle atmosphere dynamics might be modulating the annular modes at the surface.

Isolating the contribution of stratospheric jet variability to the SAM is, however, complicated because tropospheric processes have a strong impact on stratospheric circulation throughout the winter-spring season. Dynamics of both the stratospheric and tropospheric components of the annular modes involves interaction with the up-welling wave activity forced at the surface. In the troposphere, the variability of the SAM can be approximated as a response to the anomalous eddy momentum forcing resulting primarily from the refraction of wave activity in the meridional plane and latitudinal shifts of the maximum baroclinicity regions [Lorenz and Hartmann, 2001-2003]. In the stratosphere, intraseasonal variations of the polar stratosphere have been linked to the forcing of the planetary-scale waves propagating in the vertical [Charney and Drazin, 1961] and can be approximated rather well by the lower-stratospheric eddy heat fluxes [Fusco and Salby, 1999; Weber at al., 2003; Salby et al., 2012].

The “upward” mechanism linking tropospheric and stratospheric components of the SAM can be understood in terms of wave refraction [Limpasuvan and Hartmann, 2000]. During the positive phase of the SAM, the vertically propagating wave activity is refracted equatorward upon reaching the upper troposphere. This results into anomalous poleward momentum fluxes and reinforcement of the westerlies along 60°S. Deflected towards equator, the waves are less likely to propagate upward in the stratosphere and perturb the polar vortex since they encounter the critical line of the tropical stratospheric easterlies. The opposite occurs during the negative phase of the SAM. The up-floating waves are redirected poleward and guided up into the stratosphere through the westerly waveguide where they drive meridional circulation and poleward transport of heat and ozone. Changes in the latitude of a source region of the upward propagating wave activity which accompany migration of the jet

can also have an impact on the stratosphere. Waves originating at the midlatitude source region are more likely to reach the stratosphere compared to those from the subtropical source region [Randel, 1985].

Observational analyses and experiments with mechanistic and global circulation models suggest, however, that at times vacillations of the stratospheric jet can propagate downward [Holton and Mass, 1979; Christiansen, 1999-2000] and affect the tropospheric variability related to that of the annular modes [Baldwin and Dunkerton, 1999; Kuroda and Kodera, 2001; Cristiansen, 2001-2005; Graversen and Christiansen, 2003]. The downward dynamical coupling with the stratospheric polar vortices was shown to be preceded by the upward pulses of wave activity [Graversen and Christiansen, 2003; Polvani and Waugh, 2004] and in the Northern Hemisphere also to be accompanied by the downward progression of wave activity [Graversen and Christiansen, 2003].

In the Southern Hemisphere, the downward propagation of the polar night jet anomalies from the middle towards the lower stratosphere has been shown to be closely locked to the annual cycle. The study by Kuroda and Kodera (1998) extracted an interannual mode of variability characterized by the slow poleward and downward progression of the polar vortex anomalies from May to October and accompanied by changes in the wave activity. The mode owes its existence to the non-linear interactions between vertically propagating waves and the mean profile of the polar-night jet. Figure 3.1a shows variance of the SAM index as a function of calendar month and height and the seasonal cycle of zonal wind averaged along 60°S (adapted from Thompson at al., 2005). The SAM index was defined as the leading EOF of geopotential height at different pressure levels. The variance of the SAM maximizes at 10mb level during early spring and shows a tendency to descend from the middle into the lower stratosphere from August untill November. Towards the early summer, the anomalies in the polar vortex appear to descend into the troposphere. Arguably, most of this “top-down” connection is limited to the final warming events and the break-down of the polar vortex taking place around November. These strong perturbations of the stratospheric flow induced by irregularly occurring bursts of wave activity have been shown to be followed by the anomalies in the SAM which tend to persist for up to 3 months [Thompson at al., 2005].

The condition of the stratospheric polar vortex during spring-time and its susceptibility to perturbations by planetary waves depends on dynamical processes during the entire previous season [Newman and Nash, 2005; Salby at al., 2012]. The polar vortex is said to be “pre-conditioned” whereby the up-welling wave activity will be directed into the jet decelerating it only when it is already weak enough. In contrast, when the polar stratosphere

a)

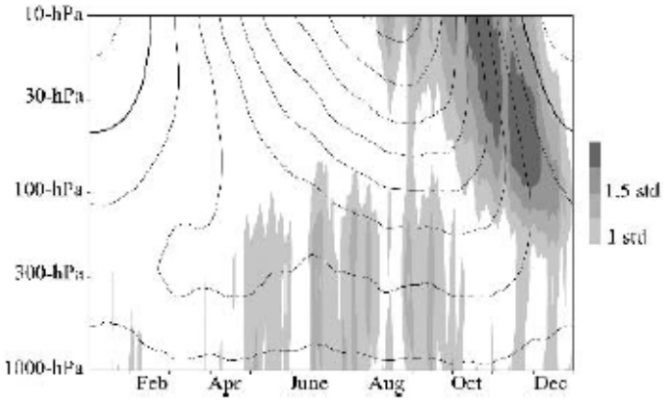

b)

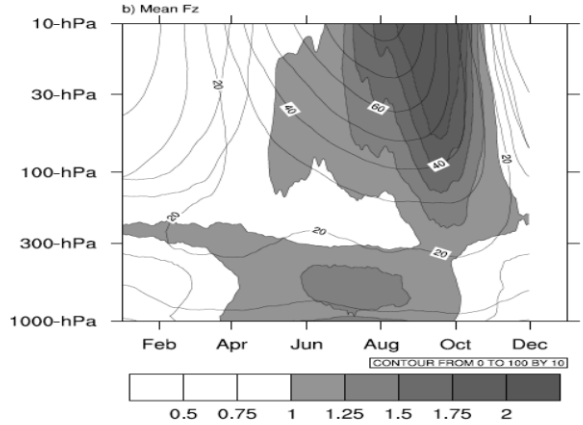

c)

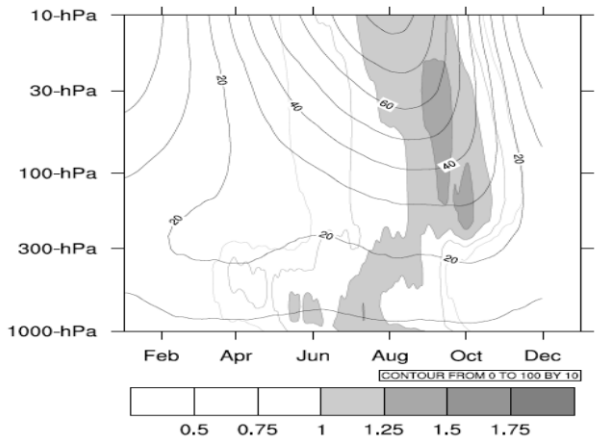

Figure 3.1 (a) Variance of the SAM index (shading) as a function of pressure level and calendar day and the strength of the zonal mean flow along 60°S (contours), adapted from Thompson at al., 2005; (b-c) Annual cycle of the mean (b) and variance (c) of the standardized vertical component of Eliassen Palm Flux averaged between 30° and 90°S (shading) and the strength of the zonal mean flow along 60°S (contours).

is cold and the vortex is strong, the up-floating wave activity will be deflected equatorward leaving the vortex unperturbed. The pre-conditioning depends on anomalous tropospheric processes, such as intensity and direction of the up-floating waves during the preceding season. At the same time, it can be amplified by internal stratospheric processes. The propagation of planetary-scale waves into the stratosphere can be limited by the refractive properties of the polar-night jet. The structure of the zonal wind along the tropopause is known to act like a valve for the up-floating wave activity [Charney and Drazin, 1961]. In the absence of planetary wave forcing from below, the polar stratosphere would cool to the radiative equilibrium and the polar-night jet would then strengthen even more. Anomalously strong westerlies in the vicinity of the tropopause would reduce the refractive index of the polar night jet further trapping wave activity in the troposphere. The opposite occurs when the polar vortex is perturbed by the waves. The deceleration of the vortex will be amplified by the anomalous downwelling and adiabatic warming associated with the descending branch of the Brewer Dobson circulation. The wave-driven Brewer Dobson circulation transports heat and ozone-rich air from equatorial regions towards the polar cap during the entire winter. During springtime, in the presence of UV radiation, the polar ozone accumulated during the previous season will further amplify the deceleration of the polar vortex through short-wave radiative heating.

The thermodynamical state of the springtime stratosphere should thus, at least to some extent, depend on the planetary wave forcing of the polar vortex during the entire previous season. It can be then expected that some part of the hypothesized downward coupling with the SAM can also be pre-conditioned and be predicted in advance. The feasibility of such forecasts has been highlighted in recent studies by Salby at al. (2012) and Son at al. (2013). This chapter attempts to understand whether the coupling between the SAM and the polar vortex is indeed pre-conditioned and to what extent. To answer this question as well as to understand the timing and best predictors of the springtime coupling, I will consider in more detail the low frequency mode of polar vortex variability driven by nonlinear interactions between waves and the mean state which is described by Kuroda and Kodera (1998). In particular, the lags observed between the vortex and its wave forcing [Rao at al., 1998] suggest an opportunity to employ the autoregressive models in describing this wave-drive mode.

The chapter is outlined as follows. Annual cycle of the polar-night jet variability and upward propagating waves is discussed in section 3.2.1. In section 3.2.2 components of the tendency equation are analyzed to identify the best proxy of the momentum forcing imparted on the stratospheric mean flow by the wave activity. A statistical model is then used to

approximate the wave-driven evolution of the polar night jet at 10 mb level in section 3.2.3. The back-effect of the polar-night jet on the propagation of waves is addressed in section 3.2.4. Section 3.2.5 addresses the pre-conditioned downward stratosphere-troposphere coupling. The chapter concludes with summary of results and discussion (Section 3.4).

3.2 Results

3.2.1 Annual cycle

In this section some results regarding differences in the annual cycle of the downward propagation of the polar night vortex anomalies and upward propagating wave activity are presented.

Shown in Figure 3.1b-c is the seasonal cycle of the mean and the standard deviation of the wave activity at different pressure levels in the stratosphere, as approximated by the vertical component of Eliassen Palm flux (F_z) averaged between 30 and 90°S. The normalized mean and standard deviation of F_z have been calculated based on the daily data within a monthly window sliding over the calendar year. While the maximum intensity and variability in the tropospheric waves is observed during June-August (Fig. 3.1b), the annual cycle of the wave activity in the stratosphere does not coincide with it. Instead, it follows the annual cycle of the zonal wind and the downward progression of the maximum wind speeds. The pattern of F_z variance in Fig. 1c strongly resembles that of the SAM in Fig. 3.1, however, it is shifted by one month earlier in the season and to the lower levels. The variability in the F_z appears to follow the annual cycle of the maximum winds at the core of the polar-night jet as well. This suggests that the observed downward propagation of the SAM anomalies can be essentially a result of the changes in the wave activity penetrating from the tropopshere, as in the Northern Hemisphere [Christiansen, 2001-2005]. However, in the Southern Hemisphere the downward progression appears to be locked to the narrow peak in the seasonal cycle of the upward wave fluxes and to follow it with a lag greater than a month. The wave variability itself appears to follow the seasonal cycle of maximum winds at the core of the polar-night jet.

If indeed wave-driven, this lag suggests that to some extent the downward descent of the polar vortex anomalies should be pre-conditioned by the seasonal maximum of wave activity during late winter - early spring. In order to understand this dependence, it is first necessary to diagnose a relationship between the daily evolution of the stratospheric vortex and the vertically propagating waves.

3.2.2 Wave forcing of the SAM-related zonal wind changes

To identify the best proxies of the SAM-related zonal wind changes driven by waves at daily time scales, it is first helpful to examine the relationship between zonal wind tendency and components of the momentum equation in the Transformed Eulerian Mean (TEM) formulation. Under quasigeostrophic assumptions, it reduces to the balance between divergence of EP flux and the Coriolis force of the residual mean motion:

$$\underbrace{\frac{\partial \bar{u}}{\partial t}}_{\substack{Momentum \\ tendency}} = \underbrace{f\bar{v}^*}_{\substack{Coriolis \\ force}} + \underbrace{\frac{1}{\rho_0 a \cos\phi} \nabla \cdot F}_{\substack{EPflux \\ divergence}} \tag{3.1}$$

Propagating wave activity modifies the mean flow through $\nabla \cdot F$, whereby absorbed waves decelerate the flow. The wave-induced motion is then deflected by the Coriolis force driving the residual mean circulation which is proportional to $-\nabla \cdot F$.

The relative contribution of the horizontal $\partial Fy/\partial y$ and vertical $\partial Fz/\partial z$ components of $\nabla \cdot F$ to the wind tendency is different between stratosphere and troposphere and at different pressure levels. Figure 3.2a shows the cross-correlation structure at zero lag between daily momentum tendency at different pressure levels and forcing terms in equation (3.1): zonal force due to EP flux divergence $\nabla \cdot F$, it's horizontal $\partial Fy/\partial y$ and vertical $\partial Fz/\partial z$components, and the Coriolis force of the residual mean meridional circulation $f\bar{v}^*$, where y denotes latitude and z – log-pressure. The cross-correlation has been computed for the tendency of the zonal mean zonal wind averaged between 45-70°S, that is where the spring-time SAM signature in zonal wind does maximize, and based on the daily September-November 1979-2009 record. The choice of the domain definitions in Figure 3.2 is motivated by a wish to illustrate the transition in the driving forces of the SAM from the troposphere to the stratosphere. I look at the spatial fingerprint of the SAM which changes from one level to the next (it corresponds to a dipole pattern in the troposphere and variability in the strength of the polar vortex in the stratosphere), but remains fairly constant between 45-70S. However, for the stratosphere at the levels above 70hPa it could be expanded from 45-70S up to 30-90S without any difference in the results.

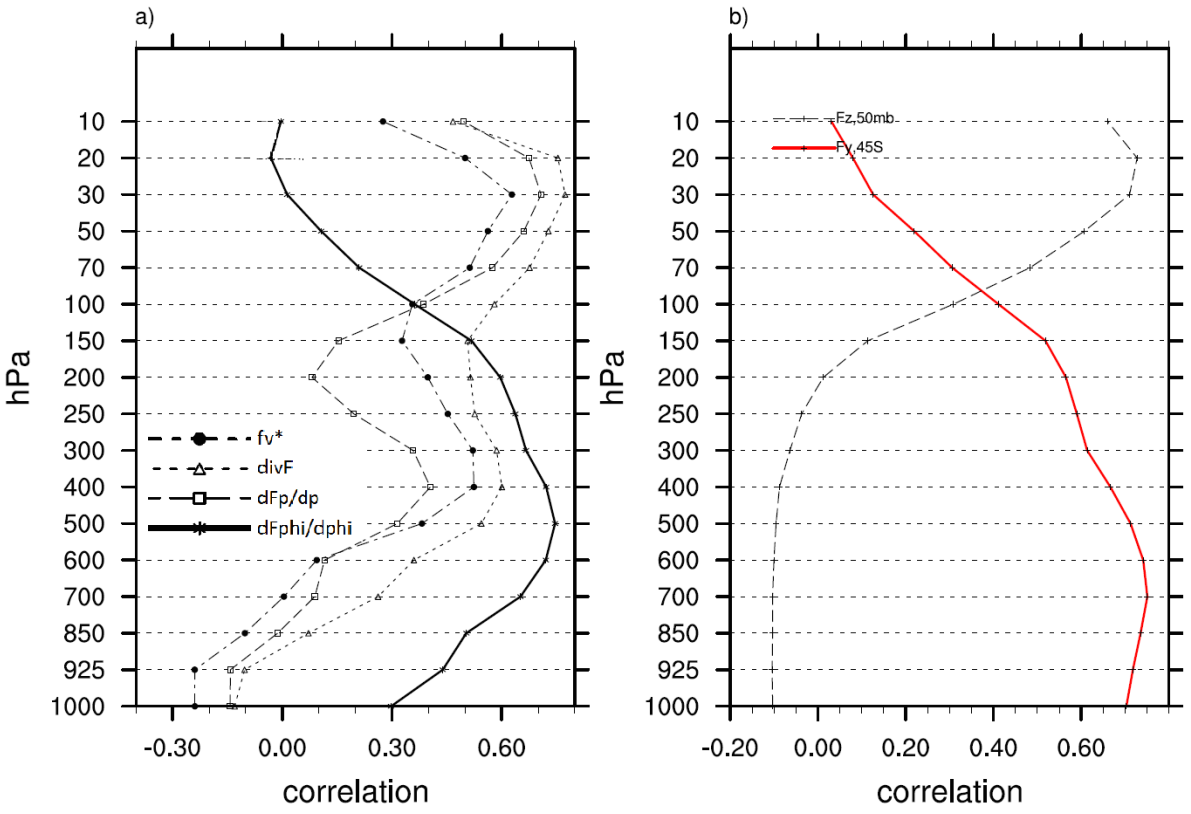

Figure 3.2. Correlation between daily zonal mean zonal wind tendency at 45-70°S, and (a) different terms of TEM momentum equation; (b) net eddy forcing terms Fy at 45°S, 1000-200mb, & Fz at 50mb, 30-90°S in September-November

In the troposphere, the main forcing in the tropospheric component of the SAM-related zonal wind appears to be through the horizontal convergence of the EP flux $\partial Fy/\partial y$ (which is proportional to the horizontal convergence of eddy momentum flux) since there tends to be a large cancellation between $\partial Fz/\partial z$ and $f\overline{v}^*$. Thus, in the troposphere, the TEM formulation gives the results equivalent to the conventional analysis (Lorenz, 1952; Hoskins, 1988). In the stratosphere, the wave forcing of the polar vortex is through $\nabla \cdot F$ which is dominated by the effect of the vertical convergence of EP flux $\partial Fz/\partial z$.

Since components of the EP Flux vector indicate the direction of wave propagation, TEM formulation makes it more convenient to analyze the effect of horizontal and vertical deviations in the wave propagation on the eddy-driven midlatitude jet and polar night jet at different pressure levels. The net effect of the horizontal and vertical shifts of the wave activity on the daily SAM-related zonal wind tendency can then be approximated by taking vertical and horizontal components of EP flux averaged at appropriate boundary levels. That is, in the troposphere, the eddy momentum forcing associated with the shifts of wave activity in the meridional plane can be approximated by a vertically averaged horizontal component of EP flux at 45°S and in the stratosphere by its vertical component averaged horizontally in the lower stratosphere.

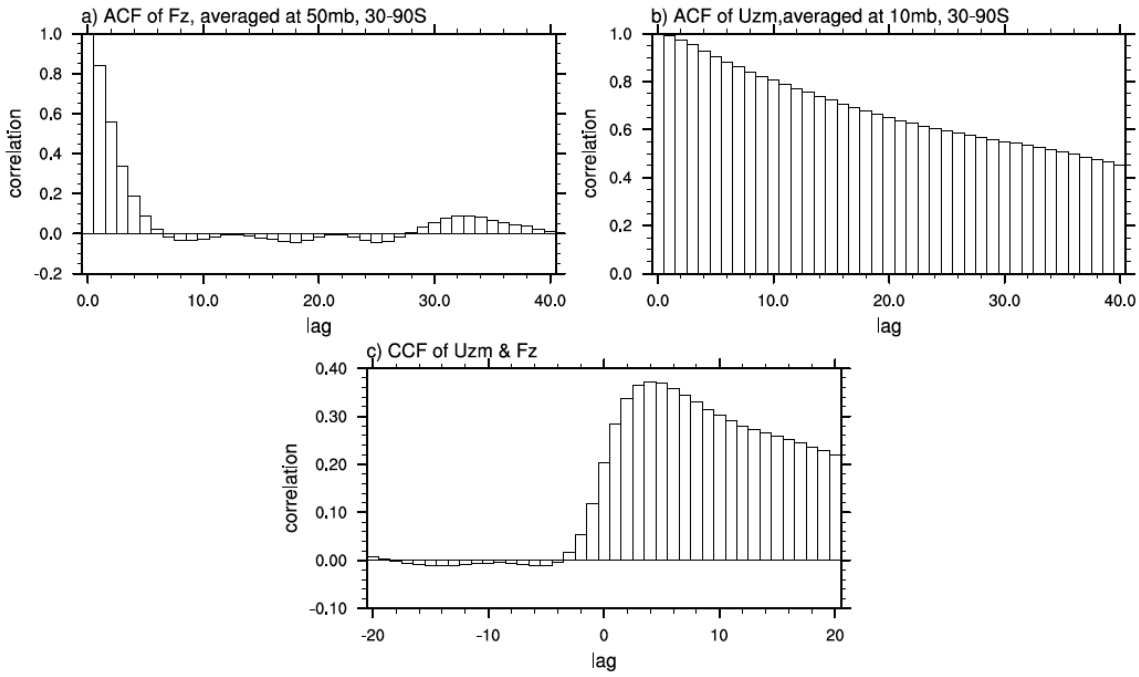

Figure 3.3 Auto-correlation (ACF) and Cross-correlation (CCF) functions of the planetary wave forcing and strength of the polar night jet at 10 mb level: (a) ACF of the daily vertical component of EP flux (Fz), averaged at 50mb, 30-90°S, (b) ACF of the zonal mean zonal wind (Uzm), averaged at 10mb, 30-90°S, (c) CCF -Fz/Uzm. Based on the daily record from 1 January 1979 to 31 December 2009.

Displayed in Figure 3.2.b are the cross-correlations between daily momentum tendency of the zonal mean zonal wind, averaged over 45-70°S, F_y, averaged vertically between 1000 and 200mb at 45°S, and F_z averaged between 30 and 90°S at 50mb and 100mb levels. The relative contribution of the eddy momentum forcing associated with F_y to the zonal wind tendency does decrease with height, while the contribution of F_z does increase above the tropopause and maximize above 50mb. Changes in F_z at 100mb approximate best the zonal wind tendency at 30mb, while F_z at 50 mb - zonal wind changes at 20 and 10mb. Below 700mb the effect of eddy momentum forcing expressed through F_y maximizes with a one day lag (not shown) consistent with the notion that momentum at the surface is maintained against friction by the eddy-induced mean meridional circulation.

Thus, the response of the zonal wind to the changes in the forcing of wave activity along 50-60°S can be assumed to have a simple form of an integrated response to the random forcing terms F_y, F_z:

$$\begin{cases} \dfrac{\partial u}{\partial t} = -F_z - \lambda_{str} u\,, & \text{in the stratosphere;} \\ \dfrac{\partial u}{\partial t} = F_y - \lambda_{tr} u\,, & \text{in the troposphere;} \end{cases} \qquad (3.2)$$

where a negative stabilizing feedback λu should be included to ensure a statistically stationary solution with respect to variance [Hasselmann, 1976; Frankignoul and Hasselmann, 1977]. The characteristic correlation time scale of the response function should be much larger than the time scale of the atmospheric eddy forcing variables. It is largely determined by the decorrelation time arising from the linear feedback λu . In the troposphere, the response time was estimated to be $(8.9\ \text{day})^{-1}$ and included a positive feedback [Lorenz and Hartmann, 2001]. Given the even stronger persistence of the variability of the stratospheric flow compared to the troposphere, the response time in the stratosphere should be much larger than in the troposphere. To estimate it, statistics of the relationship between the daily time series of the lower stratospheric wave fluxes and mean strength of polar night jet are provided in the next section.

3.2.3 Statistical model for the wave-driven evolution of polar night jet at 10 mb level

Figures 3.3-3.4 show the statistics summary for F_z at 50 mb (taken with an opposite sign) and the mean strength of the stratospheric jet at 10mb, both averaged at 30-90°S for the entire daily record from 1 January 1979 to 31 December 2009. For the cross-correlation functions (CCF) to be close to the observed one, the relaxation time in equation 3.2 should be equal to ~$(2\ \text{month})^{-1}$ in the stratosphere. The phase spectrum confirms that evolution of the stratospheric jet at 60°S can be represented as an integrated response to the forcing of the upward propagating activity. For the frequencies where variance in F_z is concentrated the phase shift approximately follows $\arctan(2\pi f / \lambda_{str})$ [Jenkins and Watts, 1969] from ~70 degrees for frequencies of $(100\ \text{day})^{-1}$ to 90 degrees for frequencies of $(10\ \text{day})^{-1}$ with $\lambda_{str} = (60\ day)^{-1}$. The spectral structure of F_z features a number of peaks in the power spectrum which apparently correspond to the different zonal wave numbers of upward propagating wave activity. The maximum variance corresponds to the frequencies typical of zonal wave number 1 and 2.

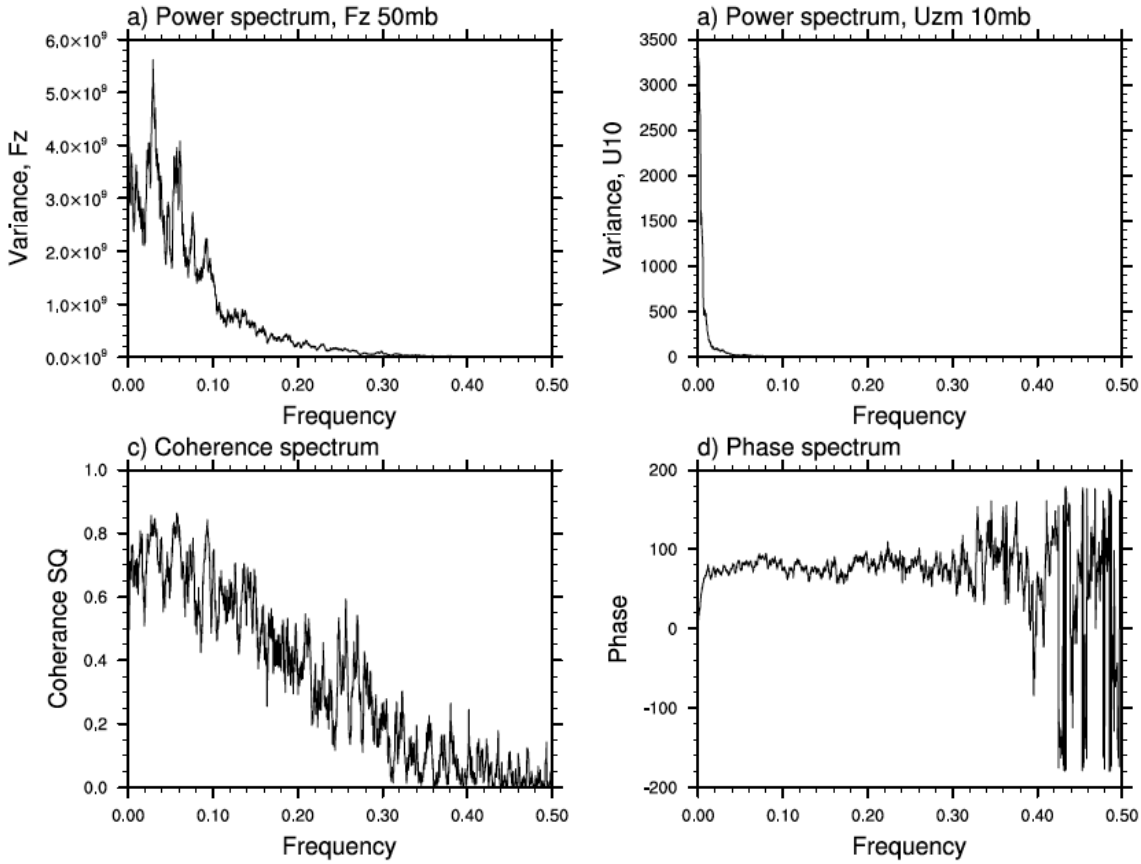

Figure 3.4 Power, coherence and phase spectra of the planetary wave forcing as measured by the vertical component of EP Flux averaged at 50mb, 30-90°S (Fz) and zonal mean zonal wind at 10 mb level, averaged between 30-90°S (Uzm). Sign of Fz has been inverted. Based on the daily record from 1 January 1979 to 31 December 2009. Frequency is given in (days)$^{-1}$.

To obtain an impression of how the ~(60 day)$^{-1}$ relaxation time affects the cross-correlation structure between the driving and the integrated process after time averaging and how the variance of an integrated process with ~60 days relaxation time changes with respect to the seasonality of variance in the driving noise, a Monte Carlo experiment was conducted. The spectral structure of F_z at 50mb (Fig. 3.4) is too complex to be accurately represented by a simple statistical model since it contains several periodicities. However, its main features can be approximated by a second-order autoregressive process (AR2) process:

$$X(t) = \phi_1 X(t-1) + \phi_2 X(t-2) + \varepsilon_t \qquad (3.3)$$

The first two serial correlation coefficients ρ_1, ρ_2 estimated from the auto-correlation function displayed in Fig.3.3a were used to compute Yule–Walker parameter estimates of $\{\phi_1, \phi_2\}$ in the fitted AR2. Figure 3.5 shows the theoretical auto-correlation function and

power spectrum of the AR2 process with parameters {1.3,-0.5} computed according to equations in Table 2.1. With the exception of an absence of the secondary variance peak in the power spectrum, they largely overlap with the estimated statistics of the observed F_z. The driving white noise time series was then multiplied by a normalized sine wave to introduce the seasonal cycle of variance in F_z typical of the observed record. Thus, 10000 samples of length [31years*364 days] were generated from AR(2) processes with parameters {1.3,-0.5} and a seasonal cycle in the variance of the driving noise.

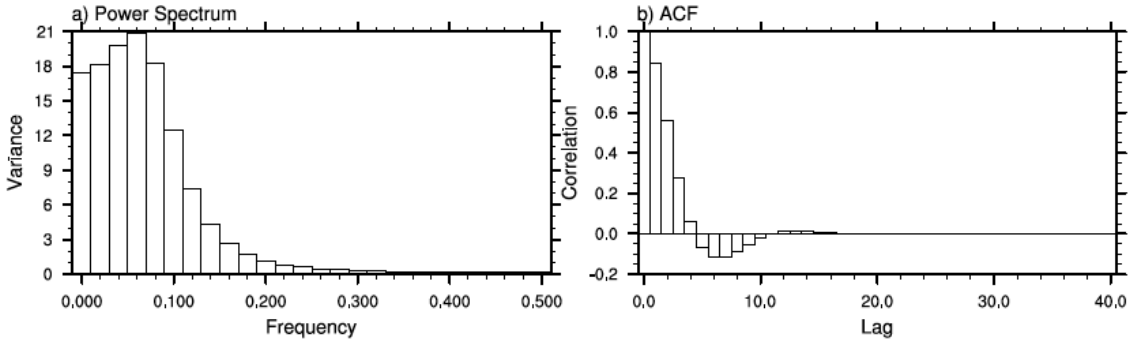

Figure 3.5. (a) Power Spectrum and (b) Autocorrelation function (ACF) of a second order Markov process (AR2) with parameters {1.3, -0.5}

In summary, the purpose of the Monte Carlo simulation is to illustrate how a one month lag between the driving stochastic forcing and the polar vortex originates when we look at that type of process with ~60 day relaxation time and to understand how lags in the monthly data should be interpreted.

3.2.3.1 Effect of the time smoothing on the cross-correlation structure between the polar jet and its wave forcing

First, it is necessary to test whether the relationship identified in Figure 3.2 holds for the monthly and seasonal mean data without being distorted by the effects of other, e.g. radiative, factors or internal feedbacks. To achieve that, the expected and observed cross-correlation function (CCF) between driving noise and integrated response is computed. Figures 3.6 a,b compare the observed and simulated cross-correlation plotted as a function of a lag and averaging period. The simulated CCF represents the mean from 10000 Monte Carlo experiments.

Theoretically, the effect of time smoothing on the cross-correlation structure between the driving noise and the response function is to increase the correlation and to reduce the lags [Munk, 1960]. For the lag to disappear completely, the averaging period must exceed the time

scale of the relaxation time of the vortex to the driving noise. The observed CCF suggests that even when monthly averages are used the lag still persists. The structure of the observed CCF is very consistent with the simulated one which confirms that the memory of the jet to the wave forcing should be around 2 months. The strength of the correlation is somewhat lower though with a maximum of 0.65 for 80-90 day average at zero lag. In the CCF from Monte Carlo experiments the maximum correlation reaches 0.75 for the same averaging period.

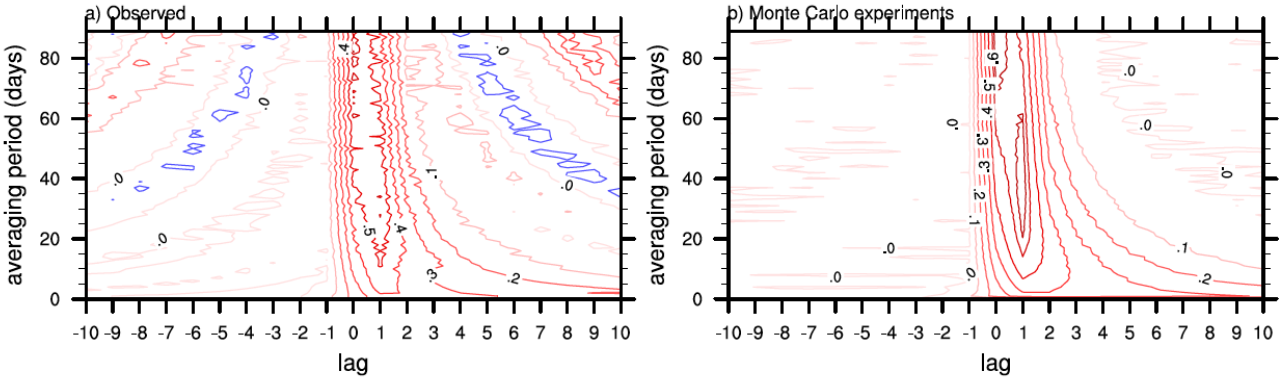

Figure 3.6. (a) Observed cross-correlation function between the vertical component of Eliassen Palm Flux at 50 mb (sign inverted) and zonal mean zonal wind at 10mb and (b) Monte Carlo simulation of cross-correlation function between AR2 (1.3,-0.5) and its integral taken with (60 days)$^{-1}$ decorrelation time plotted as a function of the lag and averaging period. The simulated CCF mean is derived from 10000 trials.

It is noteworthy that even though the integrated process in the Monte Carlo simulations is entirely determined by the driving noise, achieving correlation close to 1 would require taking averages much higher than the relaxation time. Thus, under such memory characteristics, a relatively weak correlation coefficient observed in the monthly or even seasonal mean data does not necessarily imply a weak physical relationship.

3.2.3.2 Effect of the seasonal cycle in the vertical wave propagation variability on the seasonality of variance of the stratospheric vortex

The variability in the deseasonalized F_z , the primary dynamical forcing of the stratospheric jet shows a distinct seasonal cycle which follows the annual cycle of the mean zonal wind (Fig. 3.1c). Under the relationship described by (3.3) and ~(60 day)$^{-1}$ relaxation time of the stratospheric vortex, it is to be expected that the observed pattern of F_z shown in Figure 3.1c translates into stratospheric jet variability with a lag.

To gain more insight into the lags in variance, each simulated "daily" time series was converted into "monthly" mean time series and parameter estimates of the phase shift in the

annual cycle of variance of the integrated process and that of the driving AR2 process were computed. Figure 3.7 compares the seasonal cycle of variance introduced in the driving noise and the estimated 95% confidence intervals for the seasonal cycle of variance in the integrated process. It shows that the variance of the response function tends to maximize 1 month after the maximum in variance of the driving noise.

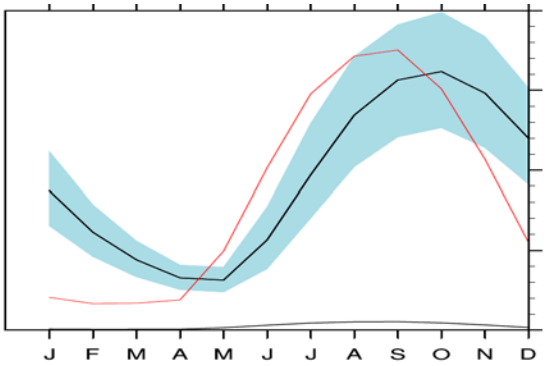

Figure 3.7. Monte Carlo simulations of the shift in the annual cycle of the std of the driving process (red) and an integrated process with λ *= (60 day)*$^{-1}$ *(black). Blue shading indicates 95% confidence intervals. The distribution is estimated from 10000 trials. Arbitrary units.*

Hence, the lag between the descent of zonal wind anomalies (Fig. 3.1a) in the stratosphere and the seasonal cycle in the variance of the vertical wave flux (Fig.3.2c) is consistent with the shifts in variance between the wave forcing and an integrated process as suggested by the Monte Carlo experiments. It appears to be the combination of 60 day memory of the zonal wind and the seasonal descent of variance in the wave forcing following changing background flow that determines the spring-time descent of the zonal wind anomalies. Thompson at al. (2005) noted that the timing of variance peak is determined by the theoretical criteria outlined by the Charney and Drazin theorem (1961), that is, the winter vortex is too strong to permit the propagating wave activity. However, the observed seasonal maxima in F_z suggest the opposite since they collocate with the strongest winds at the jet core. The discrepancy can be eliminated by considering the refractive properties of the polar night jet which are reviewed in the next section.

3.2.4 Effect of the mean structure of the stratospheric jet on the propagation of wave activity

Figure 3.8 presents the annual cycle of the monthly climatology of the zonal mean zonal wind, the vertical component of Eliassen Palm Flux and the refractive index for the

stationary wave with zonal wave number 1 averaged at the 50 mb level. The annual cycle of the zonal-mean wind (Fig. 3.8a) shows the well-known polar-night stratospheric jet maximizing during the late winter/early spring. A broad maximum in F_z along 60°S (Fig. 3.8b) is present from the middle winter until late spring and largely overlaps with the maximum in the zonal wind. Confinement of the wave activity along the core of the jet is closely related to the refractive index maximum at 60°S shown in Fig.3.8c. At the same time, the sharpness of the strong jet results in the refractive index turning negative at its flank poleward of 70°S prohibiting the propagation of the incoming wave activity towards the pole and break-up of the vortex. The latitude of the negative refractive index south of 60°S at 50mb begins to shift poleward starting from August. The up-floating wave activity is then deflected poleward as well.

Figure 3.9a,b show the annual cycle of zonal mean zonal wind at 60°S, the refractive index for stationary zonal wave number 1 at 60°S and the latitude of the turning level. As the maximum of zonal wind at 60°S propagates downward during late winter, so does the maximum of refractive index. Towards September-October the refractive index maximizes at the 70 mb level. At the same time, following the changes in the sharpness of the jet, the latitude of the negative refractive index turns poleward permitting more upward wave propagation. It begins to shift poleward starting from August at 10mb level and from September-October in the lower stratosphere.

The interannual variability in the annual cycle of the polar night jet relaxation appears to determine the variability in the upward wave fluxes. To illustrate the feedbacks between the upward propagating waves and the polar night jet, it is helpful to plot the cross-correlation between *Fz,* averaged between 30-90°S at each pressure level and over the month when the zonal wind at 60°S maximizes, and the latitude of the negative refractive index for stationary zonal wave number 1. The CCF structure in Fig.3.9c shows that a shift of the negative refractive index poleward by 1-2 degrees S corresponds to the *1 std* increase in the upward wave flux. Thus, the downward progression of the polar-night jet anomalies is essentially wave-driven and appears to be controlled not only by the intensity of wave activity at the lower boundary but also by the variability in the spring-time weakening of the vortex which determines the width of the westerly wave-guide and, hence, the wave forcing of the stratospheric flow.

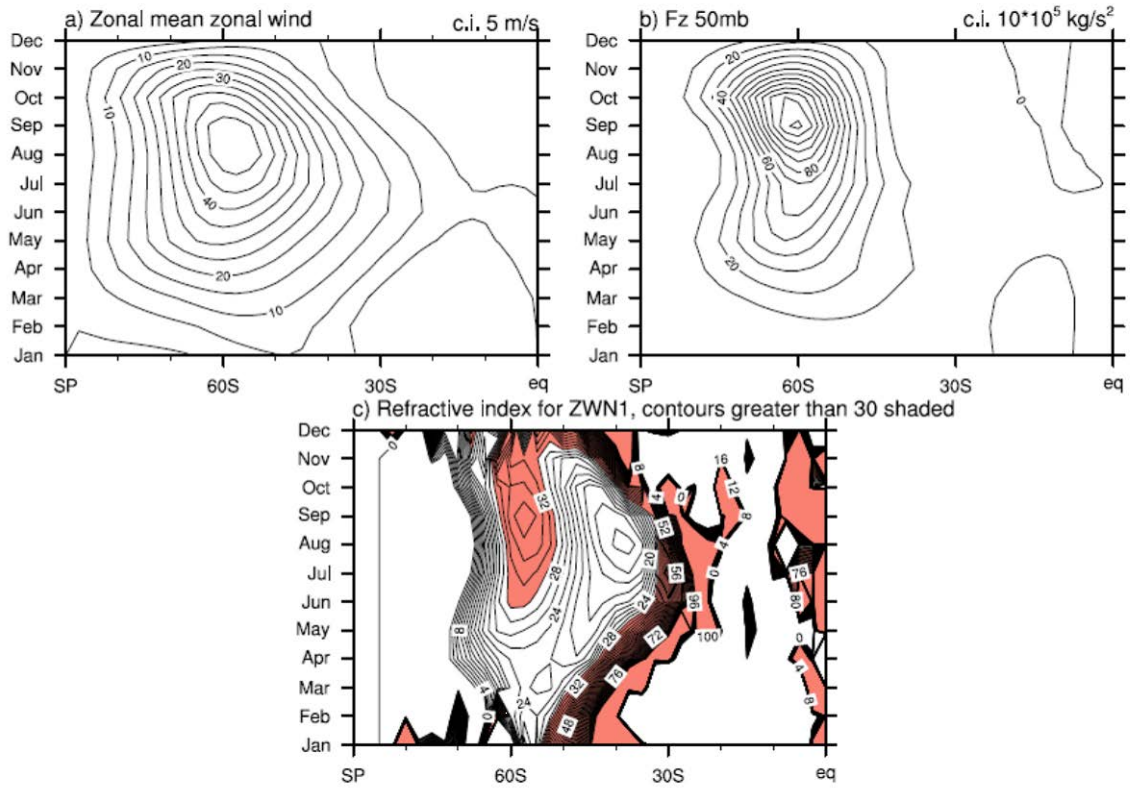

Figure 3.8. Seasonal variations in the (a) zonal mean zonal wind, (b) vertical component of EP Flux (Fz) and (c) refractive index squared $\alpha^2\eta^2$ for stationary zonal wave number 1 (nondimensional values multiplied by the radius of earth squared; contours greater than 30 are shaded) at 50mb level

3.2.5 Downward stratosphere-troposphere coupling in the austral spring

A number of studies addressed the enhanced persistence of the Southern Annular Mode with some observational analyses suggesting that the stratosphere can contribute to the "redness" of the SAM during late spring-early summer. Thus, Thompson and Wallace (2000) argued that most of the stratosphere-troposphere coupling in the Southern Hemisphere occurs during a 6-8 week interval around November and is associated with the final warming which breaks down the polar vortex. Thompson and Solomon (2002) also demonstrated that surface SAM in December-January weakly correlates with the parameters of the polar stratosphere in November, such as total ozone content and 30 mb geopotential height/temperature.

a)

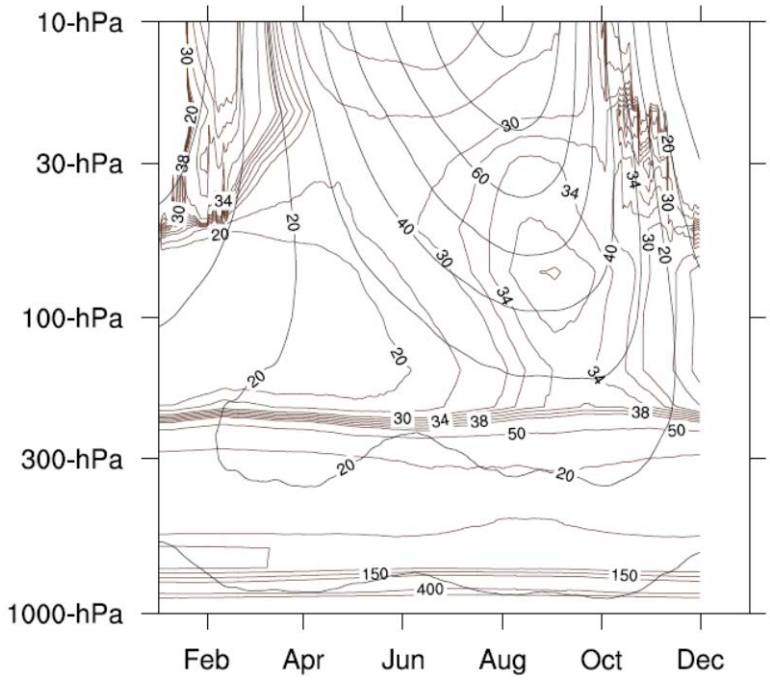
10-hPa
30-hPa
100-hPa
300-hPa
1000-hPa
Feb
Apr
Jun
Aug
Oct
Dec

b)

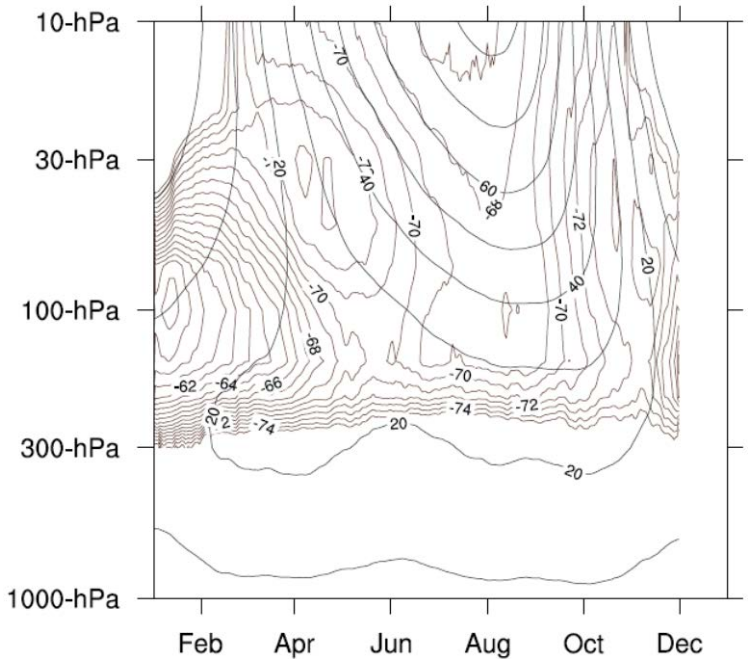
10-hPa
30-hPa
100-hPa
300-hPa
1000-hPa
Feb
Apr
Jun
Aug
Oct
Dec

c)

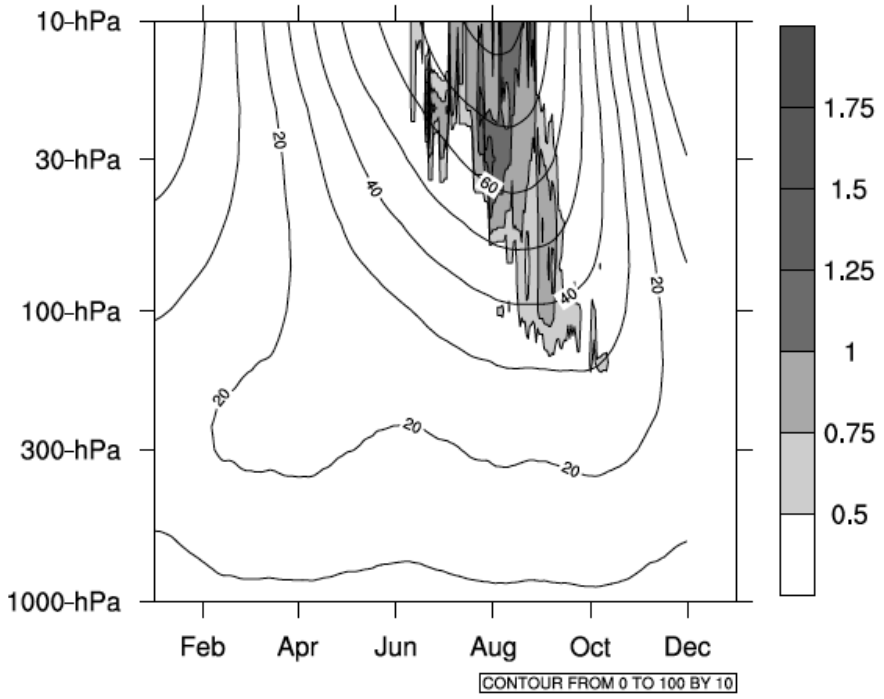

Figure 3.9. Zonal mean zonal wind (black) at 60°S and (a) refractive index for stationary wave with zonal wave number 1 at 60°S (brown), (b) the latitude of the turning level for stationary wave with zonal number 1 (brown), (c) anomalies in the latitude of turning level (shading, units in deg.S) which correspond to 1 std increase in the vertical component of EP Flux (significant at 95% level) plotted as a function of pressure level and calendar day

In fact, the downward stratosphere-troposphere coupling is not limited to November and can be tracked during the entire spring-early summer season. The spring-time relationship between stratospheric and tropospheric components of the SAM can be best seen at the time scales which significantly exceed $(10day)^{-1}$, that is when most of the internal variability in tropospheric component of the SAM in response to the forcing below the tropopause is averaged out.

Figure 3.10 shows correlation between F_z at 50mb level integrated up to October 1 with the 60 day relaxation time and zonal mean zonal wind at 55°S averaged over the monthly window sliding over the calendar year. Mean seasonal cycle of *Fz* at 50mb, 30-90°S is overlaid in the lower panel. As it is evident from the plot, the integrated upward wave fluxes not only pre-condition much of the stratospheric vortex variability after October, but also correlate well with tropospheric zonal wind at 55°S during October-December. The strength of correlations maximises from middle October until middle November (greater than -0.7) and decays towards December.

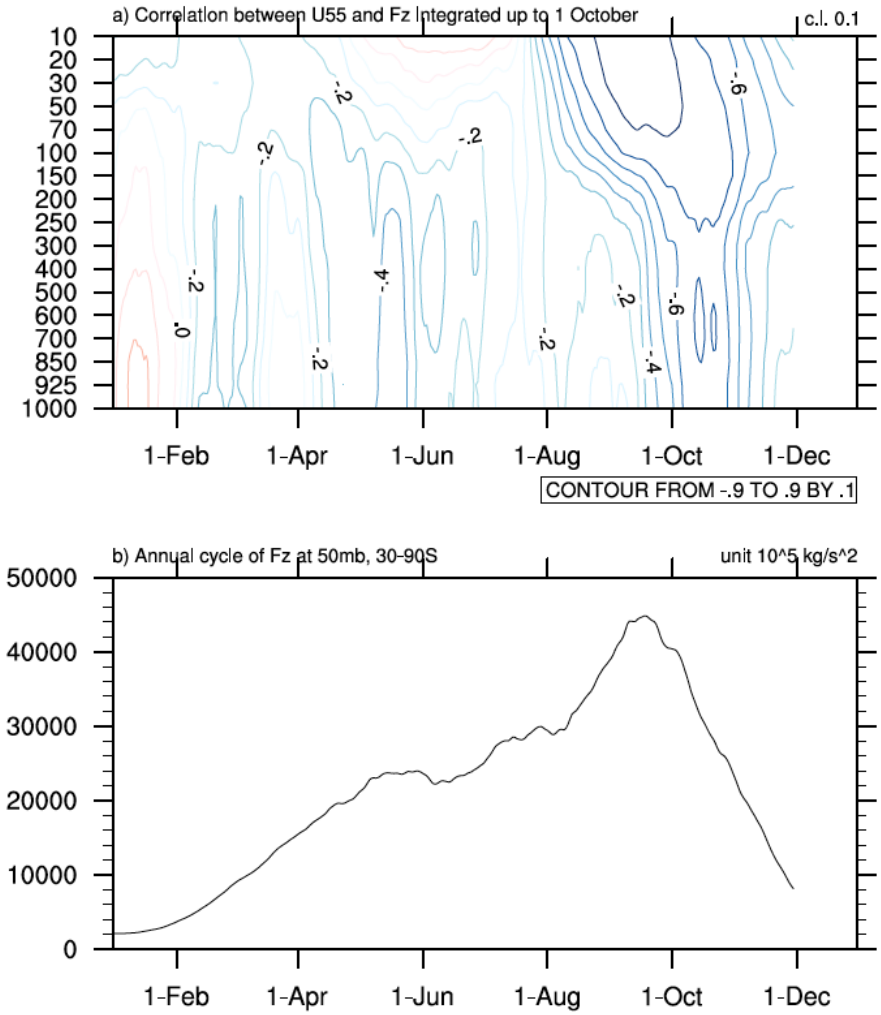

Figure 3.10. (a) Correlation between zonal mean zonal wind at 55°S and the vertical component of EP flux averaged at 50 mb level between 30 and 90°S and integrated with (60 day)$^{-1}$ relaxation time until 1 October; (b) Seasonal cycle of the vertical component of EP flux averaged at 50 mb level between 30 and 90°S. Each value is centered at the beginning of the averaging interval.

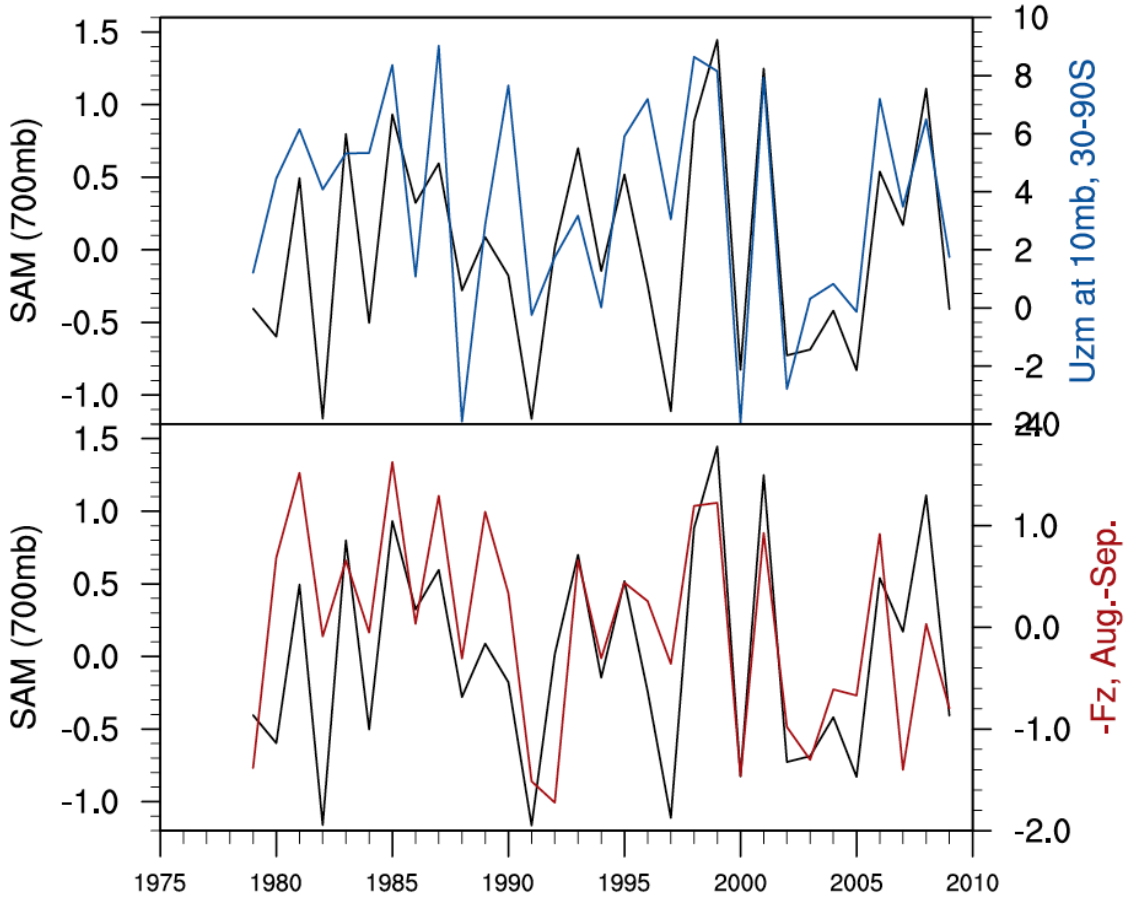

Figure 3.11. Mid-October-December SAM index defined as the first EOF of 700 hPa pressure poleward of 20S (black), mean strength of the stratospheric vortex at 10 mb (blue) and the normalized vertical component of EP Flux integrated up to mid-October with (60 day)$^{-1}$ relaxation time (red).

On seasonal time scales, this downward propagation results into downward coupling observed between the SAM and the stratospheric vortex. The top panel of Figure 3.11 shows time series of the SAM index defined as first empirical orthogonal functions of 700mb geopotential height fields poleward of 20°S, and strength of polar vortex at 10 mb averaged from mid-October to the end of December. There is a significant correlation between SAM and stratospheric variability during these months reaching 0.68. However, as shown above, the spring-time variability in the stratospheric jet mostly results from variability in the wave forcing during preceding months. The lower panel of Fig. 3.12 shows the time series of *Fz* at 50mb, integrated with (60 day)$^{-1}$ e-folding time up to the 15th October each year. Correlation with the 700mb SAM averaged for the next 3 months is strong reaching 0.73. Figure 3.12 shows correlation between *Fz* at 50mb integrated up to the 1 October, 15 October, 1 November and 1 December and SAM index computed averaged within monthly window sliding over calendar year. Consistent with Fig. 3.11 most of this relationship comes from

October, a month which follows September maximum in the seasonal cycle of stratospheric wave forcing. A somewhat weaker relationship can be also found for the lower-stratospheric wave fluxes integrated up to the 15 October and November SAM at 700mb. Since the wave forcing vanishes towards November, SAM in December shows dependence on *Fz* during the same period as SAM in November. Persistent positive correlations with the SAM extent well into early autumn.

It should be noted that some decadal variability is present in the upward wave fluxes in Fig.3.11 which complicates estimating the downward link. However, wave fluxes are sent into stratosphere from the surface and naturally contain all the climate signals. In fact, these results confirm that some of the climate signals could be communicated via stratosphere (see for example modelling studies by Ineson and Scaife (2008) and Bell et al. (2009).

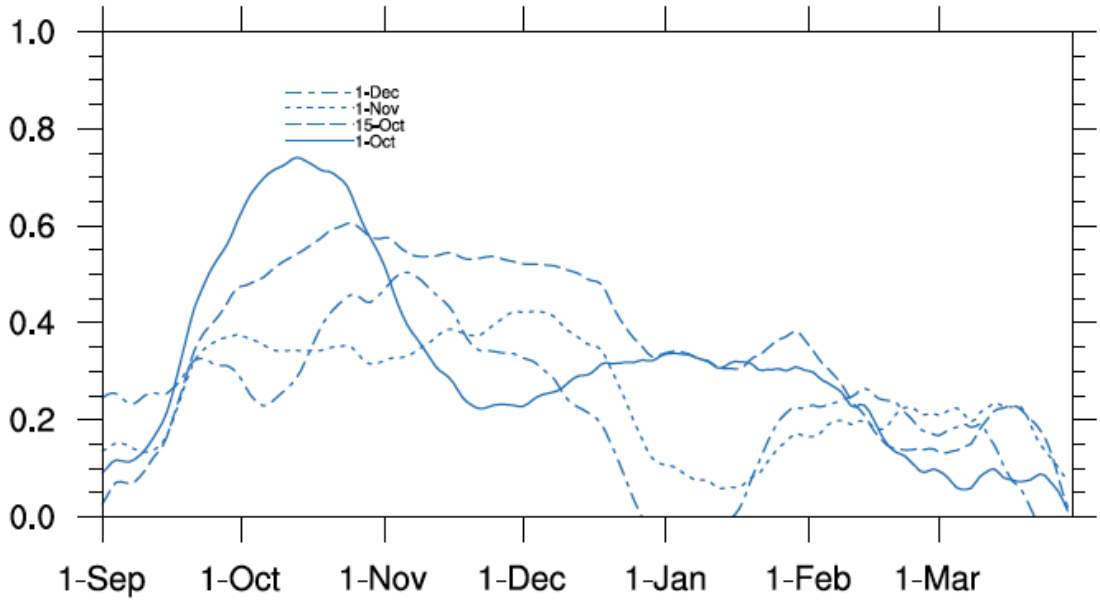

Figure 3.12 Correlation between the daily SAM index averaged within 1 month window sliding over calendar year and the vertical component of Eliassen Palm Flux averaged at 50mb, 30-90°S, and integrated with (60 day)$^{-1}$ up to the 1 October, 15 October, 1 November and 1 December.

Thus, the variability of the SAM at time-scales greater than 2-3 months during spring-time is pre-conditioned by the stratospheric wave forcing during preceding months. Even though most of the dynamical stratospheric variability originates at the surface, the strong stratosphere-troposphere coupling observed in the spring-time is mostly “top-down”, not due to the SAM extension from surface into the stratosphere. Hence, by knowing the planetary

wave forcing and parameters of the polar stratosphere during late winter/early spring, predictions of the tropospheric component of the SAM on the seasonal time scales can potentially be improved.

3.3.6 Downward progression of zonal wind anomalies in the CMIP5 models with interactive chemistry

The Global Circulation Models have been shown to displace the break-down of the polar vortex and variability in its planetary wave forcing towards the early summer [Hurwitz at al., 2010; Garfinkel at al., 2013]. The delayed break-down of the vortex affects, however, the timing of the downward coupling between the polar vortex and the SAM as it will be shown below. Table 3.1 compares downward progression of zonal wind anomalies at 55°S in the historical integrations of the CMIP5 models with interactive chemistry with the one observed in NCAR reanalysis dataset from 1979 until 2005. The latter is measured by the cross-correlation between zonal mean zonal wind at 55°S at 10 mb level and at 700 mb level taken with a 1 month lag. Additionally, one month lag correlation of 700mb zonal wind with itself is given to differentiate between downward progression and internal persistence of the surface zonal wind.

Table 3.1. CMIP5 models with interactive chemistry: lagged correlation of zonal wind at 55°S at 10 mb with zonal wind at 55°S at 700mb during the same month (left) and zonal wind at 55°S at 700mb during the next month (right)

	Grid Top	Aug/Sep	Sep/Oct	Oct/Nov	Nov/Dec	Dec/Jan
CESM1 (FASTCHEM)	2.19 hPa	0.5/0.2	-0.0/0.2	0.6/0.2	0.5/0.5	0.3/0.5
CESM1 (WACCM)	$5.1*10^{-6}$ hPa	0.3/0.6	0.2/0.5	0.1/0.3	0.3/0.2	0.3/0.3
GFDL-CM3	0.01 hPa	0.1/0.4	0.4/0.3	0.6/0.3	0.8/0.6	0.5/0.8
GISS-E2-H p2	0.1 hPa	0.0/0.0	-0.0/0.0	0.6/0.4	0.4/0.4	0.3/0.4
GISS-E2-H p3	0.1hPa	0.0/0.3	-0.2/0.4	0.4/0.5	0.6/0.6	0.4/0.4
MIROC-ESM-CHEM	0.003 hPa	0.0/0.4	0.5/0.5	0.4/0.5	0.6/0.9	0.5
NCAR reanalysis	10 hPa	0.1/0.3	0.7/0.1	0.5/0.3	0.4/0.5	0.0/0.3

Among the models selected, the Community Earth System Model CESM1-FASTCHEM captures the downward progression best despite having a relatively low top compared to the other models. However its seasonality is shifted towards the summer by one month as it is the case with the other models as well. In contrast to the observations, they show enhanced coupling with the stratosphere and enhanced persistence during November-December.

3.4 Summary

It is demonstrated that most of stratospheric jet variability on seasonal time scales during spring-time is pre-conditioned by wave forcing during preceding months. Under a rather slow response time of the stratospheric jet to the forcing of the upward propagating waves in the Southern Hemisphere, there is a significant lag between seasonal amplification of the wave forcing and the polar vortex response. At the same time, the interannual variability in the propagation of wave activity is controlled by the sharpness of the jet and in particular, the latitude of the turning level on its poleward flank. The more poleward it is, the stronger the upward flux of wave activity. Together these feedbacks create an impression of the slow descent of the polar vortex anomalies, whereby, this variability is essentially wave-driven. It is then shown that most of the vertically coherent variations in the Southern Annular Mode observed during spring-time after seasonal averaging are, indeed, top-down and can be predicted by knowing parameters of the stratospheric circulation during preceding months.

The main results of this chapter can be summarized as follows:

1) The daily evolution of the stratospheric vortex can be represented as an integral response to the forcing of planetary-scale waves excited at the surface. The wave forcing is best approximated by the vertical component of EP Flux taken at the appropriate boundary, e.g. at the 50 mb level for the evolution of the vortex at 10 mb or at 100 mb level for the evolution of the vortex at 30 mb. The relaxation time of the stratospheric jet to the net wave forcing should be equal to approximately ~$(60\ \text{day})^{-1}$ for the statistical structure of the response to be close to the observed one.
2) The ~$(60\ \text{day})^{-1}$ relaxation time of the stratospheric jet to the perturbations by a wave disturbance determines the lagged covariance structure observed in the monthly and seasonal mean fields between upward propagating waves and strength of the jet. It implies a one month delay in the zonal wind variability relative to the variability in the seasonal cycle of its dynamical forcing as is the case in the observed seasonal cycle.

3) The narrow peak in the seasonal cycle of upward propagating waves is followed by the strong coupling between polar night jet (e.g. variability of its strength) and the SAM which maximizes during mid-October and extends into December. Most of this coupling is pre-conditioned and can be predicted by wave forcing integrated over previous winter-spring months which implies its “downward” nature.
4) Though the downward propagation of zonal wind anomalies is reproduced by certain CMIP5 global circulation models with interactive chemistry, its seasonality is shifted towards November or December. The latter is likely to be related to a delay in the vortex break-down in the simulations as reported in previous studies.

Thus, the downward progression of the SAM anomalies in Fig.3.1a can be viewed as a result of the interaction between vertically propagating waves and the structure of the polar-night jet and resembles the low-frequency mode described by Kuroda and Kodera (1998). Essentially, the propagating wave activity follows the seasonal cycle of zonal mean zonal wind and refractive index of the jet, at the same time slowly modifying the flow. Under the 60 days memory, the variability in winds follows variability in the planetary waves with a one month lag. Following the seasonal cycle of the zonal wind the maximum refractive index lowers and the turning level shifts poleward. Interannual variability in this process determines variability in the upward wave flux. The appearance of downward descent of zonal wind anomalies corresponds to the descent of the level of maximum absorption of EP flux. Finally, during October-November the wave-driven downward progression of the zonal wind reaches the surface having a strong impact on the tropospheric component of the SAM.

Understanding the processes which regulate the seasonality of the dynamically induced changes in the lower stratosphere is important for seasonal prediction of the spring-time circulation at the surface. Even though most relevant are the August-September upward wave fluxes, spring-time processes might still be affected by the variability during the early and middle winter. In contrast to results presented here, Son at al. (2013) observe no significant correlations between total column ozone and the November–December SAM indices. This suggests that ozone could be only a mediator of these interactions. Since the strong coupling of winds in October follows the seasonal maximum in the upward wave fluxes, it can be speculated that the pre-conditioning of the surface SAM must could be an artifact of the downward progression of the wave activity which has been frequently observed in the observational analyses. The next chapter addresses the physical processes responsible for the observed lag between stratosphere and troposphere by tracking circulation changes

which follow a single upward propagation event, while Chapter 5 discusses processes relevant for the pre-conditioning of the stratospheric polar vortex during autumn and winter.

Chapter 4: The lifecycle of the downward coupling between stratosphere and troposphere during the austral spring

4.1 Introduction

The descent of the polar vortex anomalies down to the surface which occurs over August-December discussed in the previous chapter poses an important question as to the mechanism behind the downward coupling with the troposphere and its pre-conditioning. To answer this question several hypotheses can be proposed which rely on the following observations.

Firstly, the slow downward progression of the zonal wind anomalies along 55-60°S over several months could be an artifact of the narrow seasonal peak in the upward propagating waves. Christiansen (2001) did show for the Northern Hemisphere that downward progression of zonal wind anomalies is driven by the vertical component of the Eliassen-Palm flux and is accompanied by the downward progression of the anomalous wave forcing. Graversen and Christiansen (2003), however, found the vertical coupling in the Southern Hemisphere to be weak, rare, and failed to find any downward progression of the wave pulses. In the Northern Hemisphere, dynamical activity is high throughout the winter season and, hence, downward propagation is distributed throughout the entire season. In contrast, upward propagation events in the Southern Hemisphere are concentrated during September (Fig.3.10b). This “narrow” seasonality implies that the interaction between the waves and mean flow, such as the “downward control”, refraction or reflection of atmospheric waves which potentially can have an impact on the tropospheric circulation, should also to be concentrated during 1 month period directly following the seasonal maximum in the upward wave fluxes. The latter potentially could result into a lag between stratosphere and troposphere.

Secondly, studies by [Salby et al., 2006-2008] indicated that during austral winter and spring forcing by the planetary waves operates coherently with changes not only of the Brewer Dobson circulation, but also circulation in the deep tropics and over the polar cap. An amplification of the heat and momentum transport in the stratosphere is accompanied by cooling over the equator in the upper branch of the Hadley circulation with intensification of the organized convection and by SAM-like warming over the polar cap. They hypothesized that the driving mechanism could involve the cross-tropopause mass exchange driven by the equator-to-pole Brewer-Dobson circulation which can force upwelling motion and adiabatic cooling in the deep tropics and downwelling motion with adiabatic warming over the polar cap. Amplified by the final warming the interannual variability in the seasonal cycle of the Brewer Dobson circulation could give rise to a lag.

Thirdly, the impact of the radiative changes associated with the interannual variability in the ozone hole which develops during the same season can also play a role.

If the mechanism were dynamical, it would be possible to see it by constructing a lifecycle of a single upward propagating disturbance. To investigate the mean structure of the flow and circulation anomalies which accompany propagation of the midlatitudes waves into the stratosphere, a composite analysis is presented in this section.

4.2 Method

To construct the lifecycle I use daily NCEP/NCAR reanalysis dataset encompassing the austral late winter - early summer months (August-December) from 1979 through 2009. Prior to constructing the lifecycle, the daily time series were low-pass-filtered to the frequencies lower than $(7\ \text{day})^{-1}$. A springtime climatology was produced on the basis of the 31-yr record of daily NCEP/NCAR reanalysis fields.

Since evolution of the stratospheric flow can be represented as an integrated response to the sporadic bursts of upward wave activity as approximated by horizontally averaged vertical component of Eliassen Palm flux in the lower stratosphere (F_z) at 50mb, 30-90°S, is chosen as the reference variable for the compositing definition. Based on the F_z time series, the 70 strongest (greater than *mean + 1 std*) upward propagation events were selected (such that a distance between two subsequent events is not less than a week and background flow equally represent negative and positive phases of the SAM defined as zero). Mean strength of F_z was then computed to form a reference time series. An example evolution of F_z during 1980 is shown in Fig. 4.1. The two strongest F_z peaks correspond to the two upward propagation event identified this year.

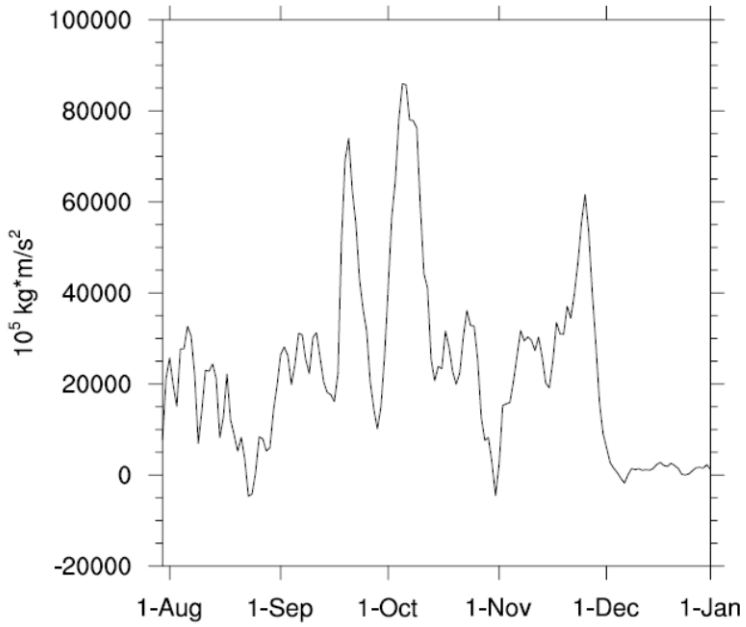

Figure 4.1. Vertical component of the Eliassen Palm Flux averaged between 30°S and 90°S at 50mb during 1980.

To characterize the associated circulation and thermodynamic features, the reference F_z time series is then regressed on the composite time series of the low-pass-filtered fields of EP flux and its divergence, zonal wind and its acceleration, refractive index, residual mass stream function and sea level pressure using the dates previously selected. The system's life cycle is illustrated by anomalous fields for days within [-15,+17] range where day 0 represents maximum wave flux at 50 mb level.

To access significance of results I performed Student's test using two-tailed 95% significance level and plotted those anomalies which exceed the reference values (for EP flux vectors - those for which the value of either horizontal or vertical component exceeds the reference value). To achieve dynamical consistency, firstly, the lifecycle anomalies are compared to those evident in the regression analysis based on seasonal mean fields and, secondly, subsamples of upward propagation events are formed to test whether a particular background flow indeed favors particular circulation features. The lifecycle results will be compared to the anomalies evident in the seasonal mean fields in the Chapter 5.

4.3 Results

4.3.1 Lifecycle: interaction between upward propagating wave activity and the background flow

In this section, anomalous dynamical structure which precedes amplification of upward propagating wave activity in the stratosphere is discussed.

Figure 4.2 presents the anomalous EP Flux cross-sections at days -7, -3, 0 prior to the lower-stratospheric wave maximum. At day -7, the anomalous EP vectors and dipole pattern in the EP flux divergence suggest that an amplification of upward wave fluxes above the tropopause lags poleward shift of a source region of wave activity at the boundary such that it is located between 50-60°S, around the Antarctic coastline. This is consistent with the climatological analysis by Randel (1985) who identified subtropical and midlatitude sources of wave activity and concluded that waves from the midlatitude source are more likely to reach the stratosphere. The convergence of EP Flux (hence, absorption of wave activity) takes place in the midlatitude troposphere and stratosphere above 700mb at day -7. Following poleward refraction of wave activity at days -3-0, it is replaced by a divergent anomaly at 60°S and poleward. This region of the absolute positive divergences at 10 mb is strong enough to be prominent even in the September-November seasonal mean.

Consistent with the modification of the zonal flow through the EP flux divergence is the spatial pattern of zonal wind changes which occurred from day –7 to day 0. Figure 4.3 shows zonal mean zonal wind tendency defined as the difference in the zonal wind which occurred over the week centered at the respective day of lifecycle. In the troposphere, a westerly acceleration has taken place poleward of 45°S, that is at the latitude of a source of the wave activity with the positive EP Flux divergences and there has been an easterly acceleration in the troposphere to the north of 45°S. In the stratosphere, a strengthening of the polar vortex poleward of 70°S and its deceleration to the north of 70°S can be observed following refraction of planetary waves from the stratospheric vortex. Hence, the zonal wind anomalies forced by the upward propagating waves form a dipole pattern of zonal wind changes extending from the surface up into the stratosphere. By day 0, following propagation of wave activity further up and equatorward, region of the positive zonal wind changes in the lower stratosphere shifts towards 60°S and merges with the tropospheric anomaly. Hence, the total impact of the upward propagating wave on the zonal mean zonal wind along 60°S is to accelerate it.

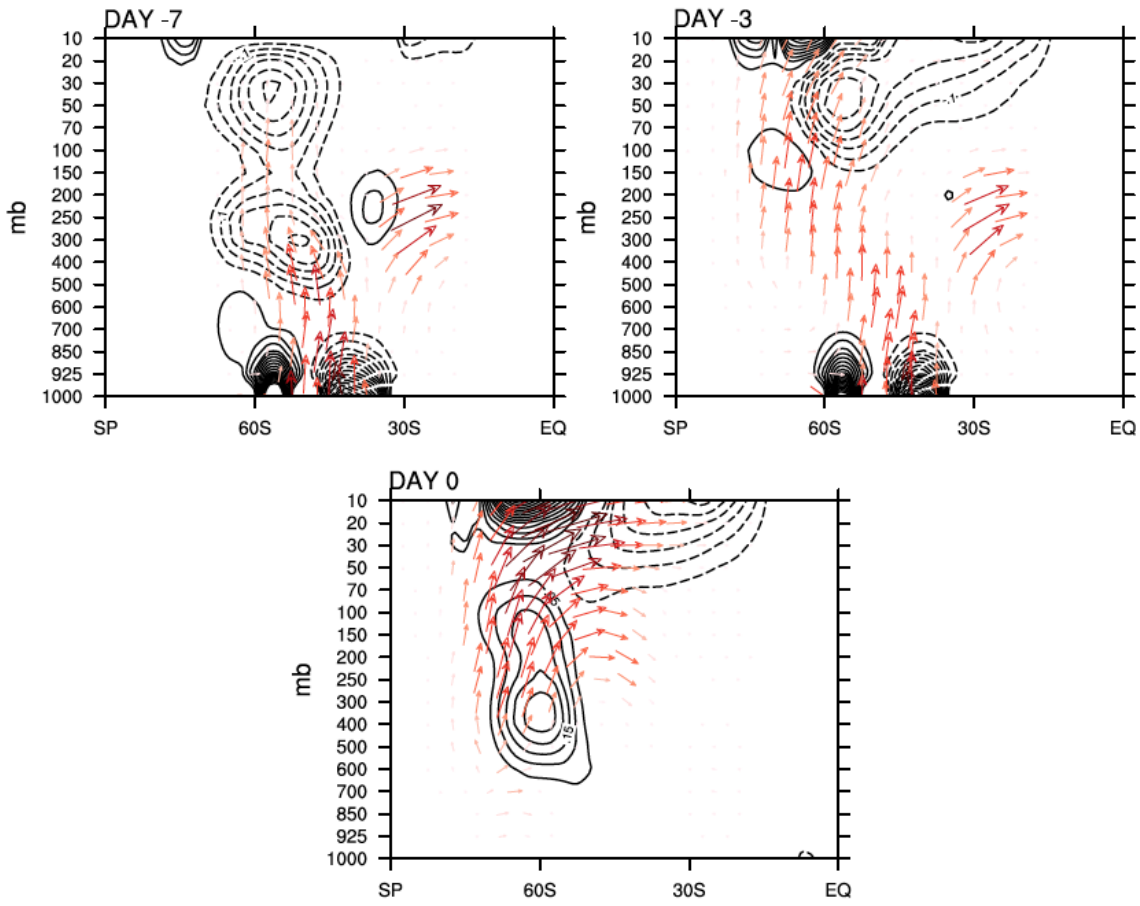

Figure 4.2. Anomalous EP Flux (vectors) and its divergence (contour, solid – positive values, dashed – negative values) which lead 1 std increase in the vertical component of Eliassen Palm Flux at 50mb level, 30-90°S, by 7, 3 and 0 days.

An interesting feature of the upward propagation is the direction of propagation above 400mb. As the atmospheric waves propagate upward, the total wave flux bifurcates into two directions above 400 mb – towards 60°S and up into the stratosphere and towards the subtropics. This appears to be a controlled by the refractive properties of the tropospheric flow. Figure 4.4 shows the climatology of the refractive index for zonal wave number 1 with zero phase speed (computed according to equations (2.12)-(2.13)). To account for non-zero phase speeds, the numerator of refractive index, the meridional gradient of potential vorticity (dQ/dy), is also plotted. The latter is not dependent on the phase speed and zonal wave number and to a large extent shapes the main features in the contours of refractive index for all waves. As it appears

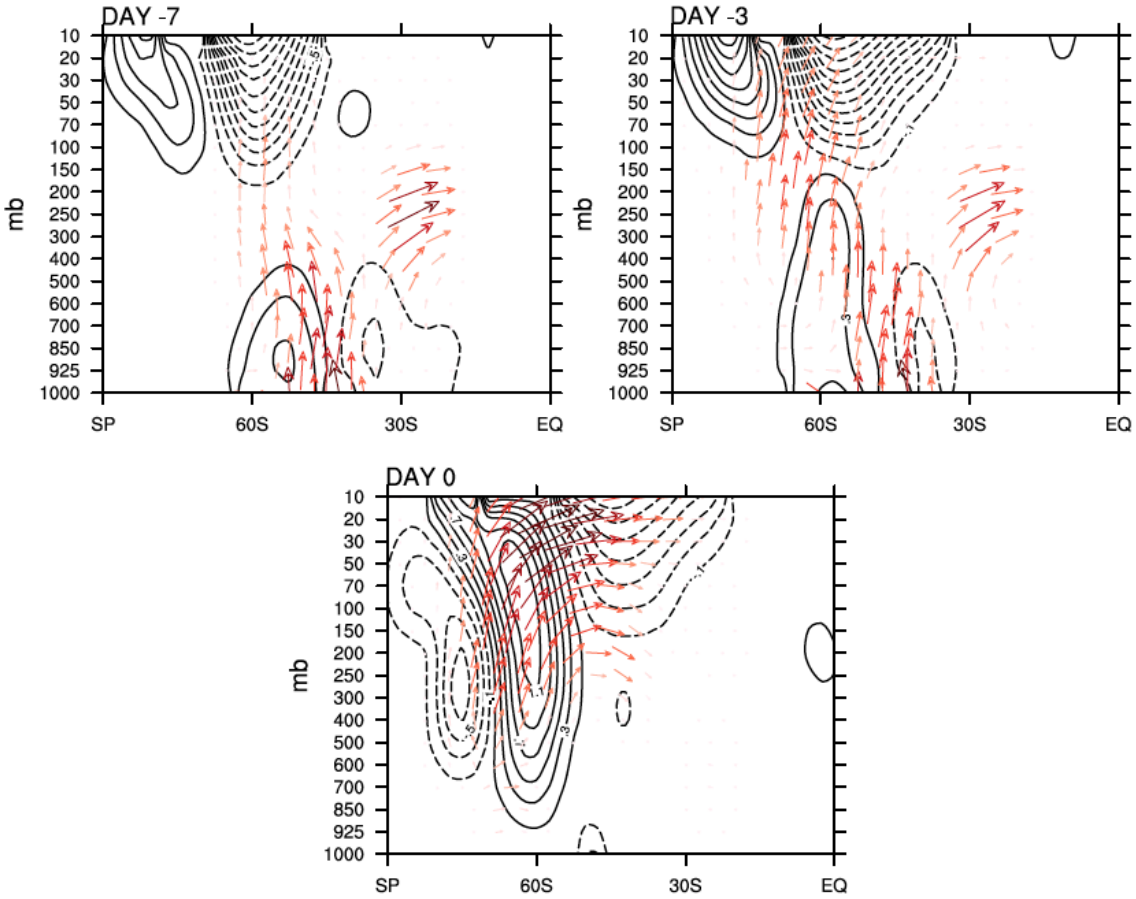

Figure 4.3. Anomalous EP Flux (vectors) and zonal mean zonal wind tendency (contour, c.i. 0.2 ms^{-1}, solid – acceleration, dashed – deceleration) which lead 1 std increase in the vertical component of Eliassen Palm Flux at 50mb level, 30-90°S, by 7, 3 and 0 days. Zonal wind tendency is computed a change of zonal wind over a week centered on the respective day.

from Fig. 4.4, the split EP flux can be largely seen as a result of the wave attraction towards larger dQ/dy (and accordingly refractive index) values. Above 500mb, dQ/dy forms two maxima – in the subtropics and in the midlatitudes. The part of the anomaly in the wave activity which is diverted towards the midlatitude one appears to be able to reach the stratosphere.

To understand how the mean state and different phases of the SAM affect upward wave propagation, anomalous EP Flux cross-sections are shown for two subsamples of the data, when the background state was typical of the positive and negative phases of the SAM. Figure 4.5 compares the propagation of wave activity based on the subsamples of data grouped according to the positive or negative phases of the SAM during days -15-0. As expected, on the background of the positive SAM phase the upward wave flux is re-directed both poleward and equatorward towards the subtropical jet, while on the background of the negative SAM phase most of the wave activity goes in the stratosphere.

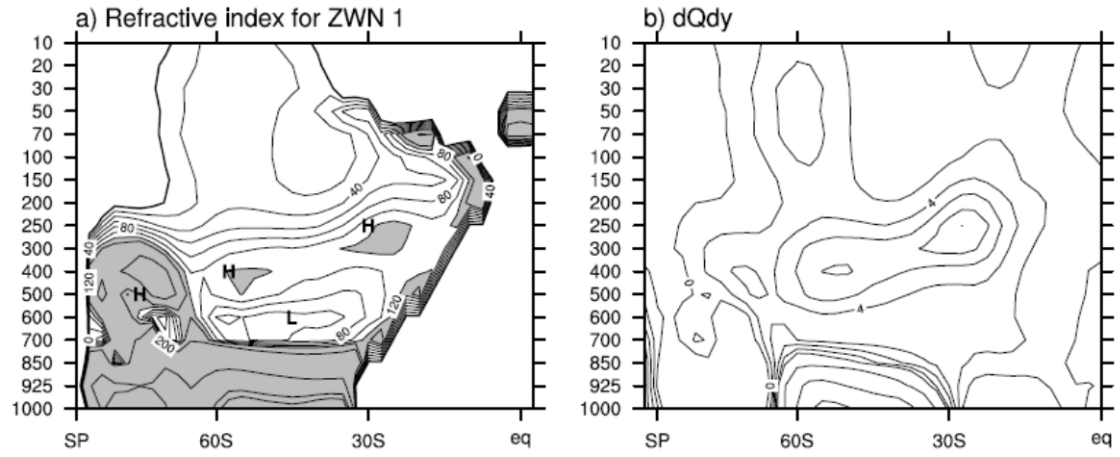

Figure 4.4. Climatology of the refractive index for stationary wave with zonal number 1 (a) and meridional gradient of potential vorticity dQdy (b). Refractive index nondimesionalized by the radius of the earth squared. Values greater than 120 are shaded.

The composites of refractive index shown at the bottom row of Fig. 4.5 suggests a weakening of the gradient in refractive index between two maxima during negative SAM, which precedes the upward propagation allowing for a larger fraction of wave activity to be deflected poleward and into the stratosphere. During positive SAM the refractive index of the subtropical jet increases and the midlatitude maximum becomes less pronounced leading to the split wave flux. The sensitivity of the SAM to the properties of the subtropical jet during these months will be further addressed in Chapter 5.

Overall, the circulation changes evident during the onset of lifecycle are comparable with results from classical baroclinic lifecycle numerical experiments (compare Fig. 5.26-27 in [James, 1995] which shows the difference between the final and initial zonal flow during baroclinic lifecycle). However, they highlight that the basic state properties of the realistic jet affect the propagation of upper tropospheric wave fluxes in the middle and upper troposphere in terms of sensitivity to the gradient of refractive index between subtropics and midlatitudes.

4.3.2 Lifecycle: wave-induced mean meridional circulation

Figures 4.6 and 4.7 shows anomalous residual mass stream function and EP flux cross-sections at days -7, -3, 0, +3 and +6. Following the absorption of wave activity in the stratosphere as indicated by regions with $\nabla \cdot \boldsymbol{F} < 0$, an intensification of the equator to pole Brewer-Dobson

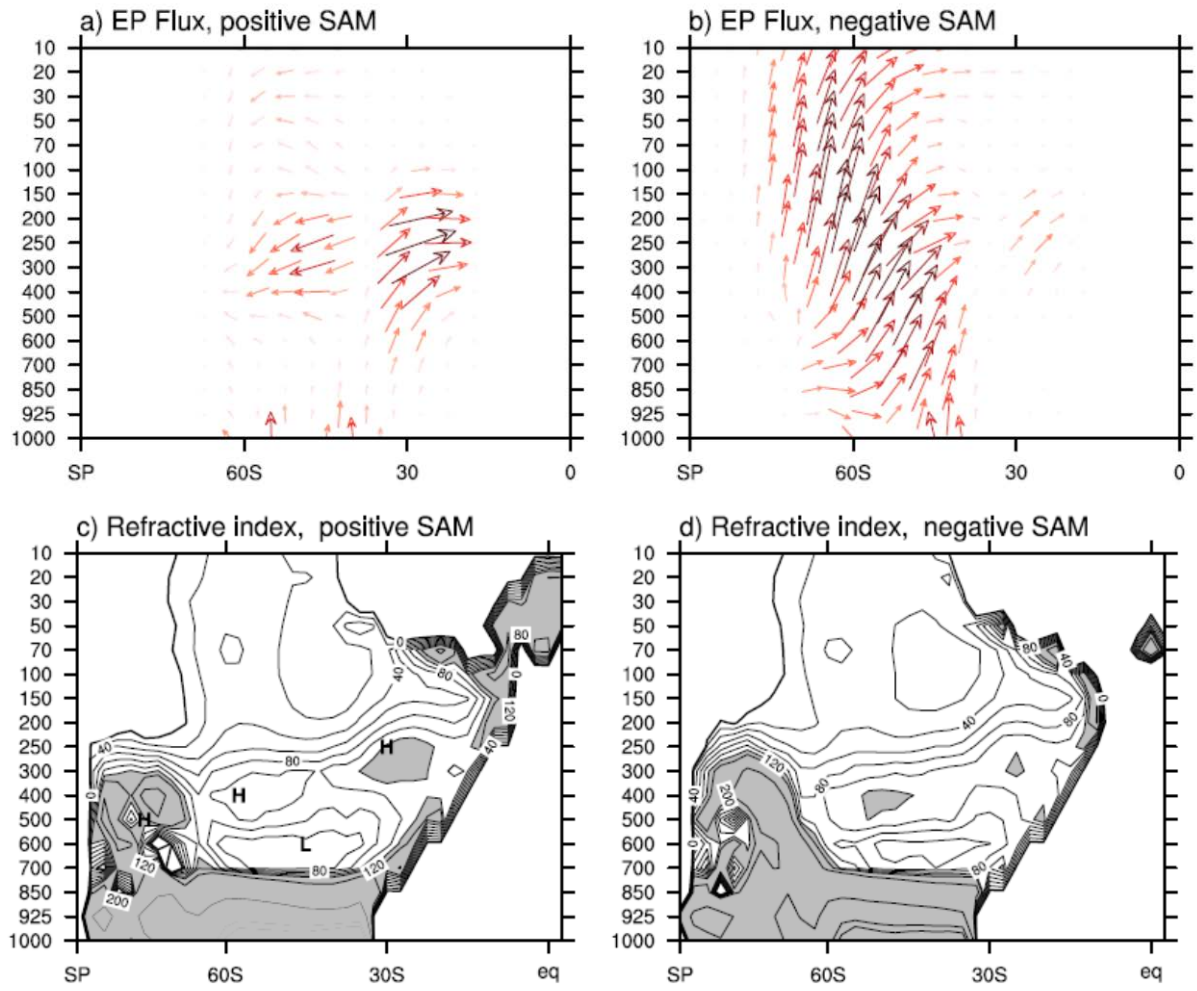

Figure 4.5. Anomalous EP Flux which leads 1 std increase in the vertical component of the Eliassen Palm Flux at 50mb level, 30-90°S, by 3 days (top) and mean refractive index for stationary wave with zonal number 1 averaged from day -15 to 0 (bottom). Left: background positive SAM; Right: background negative SAM. Refractive index nondimesionalized by the radius of the earth squared. Values greater than 120 are shaded.

circulation is observed at days -3-0 (negative anomalies in the residual mass stream function) which acts to oppose the wave induced zonal wind changes. The negative anomalies in the stratosphere which follow absorption of wave activity as indicated by regions with $\nabla \cdot F < 0$ indicate an intensification of the equator to pole Brewer-Dobson circulation.

Several days later, at day +3, a strengthening of the residual circulation is observed in the tropical troposphere which suggests an intensification of the Hadley circulation. The latter is reminiscent of the links between Brewer-Dobson and Hadley circulation observed in the seasonal mean fields and could be possibly explained through the stratosphere acting like a pump modulating mass exchange between tropics and stratosphere as suggested by Salby at al. (2006-2008). However, the EP flux cross-sections indicate equatorward pointing EP vectors

and anomalous convergence of EP flux close to equator in the upper tropical troposphere, which is contemporaneous with mean meridional circulation anomalies.

In order to see what factors control the intensification of the tropical circulation, residual mass stream function anomalies are computed during events with negative and positive background SAM during days -10-0. Comparison shows that the significant anomalies in the tropics occur only when the background state is typical of the negative SAM and wave activity is more likely to reach the deep tropics. The amount of wave activity which can reach the deep tropics is controlled by the basic state and location of the zero wind line. During spring the westerly equatorial duct begins to develop in the upper troposphere over the Pacific Ocean, which makes it easier for midlatitude waves to reach the deep tropics [Webster and Holton, 1982]. Figure 4.8 shows a map of anomalous sea level pressure at day 6 when a strengthened residual circulation is observed. The anomalously low sea level pressure is observed over the Pacific, which is supportive of the idea that the circulation changes in the tropics are essentially wave-driven and enabled through the westerly Pacific duct.

The results presented here are consistent with those by Lorenz and Thompson (2004) who found that tropical anomalies lag indices of the northern and southern annular modes by 2 weeks. However, Thompson and Lorenz (2004) suggested that relationship between the SAM and tropics is weak and limited to the June-August season, while the results presented here together with results in Salby (2008) suggest that the relationship between SAM and tropics is the strongest during the spring since the propagation of wave fluxes into the deep tropics occurs simultaneously with upward propagation into the stratosphere.

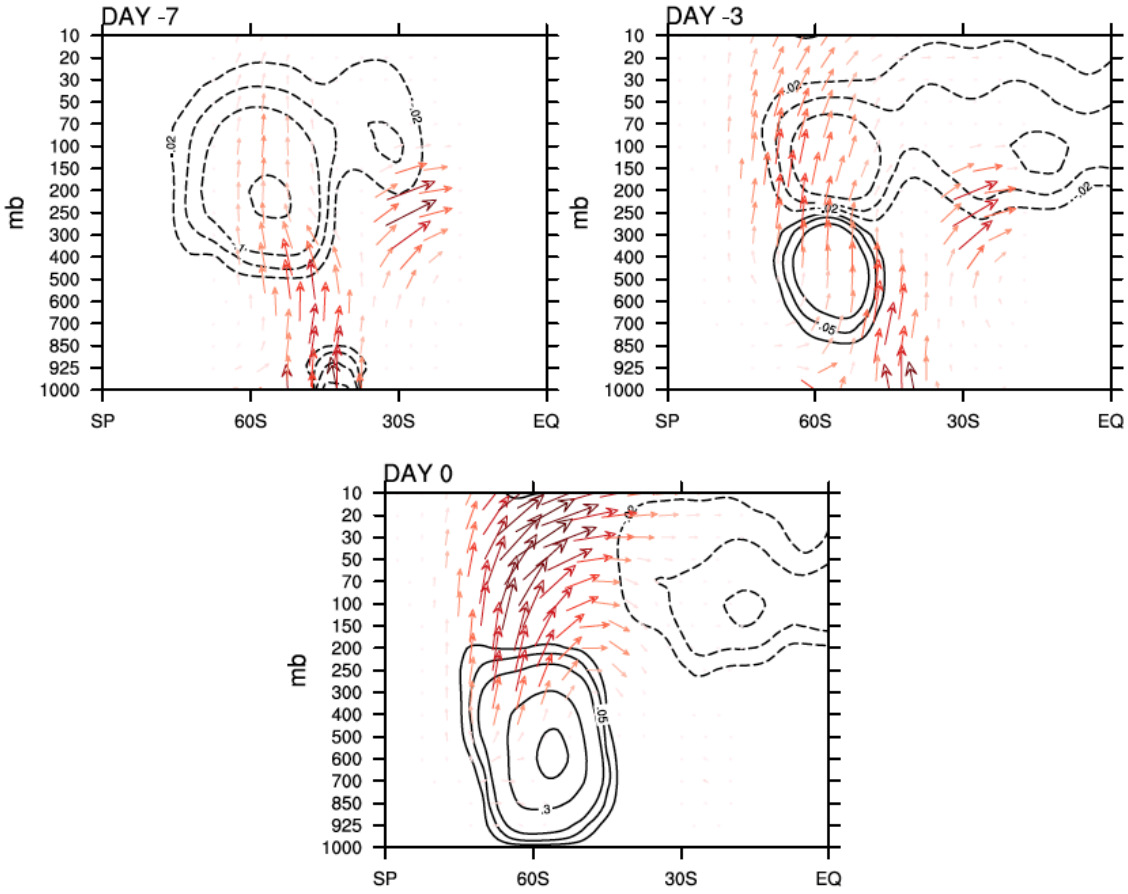

Figure 4.6. Anomalous EP Flux (vectors) and residual mass stream function (contour, unit $1.^{-10}$ kg/s ^{1}*, solid – negative, dashed – positive anomalies) which lead 1 std increase in the vertical component of the Eliassen Palm Flux at 50mb level, 30-90°S, by 7, 3 and 0 days.*

The above also has a methodological importance since it offers an explanation as to why there is no straightforward relationship between the conventional index of Hadley circulation strength such as maximum of mass stream function and the SAM in the seasonal mean [Caballero, 2007]. The pattern of the SAM-related tropical mass stream function changes represents a superposition of 2 different processes. During negative phase of the SAM the atmospheric wave fluxes reach the deep tropics and drive the intensification of the mean meridional circulation in the southern Hadley cell (as would also be evident in the maximum of mass stream function). During positive SAM phase the waves break in the vicinity of subtropics driving meridional circulation closer to its subtropical boundary. The superposition of the both anomalies evident in the seasonal mean would then appear as a stronger and contracted Hadley circulation during the negative SAM phase and weaker and expanded Hadley circulation during the positive SAM phase. When seasonally averaged, the maximum of the mass stream function would, however, show no link to the SAM or extent of the tropics.

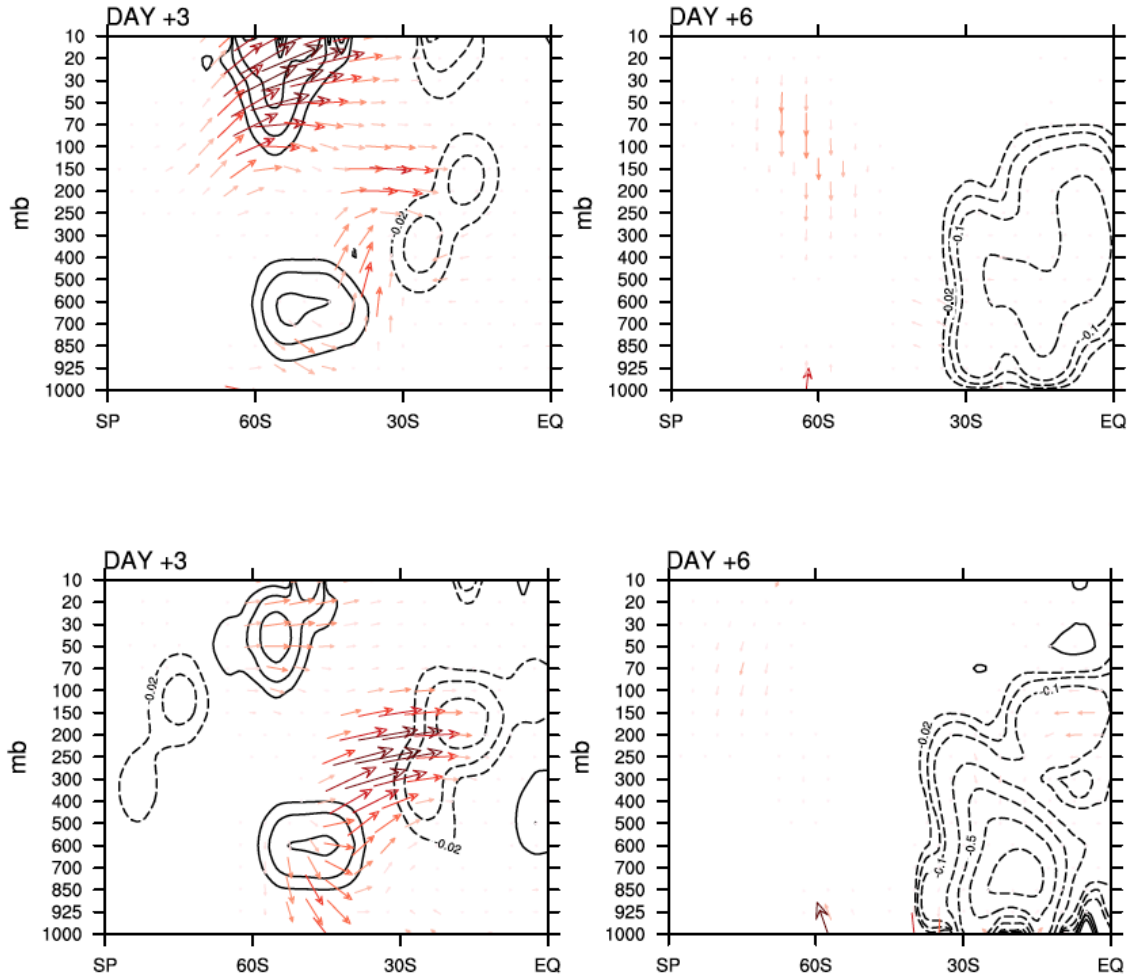

Figure 4.7. Anomalous EP Flux (vectors) and residual mass stream function (contour, unit $1.^{-10}$ kg/s ^{1}*, solid – negative, dashed – positive anomalies) which lag 1 std increase in the vertical component of the Eliassen Palm Flux at 50mb level, 30-90°S, by 3 and 6 days: (Top row) all events; (Bottom row) events with background negative SAM.*

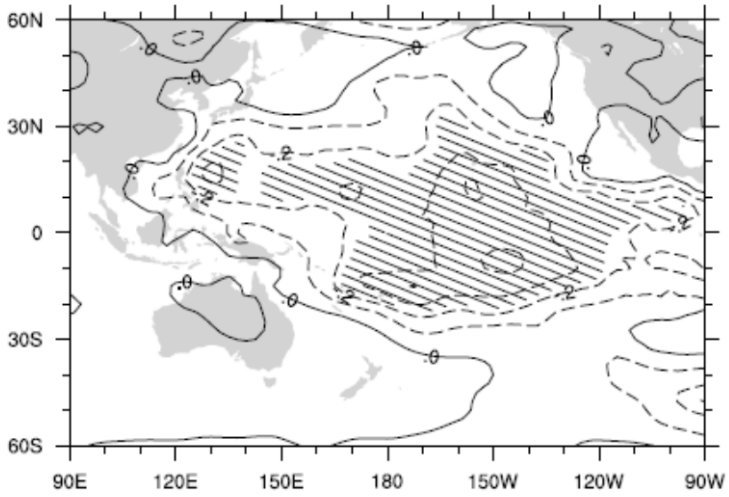

Figure 4.8. Anomalous sea level pressure field (contour, shown as correlation, levels significant at 95% are shaded) which lags 1 std increase in the vertical component of Eliassen Palm Flux at 50mb level, 30-90°S, by 6 days

4.3.3 Lifecycle: downward progression of wave activity and descent of the polar vortex anomalies

At the last stage of the lifecycle, a SAM-like signature in zonal wind does appear which overall resembles the descent of stratospheric polar vortex anomalies following perturbations of stratospheric vortex as described by Graversen and Chritiansen (2003), Thompson at al. (2005). Figure 4.9 shows anomalous EP flux cross-sections and zonal wind at day +10. Clearly, zonal wind changes along 50-55°S, which follow perturbations of stratospheric vortex, are preceded by the poleward refraction of wave activity as indicated by EP vectors in the upper troposphere at 45°S. The latter is in line with results in Limpasuvan and Hartmann (2004) who showed that the tropospheric response to the stratospheric perturbations in the Northern Hemisphere involves changes of wave propagation in meridional plane.

The composite analysis, however, fails to show any significant changes in the mean state (e.g. meridional gradient of potential vorticity or refractive index) at this stage. But the timing of the zonal wind anomaly at day +13 roughly coincides with the decaying stage of wave activity burst in the stratosphere. As shown by Randel (1985), the typical upward propagation event in the stratosphere tends to end with a downward wave flux emanating from the stratosphere. Though the exact nature of such events is not understood, their occurrence during the decaying stage of wave activity bursts suggests either reflection of wave activity from the polar vortex or a source of wave activity in the stratosphere. The exact events are difficult to isolate since the observed daily fields represent a superposition of

upward and downward wave fluxes occurring at different times and latitudes throughout the stratosphere. But, the strongest or, at least, detectable events can be diagnosed in the Fz,50mb reference time series used above. To understand whether anomalous tropospheric structure during the last phase of the lifecycle is indeed related to the downward stratospheric wave fluxes, we then form 2 subsamples of upward propagation events. The first one includes 41 events, which were followed by a negative Fz averaged at 50mb, 30-90°S, within 15 days after Fz maximum; the second includes 30 events when the downward wave flux was undetectable.

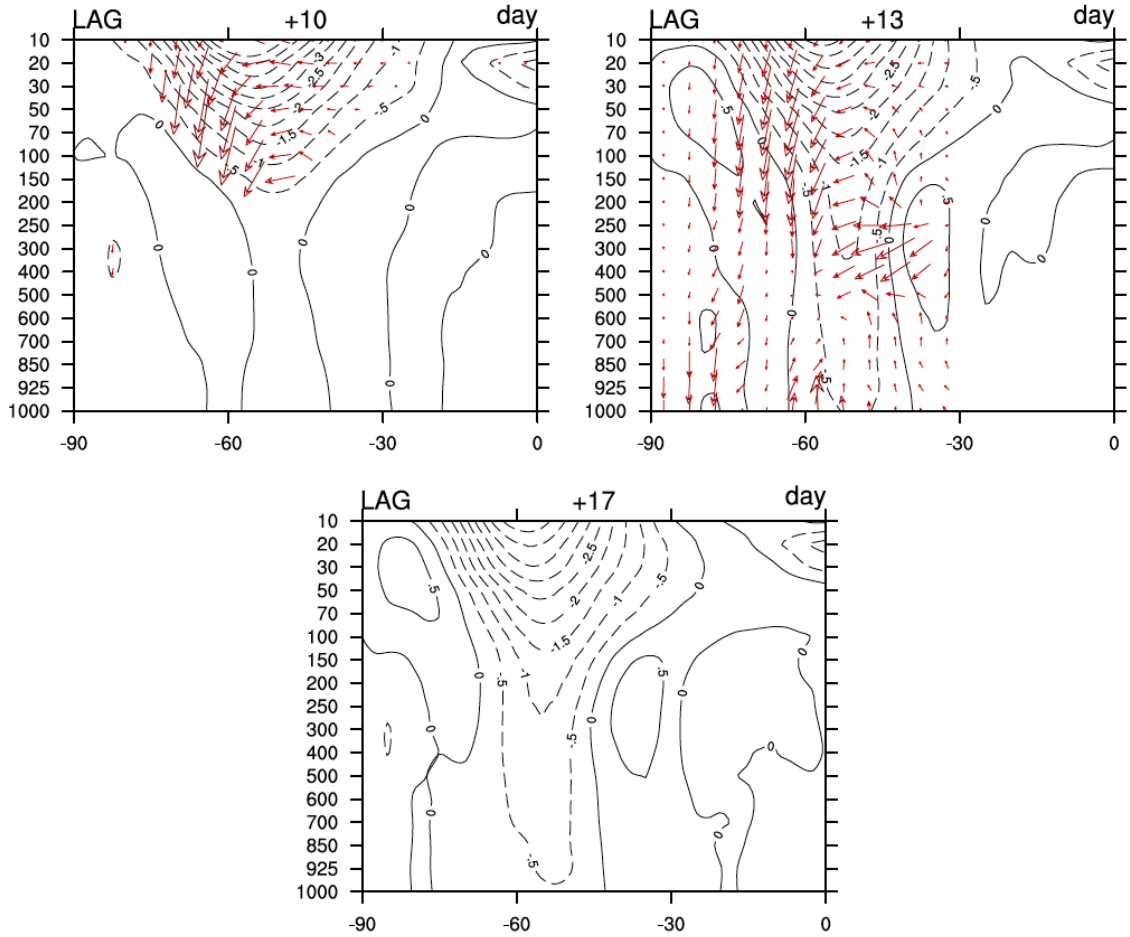

Figure 4.9. Anomalous EP Flux (vectors) and zonal mean zonal wind (contour, unit 0.5 m/s, *solid – positive, dashed – negative anomalies) which lag 1 std increase in the vertical component of the Eliassen Palm Flux at 50mb level, 30-90°S, by 10, 13 and 17 days. Based on all events.*

Comparison of the composites shows that occurrence of a significant zonal wind anomaly in the troposphere is limited to the wave activity bursts followed by the downward wave fluxes. Figure 4.10 shows anomalous EP flux and zonal wind based on the first subsample during days 10,13 and 17. By construction, the downward pointing vectors in the stratosphere indicate both a decay of wave bursts and wave activity emanating from the stratosphere. The weaker polar vortex anomalies at this stage indicate its deceleration by

upward propagating wave activity. As the vectors begin to point down, the polar vortex anomalies extend downward closer to the tropopause as well, however, they do not reach the troposphere. At days 13 the latter are followed

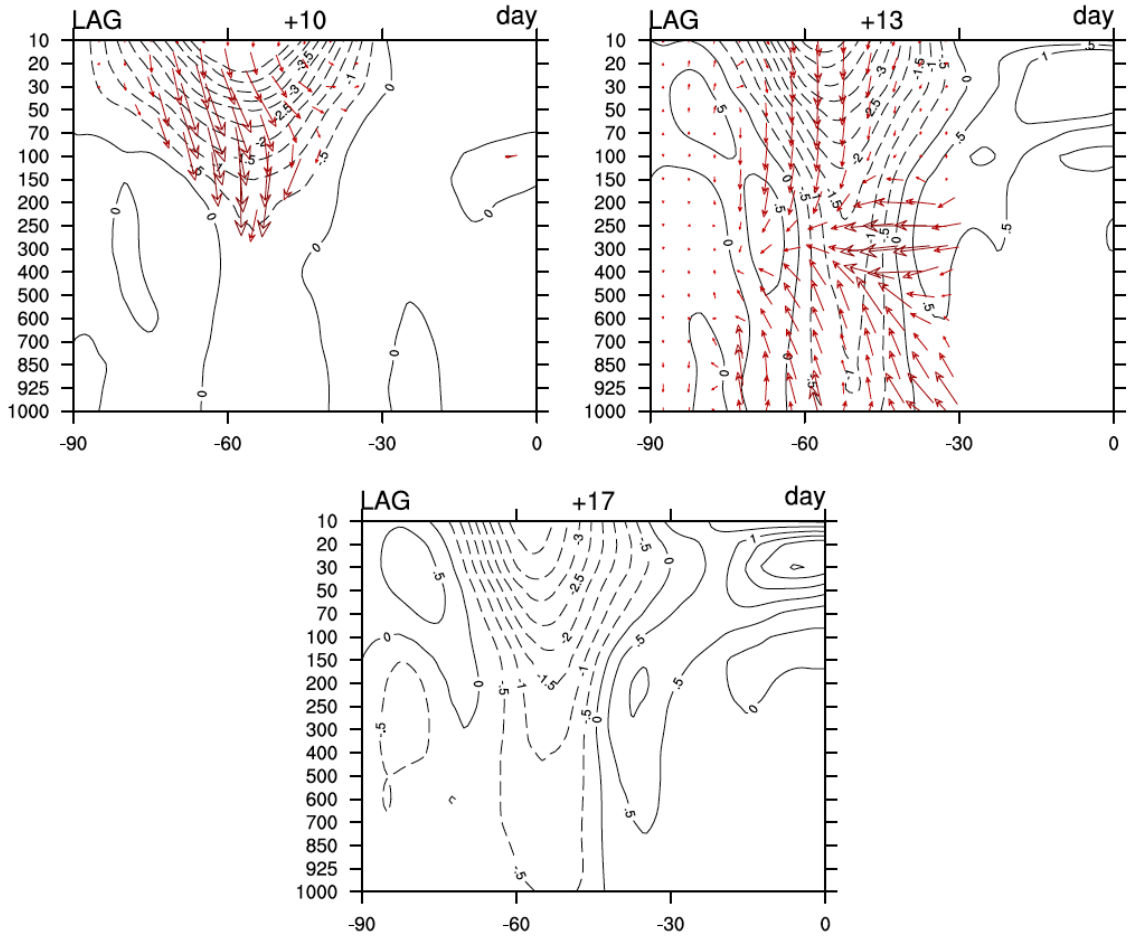

Figure 4.10. Anomalous EP Flux (vectors) and zonal mean zonal wind (contour, unit 0.5 m/s, *solid –positive, dashed – negative anomalies) which lag 1 std increase in the vertical component of the Eliassen Palm Flux at 50mb level, 30-90°S, by 10, 13 and 17 days. Based on events when the downward wave fluxes were observed.*

by the poleward refraction of wave activity and consequent zonal wind anomalies in the troposphere, which migrate poleward evolving into a SAM-like dipole structure over a course of several days. The timing of tropospheric anomalies and the difference between the 2 subsamples is then illustrated in Figure 4.11 which shows the time evolution of correlation coefficient between reference *Fz* time series and *Fy* at {400mb, 45°S} and 700 mb zonal wind at 55 S and the SAM. Overall, the above suggests that the appearance of the SAM-like zonal wind changes in the stratosphere followed by perturbations of the stratospheric vortex could be related to the interference of downward propagating and tropospheric waves.

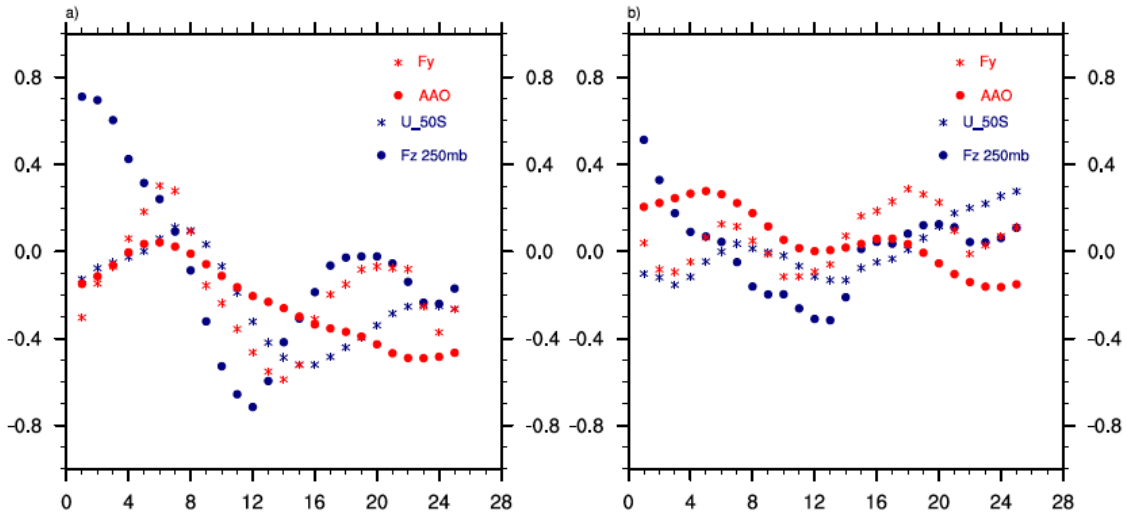

Figure 4.11. Correlation between Fz, 50mb at day 0 and Fz at 250mb, index of the Southern Annular Mode, zonal mean zonal wind at 55°S , horizontal component of EP Flux at 400mb, 40°S during days 0-30. (a) Events with downward wave fluxes; (b) Events without downward wave fluxes.

The result is in line with the theoretical study by Lindzen at al (1981) who described the potentially possible origin interference-induced vacillations in the mean flow. The essence of the vacillation mechanism due to interference can be understood from the equations for the time rate of change of the energy associated with the eddy and the zonally averaged basic states (see equations 1 and 2 in Lindzen at al (1981) which basically demonstrate that the sum of the both eddy and zonally averaged fields remains constant, i.e. eddies grow at the expense of the mean flow and vice versa. Namely, two waves with the same zonal wavenumbers and different phase speeds will interfere with each other in a constructive or destructive way with a time period dependent on the wave period. Then a periodic interference must lead to a vacillation in the mean flow as well. Their analysis has further suggested that the interference of long stationary waves with travelling Rossby waves of the same wavenumber can account for the observed periods and amplitudes of the annular modes.

4.4 Conclusions

The lifecycle of upward propagation event has been presented. The lifecycle spans approximately 3 weeks and tracks circulation anomalies which accompany penetration of wave activity into the stratosphere, into the deep tropics and downward reflection of wave

activity. Changes in the mean state which affect the lifecycle are described by constructing lifecycles of upward propagation which occur on the background of different mean states.

The anomalous dynamical structures revealed in the lifecycle of wave propagation are consistent with those expected in theory, however, they highlight the processes relevant under realistic present-day conditions, such as the role of subtropical jet in modulating propagation of wave activity and a greater likelihood for upward propagating waves to reach deep tropics and force tropical circulation on the background of the negative SAM phase.

The main results can be summarized as follows:

1. Upward propagation in the stratosphere is affected by the gradient of refractive index and the meridional gradient of potential vorticity between the subtropical and the eddy-driven jets;
2. An observed feature of the lifecycle is that on the background of the negative SAM, upward propagating waves are more likely to reach both the stratosphere and the deep tropics simultaneously, driving stronger intensification of the Brewer Dobson circulation and a stronger upwelling motion close to the equator than under the positive SAM. The anomalies in the tropics are observed in the Pacific region where the westerly equatorial duct enables propagation of the wave activity;
3. Downward propagation of the zonal wind anomalies is observed at the decaying stage of the upward propagating event. The timing of this event is coincident with the downward progression of wave activity along 50-55°S and its interference with the tropospheric waves. The zonal wind changes along 50-55°S evolve then into the SAM-like dipole.

Since the seasonal maximum of upward propagation events is observed during late September and each upward propagation event spans 2-3 weeks, the decaying stage of each lifecycle, when the downward propagation occurs, will be shifted into October. Additionally, the downward progression of zonal wind anomalies maximizes along 50-55°S and evolves into the SAM over a week. Thus, the apparent lag observed between upward wave fluxes integrated up to September and the SAM in October-December is likely to be an artifact of the "narrow" seasonality of upward propagation events and reflects the downward propagation of zonal wind anomalies at their decaying stage.

The results presented here highlight that wave reflection can have significant impact on the tropospheric weather systems. The latter is consistent with the results obtained by

Shaw and Perlwitz (2013) who constructed the lifecycle of wave coupling in the Northern Hemisphere and found significant changes in the troposphere following downward fluxes from the stratosphere. Due to the strong dynamical activity, the Northern Hemisphere daily fields represent a superposition of upward and downward propagating waves and, hence, it is more difficult to isolate a significant signal on the background of overall noise. The Southern Hemisphere example with its narrow seasonal peak demonstrates, however, that impact of wave reflection can be indeed strong as it is manifest in a strong lagged correlation between upward wave flux and surface SAM during September-October.

Potential influence of the wave reflection on the troposphere was first hypothesized by Bates (1977), Schmitz and Grieger (1978), however, in the absence of reliable stratospheric data and long enough datasets it was then impossible to isolate a significant downward signal in observations. Further investigation will be necessary to understand conditions under which downward wave fluxes can form and can affect the tropospheric flow. Downward wave fluxes are occasionally observed throughout entire winter-spring season. However, it remains a question whether they can affect the surface only under certain configurations of the tropospheric flow, such as the ones prevalent during late spring. So, there are notable difference between the Northern and Southern Hemispheres. Formation of reflecting surfaces depends on the structure of the stratospheric flow itself. Thus, Harnik and Lindzen (2001) found that the zonal mean zonal wind at 5 hPa can be a good indicator of the reflective and non-reflective years with a stronger polar vortex resulting in downward reflection of wave activity and re-inforcing of tropospheric westrelies. The results presented here suggest, however, that the strength of the downward wave flux (being proportional to the upward flux) varies coherently with the zonal wind anomalies in the opposite way leading to the deceleration of zonal wind along 50°S followed by a negative SAM anomaly. The necessity of an upward precursor to wave refection was also highlighted in the study by Harnik (2009). One of the possibilities to understand the discrepancy between hemispheres involves formation of a secondary turning level in the vicinity of the tropical easterlies prior to encountering their critical line. Hartmann (1988) found that the strong polar-night jet in the Southern Hemisphere does possess two zones of instability with the negative meridional gradients of the potential vorticity values along 60°S and 40°S. Apart from being a potential source of wave activity these negative dQ/dy values would lead to the refractive index turning negative and refracting wave activity. In fact the direction of anomalous EP vectors in Fig. 4.2 and 4.9 suggests that following deflection of wave activity towards equator it is refracted back, first poleward and then down to the surface.

Overall the analysis suggests that a realistic representation of the stratospheric flow and its reflecting properties presents an opportunity to improve predictions of the SAM on lead times beyond 1 week. The occurrence of the downward coupling in the end of an upward propagation event also explains the lagged relationship observed between the seasonal peak of the planetary waves and the SAM shown in Figure 3.12. The typical period of the burst of the wave activity spans 3-4 weeks and the descent of the stratospheric vortex anomalies to the surface occurs in the end of such event following the downward propagation of the wave activity. Thus, the impact of the upward propagating events which occur during mid-September on the SAM will be evident only during October. Analogously, the impact of upward propagation events which occur during early October will maximize only towards the end of the month or later. Internal eddy-zonal flow feedbacks can then maintain the persistent anomalies in the SAM extending them into the summer.

Chapter 5: Pre-conditioning of the spring-time stratosphere during winter

5.1 Introduction

Seasonal variability of the ozone hole and hypothetically of the spring-time circulation at the surface largely depends on anomalous winter-time dynamical processes. The latter set up the polar vortex making it more or less susceptible to planetary wave forcing during springtime. Even though most relevant for the springtime stratosphere is the planetary wave forcing during August-September [Salby at al., 2012; Chapter 1], the spring-time dynamics might be still pre-conditioned during early and middle winter. An example of such effect is the evolution of the stratospheric vortex during 2002 [Newman and Nash, 2004] when the first ever sudden stratospheric warming over the Antarctica and a split ozone hole were observed. A sequence of 11 large-amplitude wave events spanned 2002 winter over the course of May-October. After each of them the stratosphere warmed and the polar vortex weakened. The anomalously weak stratospheric mean flow made it then even easier for the waves to propagate into the stratosphere. The excessive tropospheric forcing together with the more conductive stratospheric flow culminated in the early polar vortex break-down, the split ozone hole [Newman and Nash, 2004] and anomalously low Southern Annular Mode index in the troposphere [Thompson et al., 2004].

The susceptibility of the springtime vortex to forcing from below largely depends on winter dynamics and, in particular, the phase of the Southern Annular Mode and the mechanisms which affect it during these months. During the positive phase of the SAM the waves are refracted equatorward which results in poleward momentum fluxes and reinforcement of the eddy-driven jet and at the same time leaves the stratospheric vortex unperturbed. The opposite occurs during the negative phase of the SAM. As suggested by the recent observational studies, SAM-related climate variability during winter can be affected by the anomalous processes in the subtropics and in particular by the strong subtropical jet which bounds the cross-equatorial cell of the Hadley circulation. So, Ding at al. (2012) showed that during austral winter the Southern Annular Mode depends on the tropical sea surface temperatures in the Pacific. They detected an instability region associated with subtropical jet over the Australia and hypothesized that the wave train emanating from it might play a role in shaping the SAM. Additionally, Newman and Nash (2004) suggested that anomalous processes in the subtropics might have played a role in the 2002 winter. They showed that anomalous southward wave-1 propagation from the subtropics resulted into reinforcement of wave 1 in the lower stratosphere. However, they failed to find any straightforward relationship in the interannual variability between tropics and midlatitudes. Salby at al. (2004-

2008) report coherent changes between the Brewer-Dobson circulation, the SAM and the deep tropics during austral winter and spring. The lifecycle of the upward propagation events shown in Chapter 4 suggested a two-fold link between stratosphere, SAM and tropics. Firstly, the refractive properties of the subtropical jet might modulate the amount of wave activity being able to penetrate into the stratosphere. Secondly, stronger upward propagation events under the negative phase of the SAM favor propagation of wave activity towards the deep tropics.

The focus of this chapter will be on the interconnections between the Brewer-Dobson circulation, the tropics and the SAM observed during the winter and spring. The latter will be addressed from the stratospheric perspective in an attempt to understand the climate factors which favor the propagation state conductive to upward pulses of wave activity during springtime.

The analysis begins with the discussion of factors relevant for setting up evolution of the stratospheric polar vortex during winter (Section 5.2.1) followed by discussion of a seasonal regime changes in the Southern Hemisphere climate system (Section 5.2.2) and the analysis the extratropical connection to the tropical circulation (Section 5.2.3). The chapter concludes with a discussion and summary.

5.2 Results

5.2.1 Dependence of the springtime wave forcing on the preceding winter

The dynamical processes and state of the polar vortex during late autumn and early winter arguably set up the evolution of the polar night jet in the following season [Kuroda and Kodera, 1998]. During May-June the mean state of the polar-night vortex is more conductive for the propagation of wave activity towards the South Pole compared to the middle and late winter. Even though the refractive index above the tropopause is weaker compared to the spring-time maximum, the climatology of refractive index (Fig. 3.8-3.9) shows the latitude of the turning level located poleward of 60° S which would contribute to the southward refraction of the up-floating wave activity. Consistent with that is the seasonal cycle of the upward wave fluxes (Fig. 3.8 -3.10) which shows a weak maximum during May-June. Later in the season the turning level contracts equatorward leading to the equatorward deflection of the incoming wave activity.

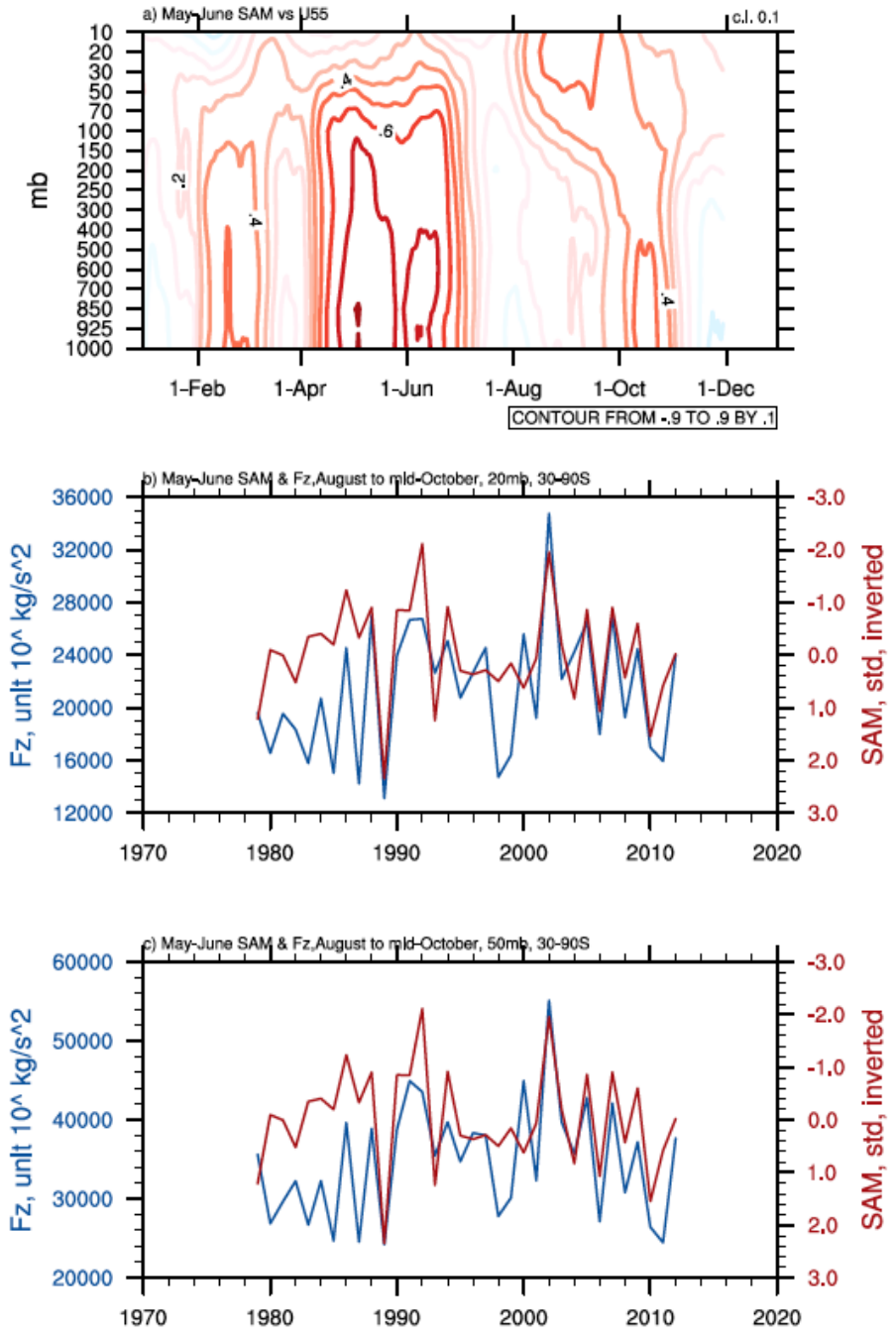

Figure 5.1. (a) Correlation between May –June SAM and zonal mean zonal wind at 55° S averaged within monthly window sliding over calendar year. (b) & (c) Time series of May-June SAM and vertical component of EP Flux averaged from August to mid-October between 30-90° S at 20 and 50 mb levels.

Hence, in order for tropospheric waves during middle winter to significantly affect the polar vortex it needs to be weakened by the wave activity during late autumn- early winter. Consistent with this idea is the observed dependence of the spring-time wave fluxes on the

thermodynamic processes at the surface during late autumn and early winter and lack of any dependence during July-August. The examination of the coherent changes between upward wave fluxes during August-October and anomalous circulation at the surface shows that most of the pre-conditioning at the surface is related to the phase of the SAM during early winter. Consequently, this early stage pre-conditioning also affects the downward progression of the spring-time polar vortex anomalies. Figure 5.1 shows the time-pressure structure of the cross-correlation between the May-June SAM and zonal wind at 55° S and time series of the vertical component of Eliassen Palm Flux (F_z) averaged between 30-90° S at 50mb and 20 mb from August to the mid-October, that is, during its seasonal maximum. The May-June SAM index correlates up to -0.63 with F_z at 50mb with the strength of connection slightly increasing with height (up to -0.67 at 20mb) and consequently captures the descent of zonal wind anomalies along 55° S. Maximum connection comes from June.

The variability behind the SAM is believed to be an intrinsic feature of the extratropical circulation and to be maintained by the internal feedbacks within the extratropical atmosphere. However, as it will be shown below, during June the dipole pattern of the SAM is centered at approximately 30° S and projects on the cross-equatorial cell of the Hadley circulation. The next section discusses the seasonal transition of the SAM and tropical influence on the upward propagating waves.

5.2.2 Influence of subtropics on the SAM-related propagation of wave activity

5.2.2.1 Seasonal transition of the SAM dipole during May-June

Figures 5.2-5.3 show the latitude-pressure structure of the zonal mean zonal wind, EP flux cross-sections and residual mass stream function regressed onto the standardized monthly June and July SAM index. Overlaid is the mean structure of zonal wind and residual mass stream function during these months. In June, the SAM index shows no classical zonal wind and mass stream function dipole centered at 45° S (see Figure 1 in Chapter 2.3). Instead, it the pattern of SAM-related anomalies strongly projects on the variability of the subtropical jet equatoward of 30° S and is associated with the strengthening of the mass stream function near the center of the cross-equatorial cell of the Hadley circulation. A similar shift in the SAM signature can be obtained in the ERA40 & ERA Interim reanalyses (not shown) which suggests that this result is not sensitive to the resolution. At the same time, Marshall's SAM index shows a similar shift in the mass stream function but little shift in the zonal wind which

suggests that stations used to compute the SAM from ground-based observations are not very representative of the June SAM.

In July, the SAM-related circulation anomalies appear to be shifting towards a conventional dipole centered at 45° S. At the same time, EP flux vectors suggest that during June, the upward wave activity still penetrates the polar vortex, while during July when the vortex is too strong it gets refracted poleward and downward to a greater extent.

The interpretation of the link between the SAM and the cross-equatorial Hadley cell can be two-fold. It can imply both the impact of the extratropical eddy stresses (which are the strongest during winter) on the tropics and impact of the tropical circulation on the growth and propagation of the extratropical waves.

For instance, the shift of the SAM dipole towards 30° S can be explained in terms of the seasonal changes in the wave propagation. The EP flux cross-sections in Fig. 5.2 show no change in the source of wave activity at the surface in the midlatitudes. Instead, under the positive phase of the SAM, the anomalous wave activity is diverted much closer towards the equator in the upper troposphere during June compared to the other months. The latter together with the bifurcation of the upward wave fluxes shown in Chapter 4 suggests that the interannual variability in the propagation of the waves in the meridional plane could be partly organized by the tropical circulation. The seasonality of the subtropical jet, its exceptional sharpness and location of the jet core equatorward of 30° S in June-July could result into an equatorward shift of propagating tropospheric waves and through that of the SAM dipole.

To demonstrate that, a test of the means based on the daily anomalies of the refractive index (for stationary wave number 1) of the subtropical jet during June is performed. That is, based on the daily data 2 samples are formed representing anomalies of the refractive index at 27.5° S, 400-250mb (that is at the core of the subtropical jet and at the levels where SAM related anomaly in EP Flux in the Fig.5.3 attains its maximum) greater or lower than (*mean +/- 0.5 std)*. The mean differences in zonal wind and the vertical component of the EP flux before and after an increase in the subtropical refractive index are shown in Figures 5.4 - 5.5.

Three days before an increase in the refractive index, the subtropical jet shifts poleward as indicated by a dipole pattern in the upper troposphere with an easterly zonal wind anomaly equatorward of its core at 27.5° S and a westerly anomaly poleward of 27.5° S. At day 0 the secondary dipole pattern develops in the midlatitudes with an easterly acceleration equatorward of 45° S and a westerly acceleration poleward of 45° S and overlaps the anomaly observed at day -3 . At day +3 westerly zonal wind anomalies maximize at 60° S in the upper troposphere and easterly anomalies span the troposphere from 40° S to 20° S overall resembling the SAM signature in June. Figure 5.5 shows difference in the vertical component

of EP flux between the days with the high and low refractive index of the subtropical jet at lags 0, +3. The strengthening of the westerlies along 60° S is accompanied by a reduced upward wave flux both in the troposphere and later in the stratosphere.

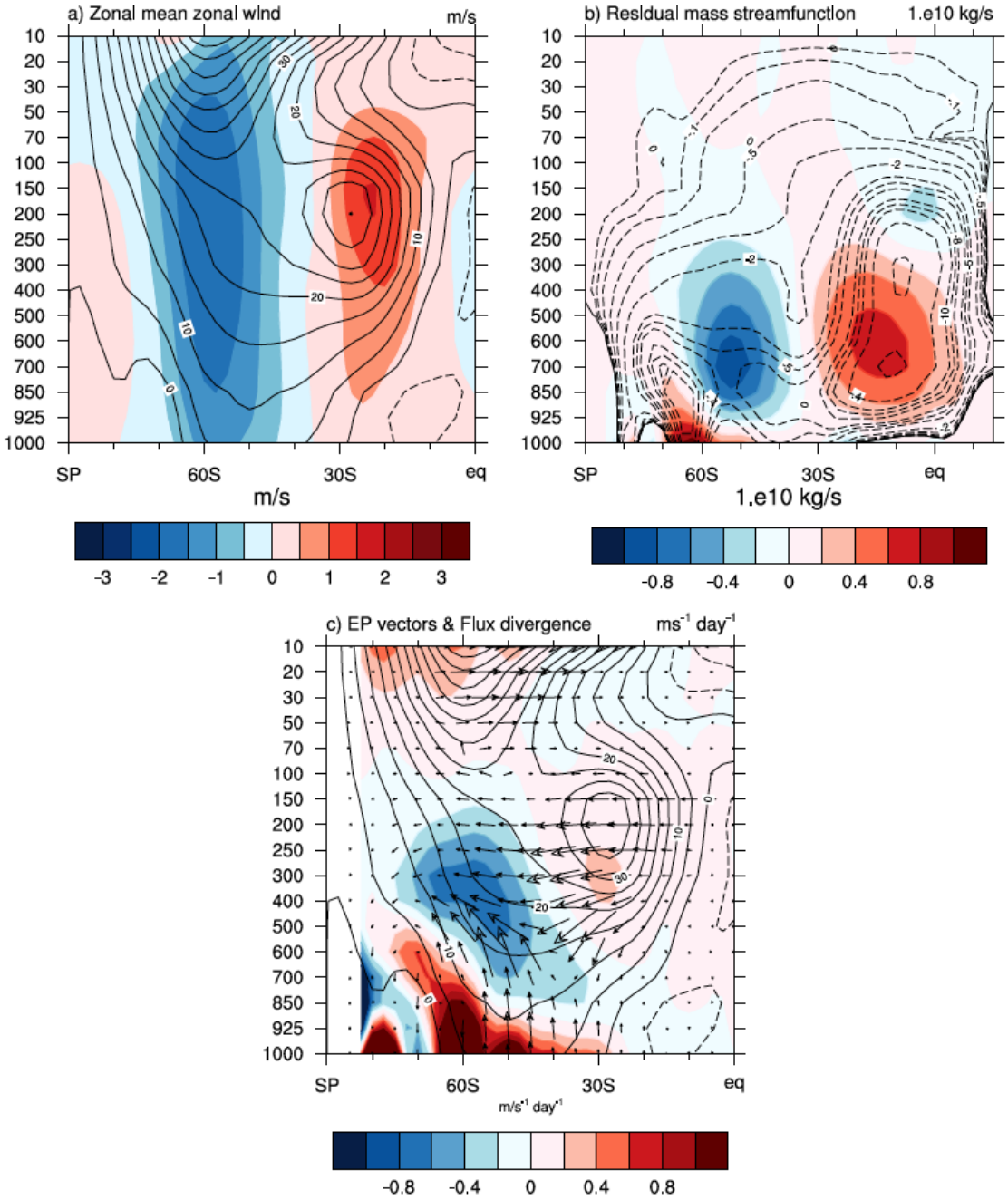

Figure 5.2 Regression patterns of (a) zonal mean zonal wind, (b) residual mass stream function, (c) EP Flux and its divergence related to the Southern Annular Mode during June. Black contour indicates the climatology of the zonal mean zonal wind (a and c) and of the residual mass stream function (b). Shown in terms of the negative polarity of the SAM.

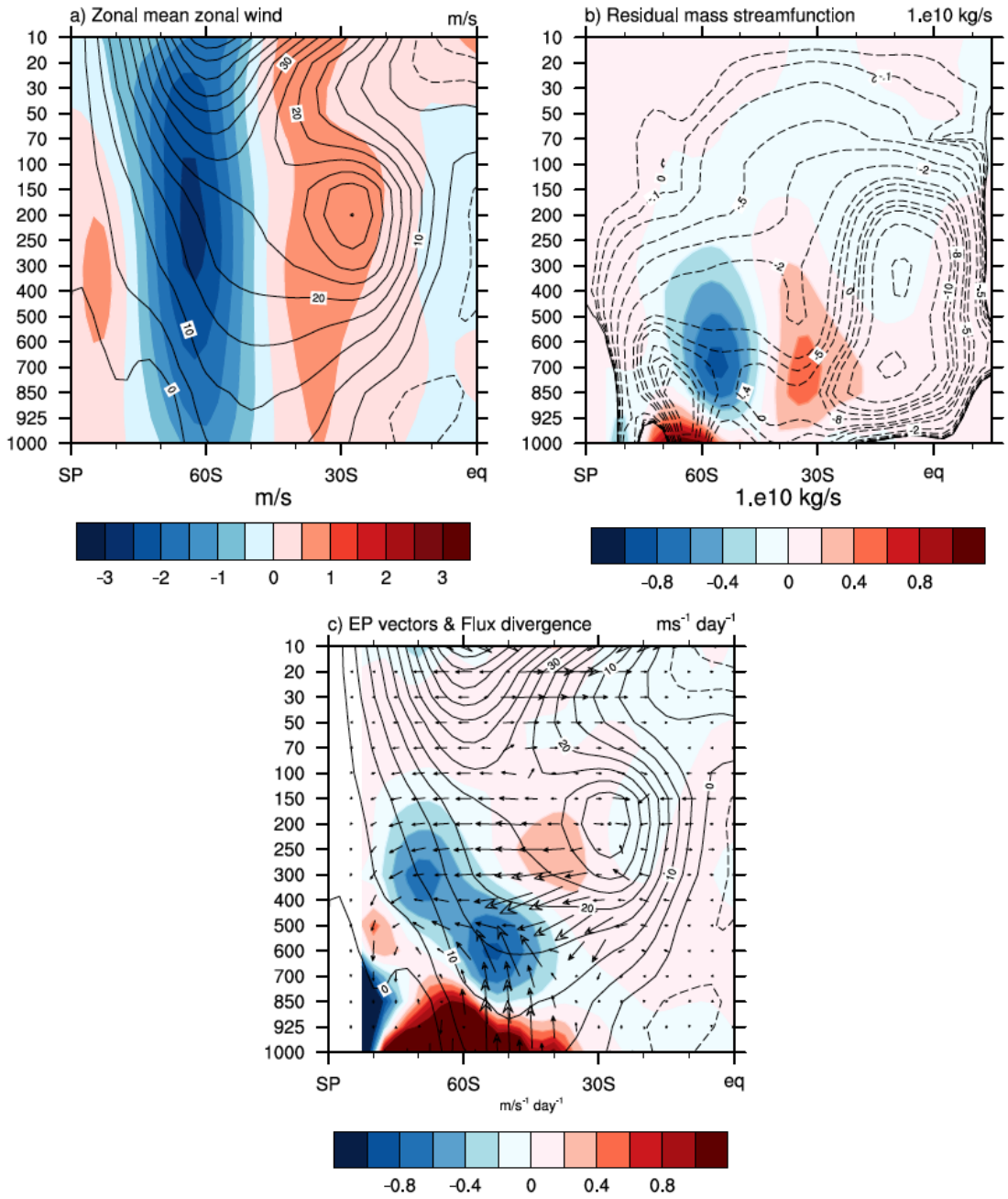

Figure 5.3 Regression patterns of (a) zonal mean zonal wind, (b) residual mass stream function, (c) EP Flux and its divergence related to the Southern Annular Mode during July. Black contour indicates the climatology of the zonal mean zonal wind (a and c) and of the residual mass stream function (b). Shown in terms of the negative polarity of the SAM.

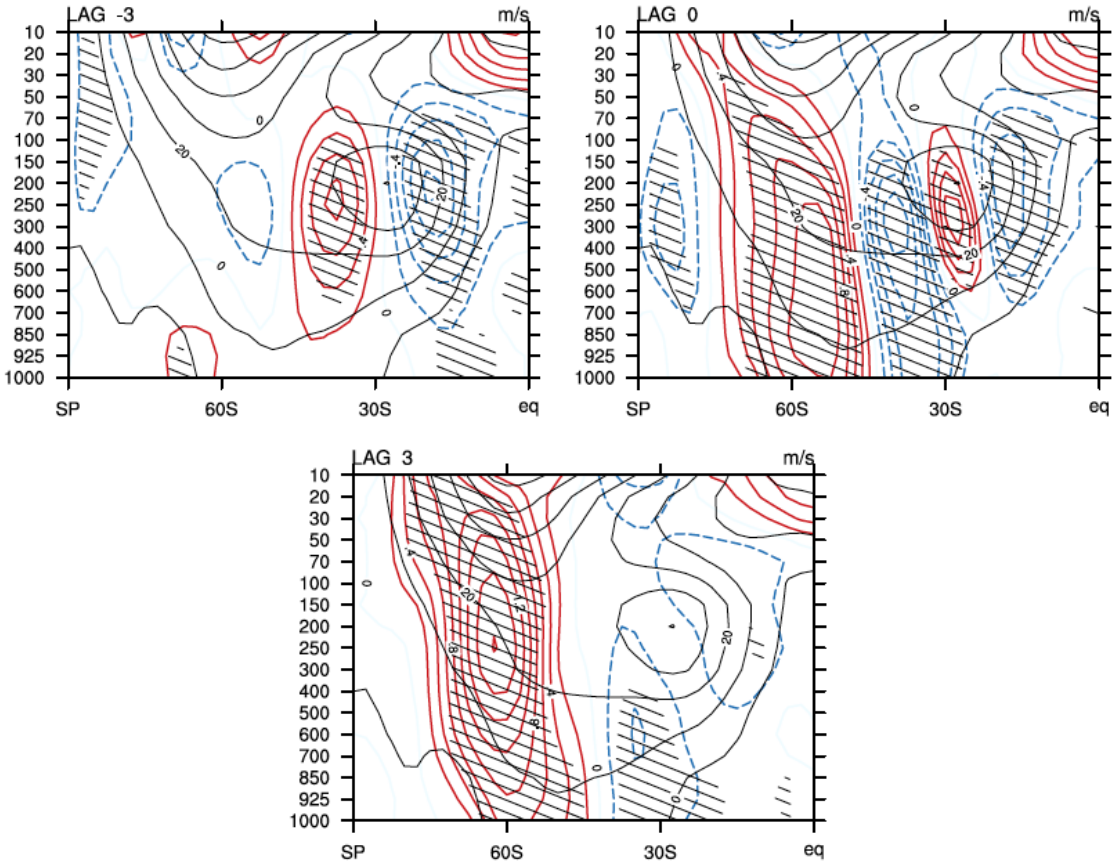

Figure 5.4 Composite zonal mean zonal wind differences which precede and follow a change in the refractive index of the subtropical jet during June. (contour, blue – easterly, red – westerly anomaly, c.i. 0.2 m/s). Overlaid is the June climatology of zonal mean zonal wind (black, c.i. 10 m/s). Shading denotes 95% level.

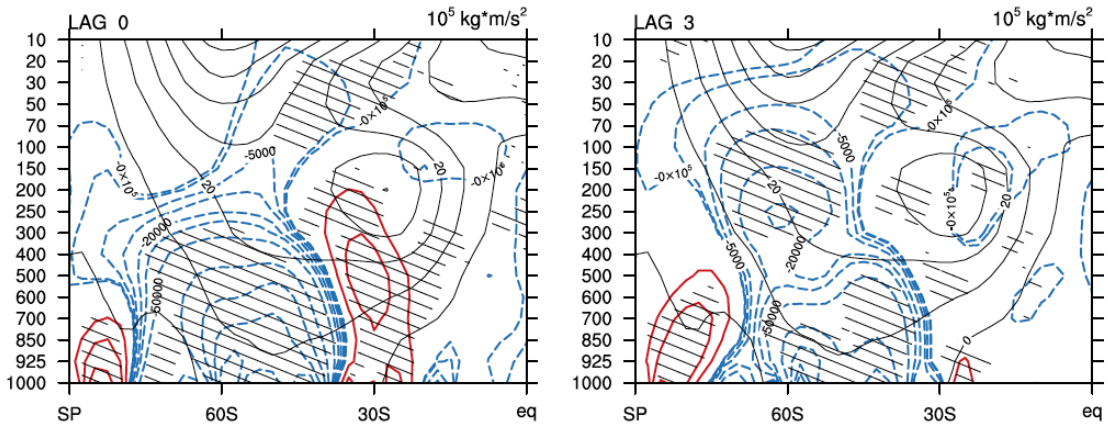

Figure 5.5 Composite vertical component of the EP Flux differences which follow a change in the refractive index of the subtropical jet during June. (irregular contours, blue – negative, red – positive anomaly). Overlaid is the June climatology of the zonal mean zonal wind (black, c.i. 10 m/s). Shading denotes 95% level.

5.2.2.2 Anomalous dynamical structure which preceded the split ozone hole of 2002

A strong latitudinal shift of the subtropical jet and its impact on the upward propagating activity can be considered as one of the factors which led to the excessive wave forcing of the stratosphere during its pre-conditioning period and resulted into the early close-down of the ozone hole during 2002 [Newman and Nash, 2004] and anomalously low SAM index at the surface [Thompson at al, 2005].

Figures 5.6a-d compare the anomalous zonal mean zonal wind, the Eliassen Palm Flux, the mean refractive index for stationary wave with zonal number 1 and the meridional gradient of potential vorticity (PV) during June 2002. The situation is reminiscent of the one in Figure 5.4 at lag 0. A poleward shift (up to 5 degrees compared to the climatology) of the subtropical jet was accompanied by the changes in the refractive properties of the jet, in particular by an increase in the meridional gradient of potential vorticity and refractive index in the middle troposphere poleward of 30° S. The latter has been accompanied by a stronger vertical wave flux into the stratosphere and the deceleration of the vortex equatorward of 60° S.

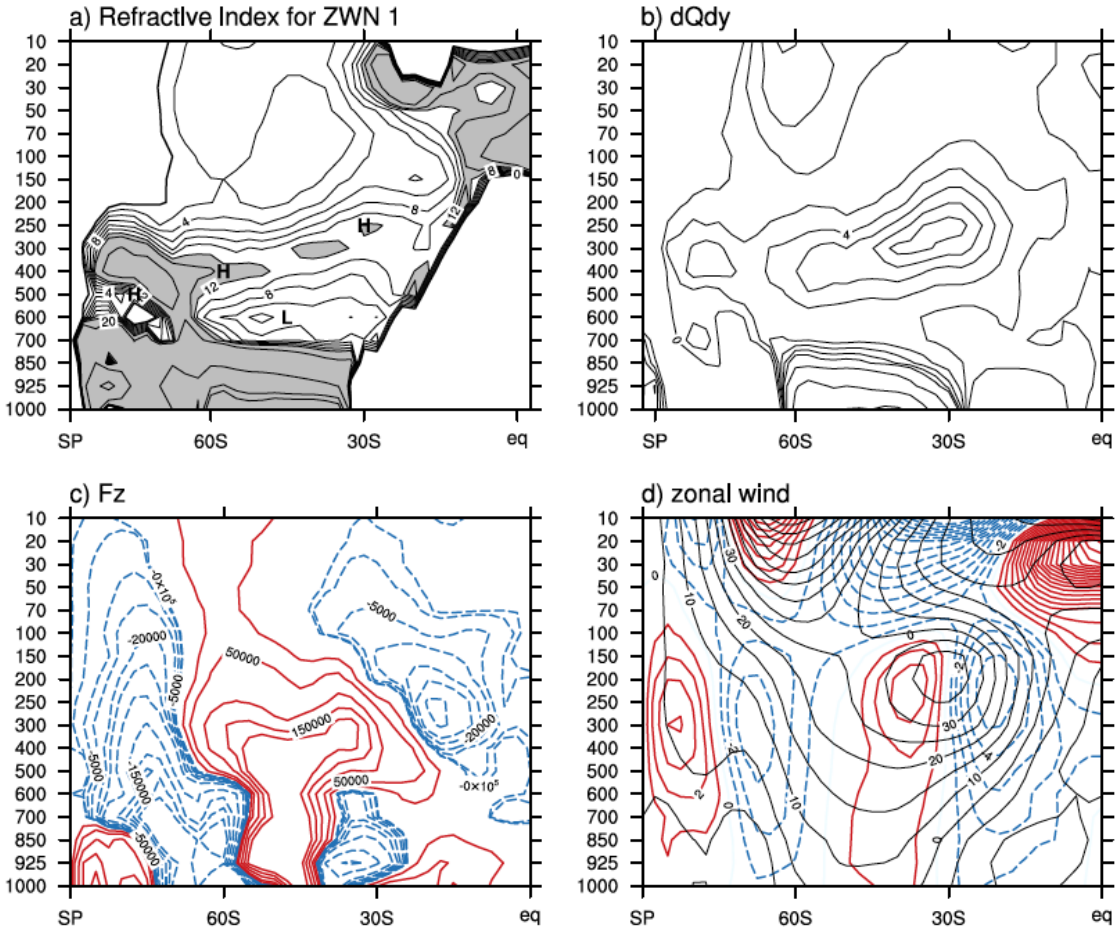

Figure 5.6 (a) mean refractive index (nondimensionalized, contours greater than 12 shaded), (b) mean meridional gradient of potential vorticity, (c) anomalous vertical component of the EP Flux and (d) zonal mean zonal wind and its anomaly during June 2002.

5.2.2.3 Dependence on the refractive properties of the subtropical jet

The effect of winter-time Hadley circulation and refractive properties of the subtropical jet which bounds it on the Southern Annular Mode and upward wave fluxes is not limited to June and July. The lifecycle investigated in Chapter 4 revealed a bifurcation of total upward wave flux towards the subtropics and midlatitudes during September-November as well. The latter is consistent with the seasonal mean signature of the SAM in the Eliassen Palm Flux. Figure 5.7 shows the May-November seasonal mean structure of the refractive index for stationary wave with zonal wave number 1 and the meridional gradient of potential vorticity. The latter represents the largest contribution to the refractive index determining the existence of 2 distinct maxima in the upper troposphere – at ~(27S, 300mb) and (50° S, 500mb). For phase speeds greater than zero, the refractive index maxima will resemble the meridional profile of PV gradient even closer, as implied by equation 2.12-2.13 in chapter 2.

The changes in zonal wave number just shift the refractive index up and down without affecting its meridional profile. Overlaid in Figure 5.5b are the EP Flux vectors regressed on the Southern Annular Mode index.

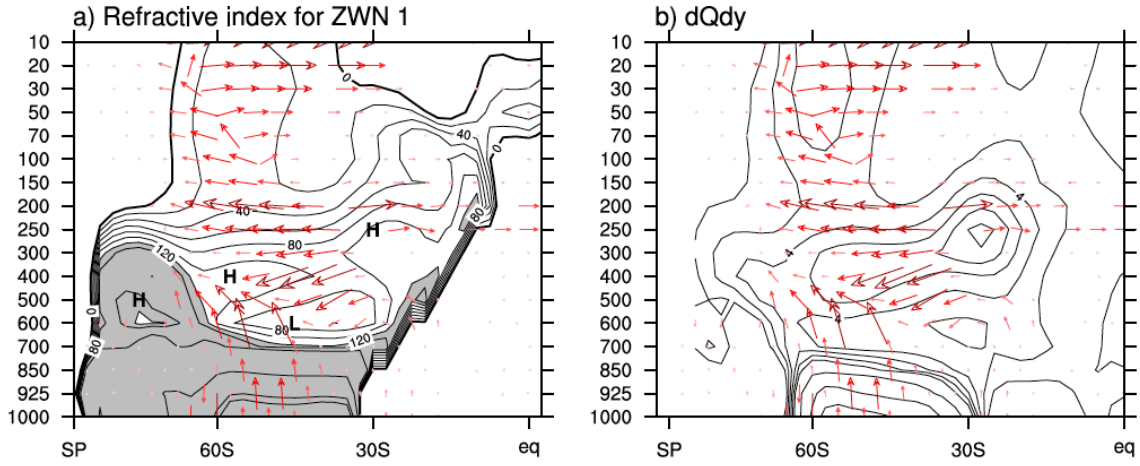

Figure 5.7. SAM-related anomalies in the Eliassen Palm Flux (vectors). Superimposed is the climatology of (a) refractive index for stationary wave number 1 (nondimesionalized by the radius of the earth squared, contours greater than 120 are shaded) and (b) meridional gradient of potential vorticity. June-November, 1979-2009.

The largest contribution to the variability in the SAM index comes from eddy momentum flux convergence in the upper troposphere which could be equivalently represented by changes in the vertically averaged horizontal component of EP flux at 45° S, reflecting the net momentum forcing associated with refraction of vertically propagating waves in the meridional plane (Fig. 3.2). When discussing the feedbacks of SAM, Lorenz and Hartmann (2001) emphasized the changes in the refractive index between 50-60° S, that is the local midlatitude maximum in Figure 5.5a,b. However it is evident in Figure 5.5b, that at seasonal time scales anomalous propagation of wave activity in the upper troposphere which maintains the SAM closely follows the isolines of the refractive index between its subtropical and midlatitude maxima.

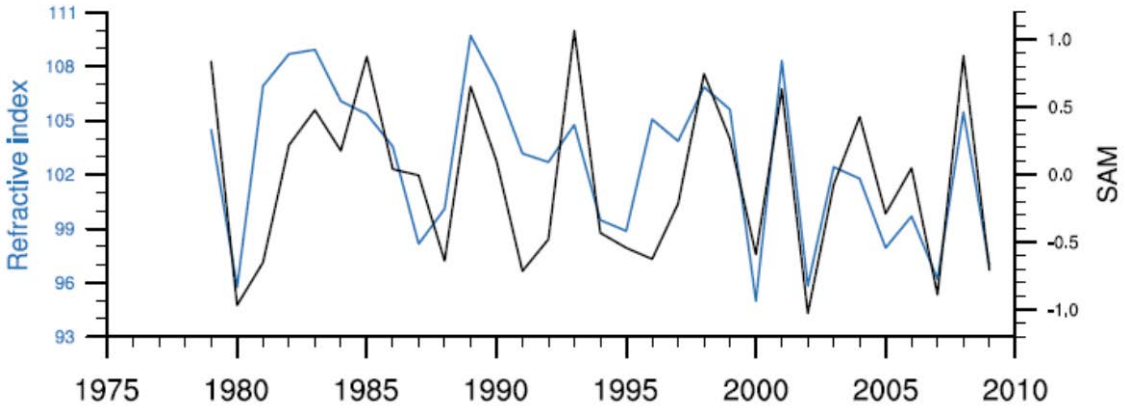

Figure 5.8 Southern Annular Mode index (black) and refractive index of subtropical jet (blue) during June-November

The subtropical maximum is located well outside of the SAM-related dipole in zonal wind and so should depend entirely on the parameters of the tropical circulation. Figure 5.8 shows time series of the subtropical refractive index maximum (one point maximum) and the SAM averaged over May-November. The correlation coefficient is equal to 0.65 and is significant at 95% level. The positive sign of relationship is consistent with the one expected from wave refraction. An equatorward shift of wave activity due to an enhanced subtropical refraction index should result into poleward momentum fluxes, reinforcement of zonal wind anomalies poleward of 45° S and a shift towards positive phase of the SAM.

Thus, the propagation of wave activity and through that the variability of the Southern Annular Mode can be partly controlled by tropics through the refractive index of the subtropical jet. The dependence is not limited to the austral winter and spring. Analogous links but at different levels due to seasonal changes of subtropical jet can be found during the austral summer as well.

5.2.3 Coherent changes between the Brewer-Dobson circulation, the SAM and the tropical circulation driven by the extratropical waves

While the subtropical jet appears to be modulating propagation of the extratropical wave activity, in particular, during early winter, the lifecycle also revealed that under the negative phase of the SAM the extratropical wave fluxes are more likely to reach the deep tropics leading to intensification of the meridional overturning circulation. The latter could explain the coherent changes between the Brewer Dobson circulation, SAM and the deep tropics observed in the Salby at al. (2004-2008). To understand the nature of the coherent

changes between Brewer-Dobson circulation, SAM and the deep tropics, it is first necessary to review the Hadley circulation theory.

While tropical and extratropical circulations are coupled in two ways throughout the year, it might be argued that the previous discussion is biased towards tropical influence. The analysis of Rossby wave numbers and the theoretical ideas which underly them could help however to illustrate the degree to which tropical circulation is affected by the extratropics during early winter and whether the above-mentioned relationships suggest tropical or extratropical influence.

5.2.3.1 Characteristics of the climatological mean Hadley circulation

Theories of the Hadley circulation and studies based on simulations with idealized general circulation models [Schneider and Bordoni, 2008] suggest that the Hadley circulation might undergo significant regime shifts in the seasonal cycle. The difference is likely to be imprinted not just in the strength and position of the winter and summer cells but also in the character of its parameter dependencies: the relative role of thermal driving and extratropical eddy stresses in the Hadley circulation strength. The latter might have important implications for the entire Southern Hemisphere climate system.

The zonal momentum balance in the upper troposphere in the vicinity of the Hadley cell center can be approximated by the balance between deceleration by eddy momentum fluxes and acceleration by angular momentum advection by the mean meridional circulation [Walker and Schneider, 2006]:

$$(f + \bar{\zeta})\bar{v} = (1 - Ro) f\bar{v} \approx S \tag{5.1}$$

where f is the Coriolis parameter, $\zeta = -(a\cos\phi)^{-1}\partial_\phi(u\cos\phi)$ is the relative vorticity, Ro defined as $-\zeta / f$ the local Rossby number, and S is the horizontal momentum flux divergence. Schneider (2006) showed that Ro can be used as a nondimensional measure of the role of the eddy momentum fluxes in the strength of the Hadley cell. When Ro approaches 0, changes in the Hadley cell are almost entirely due to changes in the horizontal eddy momentum flux convergence, when it is close to 1, the mean meridional circulation is "decoupled" from impact of the eddy fluxes. The contrasts are expected to be especially strong in the Southern Hemisphere which features a split jet and a strong Hadley cell in the annual mean.

It is worth to review the seasonal differences by looking at the structure of the Eulerian mean mass streamfunction Ψ. Following Oort and Yienger (1996), Ψ is defined by:

$$[\bar{v}] = g\frac{\partial\Psi}{2\pi R\cos\phi\partial p} \tag{5.2}$$

$$[\bar{\omega}] = -g\frac{\partial\Psi}{2\pi R^2\cos\phi\partial\phi} \quad , \tag{5.3}$$

where v is meridional velocity, ω is the vertical velocity, R – radius of the Earth, p – pressure, square brackets stand for temporal averaging, overbars – for zonal averaging. The field of mass streamfunction is obtained by integrating (2) downward to the surface. Prior to that the $[\bar{v}]$ field was corrected by removing its mass-weighted vertical mean value to ensure the vertical-mean mass balance.

Figure 5.9 shows seasonal variation in the climatological mean (1979-2009) mass streamfunction Ψ and the local Rossby number Ro. Consistent with the theory of axisymmetric circulations developed by Lindzen and Hou (1988), seasonal changes in the mean meridional circulation follow displacements in the latitude of maximum heating. The upwelling branch of the Hadley circulation is located directly above latitude of maximal sea surface temperatures throughout the year. Solsticial circulations are dominated by a presence of a strong cross-equatorial winter cell. The southern winter cell is up to $2\cdot10^9 kg\cdot s^{-1}$ stronger than the northern winter cell which corresponds to the seasonal drift of thermal equator from 15° N-20° N in December-February to 5° N in June-August. However, the second weaker summer cell does not disappear completely, as expected for symmetric circulations studied by Lindzen and Hou: a pair of equatorially symmetric Hadley cells is a robust feature of the circulation present throughout the year and most prominent during equinoxes [Dima and Wallace, 2002]. It is noteworthy that the SON southern cell is still comparatively strong and is more characteristic of JJA conditions, while MAM cell is of DJF.

Superimposed in Figure 5.9 is the local Rossby number, a measure of the proximity of the circulation to the axisymmetric limit. With the annual mean Ro in the vicinity of mass stream function maximum around 0.5 (as discussed by Schneider), the observed circulation

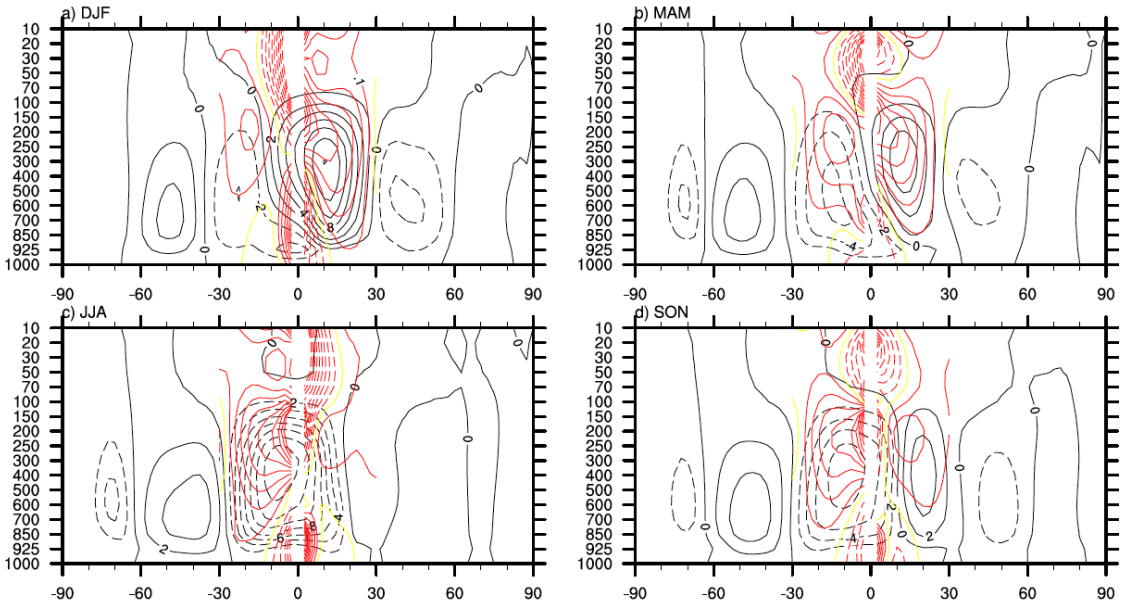

*Figure 5.9 Seasonal variations in the mass stream function (black, c.i. 2*1.$^{-10}$kg/s, negative values dashed) and local Rossby number (red, c.i. 0.1)*

represents an intermediate regime between "pure eddy-" and "pure thermally-" forced circulations. However, the strong seasonal difference between summer and winter Hadley circulation is apparent. Maximum of DJF mass stream function is located approximately at 12.5° N at 300mb level and overlaps with upper-branch Ro contours of 0.4-0.5. The JJA winter cell, located much closer to equator at ~(5° S,300mb) (thus contribution of Coriolis parameter is large) corresponds to higher Ro values ranging between 0.7-0.9. Southern winter conditions thus are relatively close to the "inviscid limit". High Ro values extend deeper poleward in the SH than in the NH: Ro values over the entire extent of the southern cell are higher than over the northern cell throughout the year. On the other hand, summer circulations in both hemispheres feature Ro below 0.2 and should be strongly affected by the extratropical eddy stresses.

Therefore, seasonal changes in upper troposphere local Rossby number over the center of Hadley cells suggest that winter circulation should be decoupled from the effect of extratropical eddy stresses due to a large role of the Coriolis parameter.

5.2.3.2 EOF analysis of tropical-extratropical connection

To see whether differences suggested by Ro are indeed imprinted in the dependence of Hadley circulation parameters and to identify patterns of simultaneous variation between the

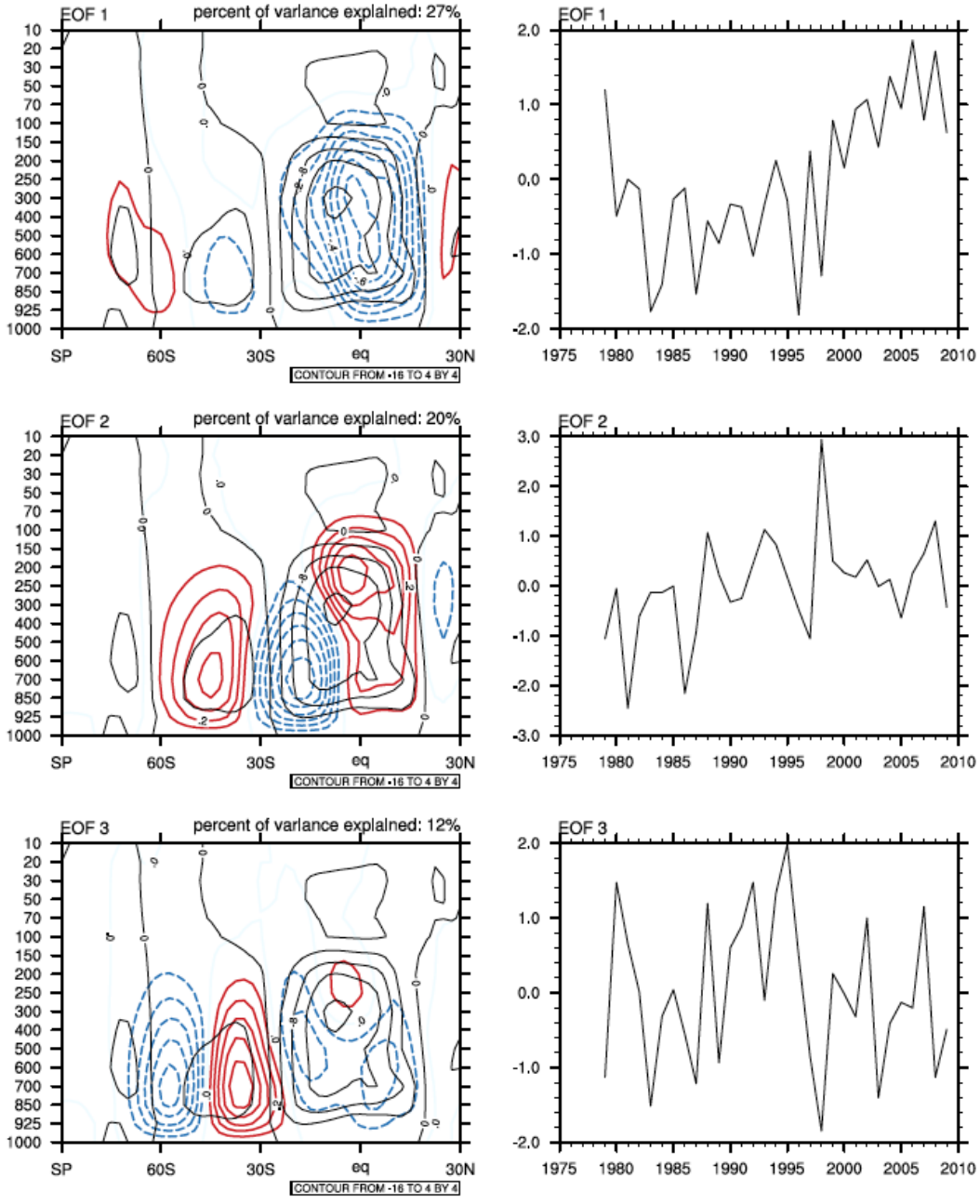

*Figure 5.10 (a) First three empirical orthogonal functions of the 30° N-90° S, 1000-10mb mass stream function field during JJA. Left: regression on mass stream function (color, c.i. 0.1*1.$^{-10}$kg/s). Right: time series. Overlaid in mass stream function climatology (black, c.i. 4*1.$^{-10}$kg/s).*

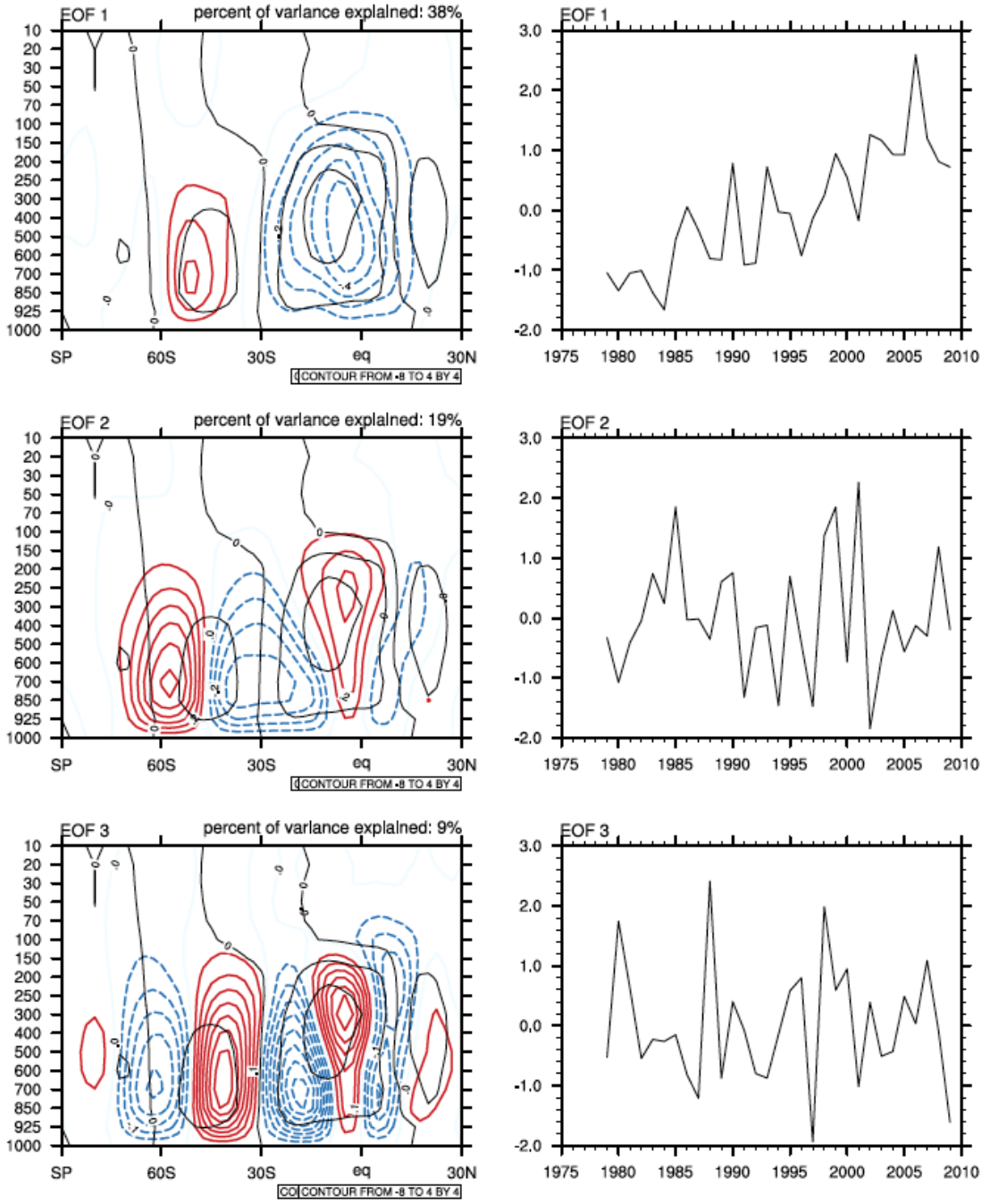

Figure 5.10 (b) First three empirical orthogonal functions of the 30° N-90° S, 1000-10mb mass stream function field during SON. Left: regression on mass stream function. Right: time series.

Handley circulation and extratropics, I calculate main EOF's of the seasonal mean mass streamfunction fields taken between 30° N and 90° S. Prior to computing, data has been weighted by the square root of cosine of latitude and increments of the pressure they represent.

Figure 5.10 summarizes first 3 EOFs of the mass stream function during JJA and SON. Characteristic of austral winter and spring conditions is a uniform strengthening/weakening of the winter cell with an oppositely signed anomaly in the stratosphere. Overall, the first EOFs are identical to those derived by von Storch (1998) based on 200mb global mass stream function. They are related to the increase in zonal mean precipitation at the latitudes of the upwelling branch and vertically averaged relative angular momentum (not shown). The first EOFs of JJA and SON mass stream function field are remarkably similar, which is not evident during austral winter and autumn and agree with the seasonal differences in the local Rossby number in Fig.5.9. The winter and spring first EOF's are in fact significantly correlated up to 0.5. Overall, they appear to feature tropical variability developing in the absence of eddy influence as implied by the local Rossby number.

An advantage of using an EOF based on the mass streamfunction instead of the conventional SAM index is that it captures mass transports by the Hadley circulation much better than the geopotential height field. When extended up to 30° N, EOF analysis acts as a kind of a filter to eliminate noise and unrelated processes showing a far clearer SAM signature in the tropics.

The 3rd EOF in JJA and the 2nd in SON can be clearly identified with the SAM and explain 13% and 25% of total variance respectively. Cross-correlations with SAM are high reaching 0.82 during both JJA and SON. The second EOF during JJA is associated with the intensification of the Ferrel cell. The 4th (not shown) and 3rd are associated with ENSO. Exceptional is the austral winter (not shown) when ENSO and SAM are very strongly interrelated [L'Heureux and Thompson, 2006] and their signatures can't be separated.

Figure 5.11 shows the correlation between the SAM-related EOFs and the residual mass streamfunction. Coherent changes between tropics and extratropics are evident during both seasons. They involve changes in both strength of the upwelling branch and latitudinal extent of the Hadley circulation. That is, an equatorward shift of the extratropical circulation during the negative phase of the Southern Annular Mode is accompanied by a contracted and stronger Hadley cell with the opposite observed during the positive phase of the SAM. During September-November correlations are strong exceeding 0.5 resulting into strong coupling between the tropical, the extratropical troposphere and the Brewer Dobson circulation.

Figure 5.12 shows correlation between the SAM-related EOFs on the EP flux and its divergence. Amplification of residual circulation in the inner tropics is coincident with anomalous EP flux in the upper troposphere between 150-250 mb. In JJA the EP flux anomalies appear to 5° S, while in SON at 10° N, that is right above the upwelling branch. The overlap between residual mass stream function and EP Flux anomalies suggests that

connection between SAM and tropics revealed here results from anomalous absorption of the extratropical eddy fluxes in the upper branches of the Hadley circulation. The difference between winter and spring results primarily from the existence of the equatorial westerly duct which begins to develop in the spring and shifts the zero-wind line allowing for the extratropical wave activity to reach equator. Additionally, negative SAM and El Nino events tend to enhance the eddy fluxes and circulation throughout the Southern Hemisphere (Fogt at al, 2011).

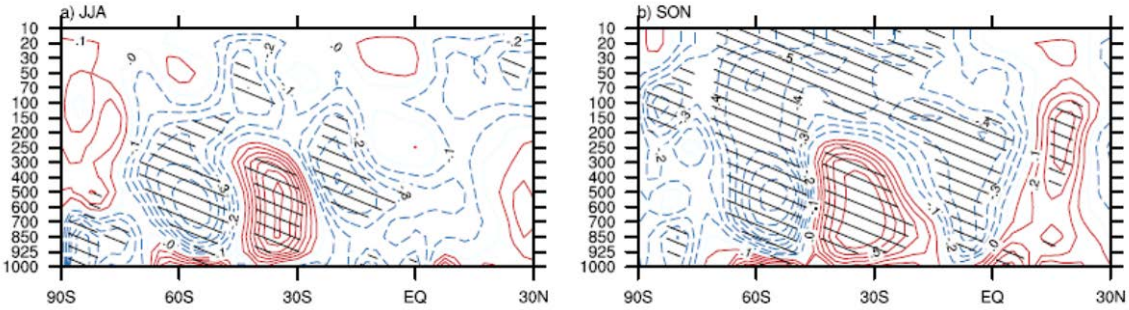

Figure 5.11 Correlations between SAM-related EOFs and the residual mass stream function (shown in terms of negative SAM polarity). Shading denotes correlation significant at 95% level, red – positive, blue – negative correlation.

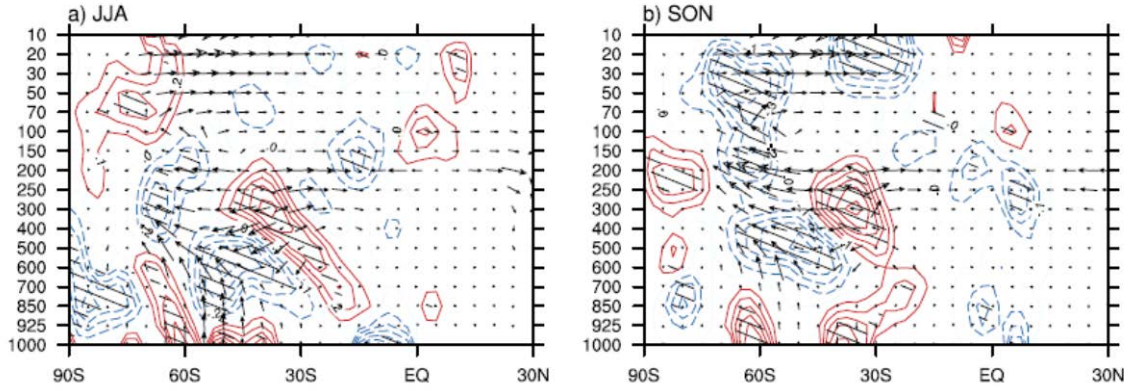

Figure 5.12 Correlations between the SAM-related EOFs, Eliassen Palm Flux (vectors) and its divergence (contour). Correlations are shown in terms of the negative SAM polarity. Shading denotes correlation significant at 95% level, red – positive, blue – negative correlation.

Together, local Rossby numbers and EOF analysis suggest that even though the winter Hadley circulation is to a large extent decoupled from the extratropical influence during austral winter and spring, the extratropical eddy fluxes still reach the deep tropics and affect the mean meridional circulation. The impact of the extratropical eddy stresses appears to be strongly related to the physical processes represented by the SAM, that is to the changes in

propagation of the extratropical waves. The impact of the eddy stresses and the SAM on the tropical circulation does intensify towards the spring season both due to the decrease in the relative role of the Coriolis parameter in the zonal momentum balance and due to the development of the equatorial westerly duct.

In addition, the theoretical and "model" regime transitions which follow the seasonal cycle of the Hadley circulation discussed by Bordoni and Schneider (2006) are indeed evident in the Southern Hemisphere, not limited regionally to the Asian summer monsoon and can be detected in the first EOFs of the mass stream function field.

5.3 Summary

Some of the main results of the analysis are:

1) The springtime stratosphere is pre-conditioned by the dynamical processes during late-autumn –early winter when the stratospheric vortex is still conductive to the upward propagating wave activity. In particular it depends on the phase of the SAM during May –June.
2) During May-June, the SAM is, however, strongly coupled to the cross-equatorial cell of the Hadley circulation with the SAM dipole in zonal wind centered at 30° S. The dependence can be explained in terms of subtropical jet impact on the extratropical waves. A composite analysis revealed that a poleward shift of the subtropical jet is first followed by changes in its refractive properties and then followed by a positive anomaly in the SAM. A relationship between the SAM and the refractive properties of the subtropical jet is evident in the interannual variability as well.
3) A strong anomaly in the latitude of the subtropical jet during June was one of the factors which resulted into the excessive wave forcing of the stratosphere and the split ozone hole of 2002.
4) At the same time, there appears to be a back-effect of the SAM on the strength and extent of the Hadley circulation. Eddy-driven changes in the tropical circulation maximize during spring following the seasonal cycle of the westerly equatorial duct and result into strong coupling between the SAM, the Brewer-Dobson circulation and the deep tropics.

The relationship between the tropics and the Southern Annular Mode identified by the mass stream function based EOF analysis reveals anomalies in the sea level pressure and SST (not shown) is similar to those by Ding at al. (2012). An active Rossby Wave Source region during JJA is indeed evident in the diagnostics such as positive EP Flux divergence or region of the negative meridional gradient of potential vorticity. However, I failed to find any straightforward relationship between them and the SAM. The SAM-related EP flux pattern does not overlap with the area of the negative refractive index and *dQdy* which indicate a source of wave activity. Instead, SAM correlates with the maximum values of the refractive index close to the core of the subtropical jet. This suggests that tropical influence on the SAM can be understood in terms of the impact of the subtropical jet on propagation of wave activity.

Chapter 6: Stratospheric and tropospheric aspects of summertime variability in the Southern Annular Mode

6.1 Introduction

The evidence of a stratospheric impact on the summertime circulation is primarily found in the context of recent trends in the Southern Hemisphere. A number of studies have attributed the observed shift towards the higher index polarity of the annular modes (analogous though weaker changes are observed in the Northern Hemisphere as well) to the combined effect of the enhanced greenhouse gases and ozone depletion on the long-term climate trends [Thompson and Solomon, 2002; Hartmann at al., 2000, Gillet and Thompson, 2003]. The trends of the annular modes maximize during boreal winter and overall can be described by the poleward migration of the extratropical circulation accompanied by an expansion of the tropical belt. The latter has been addressed by researchers through a variety of indices [Seidel et al., 2008]. Estimates of this shift, however, are not robust. They differ from diagnostic to diagnostic, ranging from 0.6 to 2 degrees of latitude per decade, leaving the exact rate of expansion under debate. The widening of the tropical zone has been accompanied by a rise in the tropical tropopause. Together, these changes represent an increase in the tropical air mass of up to 5% [WMO, 2011]. Due to its almost global coverage, poleward expansion of the circulation can partly account for the observed changes in various diagnostics of atmospheric circulation, i.e. up to 50% of the summer surface temperature increases in the northern extratropics [Thompson and Wallace, 2000], regional warming over the Antarctic Peninsula [Marshall et al., 2006], enhanced subtropical rainfall [Kang at al., 2011; Gonzalez at al., 2013] etc, and might have slightly contributed to the increase in the global mean temperature through radiative cloud feedbacks [Grise et al., 2013].

At present, different causal links between the poleward shift of the subtropical terminus and the poleward migration of the jet stream as well as the role of the stratosphere in driving these changes are not completely clear. Generally, present-day climate conditions represent an intermediate regime, whereby the Hadley circulation and extratropical waves do interact. The extent and strength of the Hadley circulation are controlled by both the thermal driving associated with the tropical SST and extratropical eddies [Schneider, 2006]. At the same time, the subtropical jet which bounds a thermally driven Hadley circulation can exert an influence on the extratropics by modifying baroclinicity and growth of atmospheric waves and through barotropic effects associated with changes in wave propagation. Indeed, both climate model simulations and observational analyses indicate that the latitudes of the secondary eddy-driven jet maxima and boundary of the Hadley circulation are interrelated on both the decadal and interannual time scales [Lu et al., 2007; Kang and Polvani, 2011], in particular during austral summer. But mechanisms proposed to explain the observed shifts largely rely on different assumptions and somewhat subjective definitions of subtropical

boundary. Though interrelated, different measures of Hadley circulation extent and strength can be controlled by different dynamical processes (different under different mean conditions as well) and, hence, the relationship between strength and extent of the upper and lower, downwelling and upwelling branches of the Hadley circulation is far from being linear [Levine and Schneider, 2011]. According to one view, the extent of Hadley circulation can be defined by the latitude where it first becomes baroclinically unstable [Held, 2000]. The increases in the midlatitude static stability projected under global warming scenario would then result into the poleward shift of baroclinicity, stabilization of subtropical jets which inhibits breakdown of thermally driven cell and shifts subtropical boundary poleward [Held, 2000; Lu at al., 2007; Frierson et al., 2007; Johanson and Fu, 2009]. Another view says that Hadley circulation boundary can be largely controlled by the extratropical eddy momentum fluxes. So Chen and Held (2007), Ceppi and Hartmann (2012) attempted to explain the change in the Hadley cell width as a result of increased eddy phase speeds associated with the stronger eddy-driven jet and a consequent convergence of eddy momentum fluxes closer to subtropical boundary. Other studies attribute it, however, to the thermal driving of the Hadley circulation and, in particular, to the impact of the increased SST over the tropical Eastern Pacific projected by most coupled models. In contrast to the typical El Niño conditions resulting into narrower and stronger Hadley cells [Oort and Yienger, 1996], the SST-forcing of a wider meridional extent has been projected to result into a "global warming"-like tropical expansion [Tandon et al, 2013]. The changes in the strength and latitude of the subtropical jet, which bounds the Hadley circulation, might in turn alter the propagation and growth of midlatitude waves affecting the annular modes. The potential importance of the last mechanism for the extratropical climate has been highlighted many times in a number of model-based studies [Nigam and Lindzen, 1989; Ferreira at al., 2001; Lee and Kim, 2003; Ceppi at al., 2013] and can be responsible for the global impact of ENSO [Seager at al., 2003], the interhemispheric connections observed in the paleoclimate studies [Goodwin at al., 2013] and on decadal time scales during 20th century [Rosanova (phd thesis, 2006); Chylek at al., 2010].

Basic dynamics suggests that the location of jet streams, and so the annular modes, should be sensitive to the spatial temperature gradients, as confirmed by simulations with numerical models [Son and Lee, 2005; Eichelberg and Hartmann, 2005; Lim and Simmonds (2008)], while different thermal forcings provide a different response. So, in an idealized GCM experiment, Butler at al. (2010) find that both polar stratospheric cooling and tropical warming in the upper troposphere result into poleward contraction of the storm tracks, while polar surface warming results in equatorward shift of jet stream. However, when combined

together, the total response does not equal the response to the sum of the forcings applied independently indicating a non-linearity in the system. Overall, coupled atmosphere-ocean GCMs and chemistry-climate models exhibit no widening unless anthropogenic forcing is included. However, they tend to underestimate the observed rate of expansion [Johansson and Fu, 2009]. In search of a missing link, some researchers have attempted to attribute the more rapid expansion in the Southern Hemisphere to ozone depletion over Antarctica and its modification of the upper atmosphere jets through the interplay of atmospheric chemistry and dynamics. Son et al. (2010) and Lu at al. (2009) found, in a series of chemistry-climate model experiments, that models only reproduce the observed expansion when stratospheric ozone forcing is included in the simulations. They argue that ozone depletion has been driving surface climate change in the Southern Hemisphere in the same direction as the increase in global mean temperature. However, the ozone recovery expected in the XXI century might cancel out some of the GHG induced changes according to recent studies [Smith at al., in press; Barnes at al, in press; Grise at al., in press; Smith at al., 2012]. The mechanism by which the stratospheric impact lags the maximum ozone losses by almost 3 months remains poorly understood. So, the maximum ozone depletion occurs during September-October, the observed lower stratospheric cooling maximizes during November-December and a maximum positive trend in the SAM (since 1979) occurs during January. At the same time, as shown in Chapter 1, the observed downward descent of stratospheric polar vortex anomalies maximizes in October directly following the seasonal maximum in the lower stratospheric heat fluxes.

The uncertainties surrounding projections of the Hadley circulation parameters in the numerical simulations [Levine and Schneider, 2011; Kang at al., in press] make it difficult to rely on models when interpreting observed relationships and trends. The analysis by Schneider and Bordoni (2007) suggests that the summer Hadley circulation regime in the Southern Hemisphere is mostly eddy-driven. However, it is well-known that the tropical Pacific SST variability related to ENSO maximizes during boreal winter and dominates variability in the tropics and the extratropical Pacific during these months. So, a study by Zhou and Yu (2004) found that models forced with historical sea surface temperatures result into a better reproducibility of the SAM, especially during summer. L'Heureux and Thompson (2006) documented a relationship between ENSO and SAM over the extended summer season (November-February). Recently, an observational analysis by Ding et al. (2012) found an association between the Southern Annular Mode and tropical Pacific SST changes, independent of ENSO. They observed that a positive trend in the SAM was coincident with the summer cooling over the Eastern Pacific and a weak negative tendency in

the SAM during winter – with the SST increases in the Eastern Pacific. At the same time, a study by Fogt and Bromwich (2006) noticed that a connection between the SAM and ENSO-related anomalies in the tropical Pacific SST is subject to decadal variability. According to their Fig.12, a strong teleconnection with the SAM prevailed during austral spring in the 1990's, however, was completely absent during previous 2 decades. Their results suggest that remote climate connections can be enabled only under certain mean state.

Therefore, despite a number of mechanisms behind accelerated changes in the Southern Hemisphere, including impacts of the ozone depletion, greenhouse gases and natural variability in the tropical SST, has been proposed, it remains a question, whether it is the polar circulation pulling the tropics away from the equator or whether it is the tropics pushing the circulation poleward during austral summer. In this chapter, a role of tropical and stratospheric variability in driving interannual variability of the SAM during summer months as well as decadal variability in these factors is analyzed.

The chapter is outlined as follows. Impact of the springtime variability in the stratosphere on the summer SAM, its timing as well as the relative role of different types of variability in the Pacific SST is discussed in Section 6.2.1. Section 6.2.2 examines a change in the dynamics of the SAM which occurs after solstice. Sections 6.2.3 addresses the mean conditions which enable tropically-forced anomalies in the SAM, while Chapter 6.2.4 examines recent changes in the factors driving variability of the summer SAM. The dynamical mechanism which explains the tendency towards stronger tropical influence on the mean state is discussed Section 6.2.5. Regression model with time-varying coefficients which incorporates both influence of the stratosphere and the PDO on the SAM is presented in section 6.6. The chapter ends with conclusions and discussion.

6.2 Results

6.2.1 SAM predictability during late spring and summer: relative role of the stratosphere and the Pacific SST variability

According to Figure 3.12 the impact of downward progression of wave activity on the SAM maximizes during October-November following the seasonal maximum of upward propagating events. The persistent anomalies in the SAM extend through December well into the autumn. The impact of stratospheric variability during summer is better seen at the seasonal time scales so that internal SAM variability is filtered out. Figure 6.1a shows December-February SAM index and its component which varies coherently with the springtime planetary wave forcing. Correlation between the upward wave fluxes during their seasonal maximum as measured by the vertical component of Eliassen Palm flux (*Fz)*

integrated until mid-October, and DJF SAM reaches -0.6 (significant at the level greater than 99.99%). However, this connection fails to capture the decadal variability in the SAM and rather represents an added noise. Figure 6.1b shows correlation between detrended zonal mean zonal wind during December-February and springtime forcing of the stratosphere by planetary waves. Correlations maximize along 55°S reaching 0.7, however, most of this connection comes from December alone, deteriorates fast starting from January, consistent with Fig. 3.12, and resembles residual persistence of the SAM.

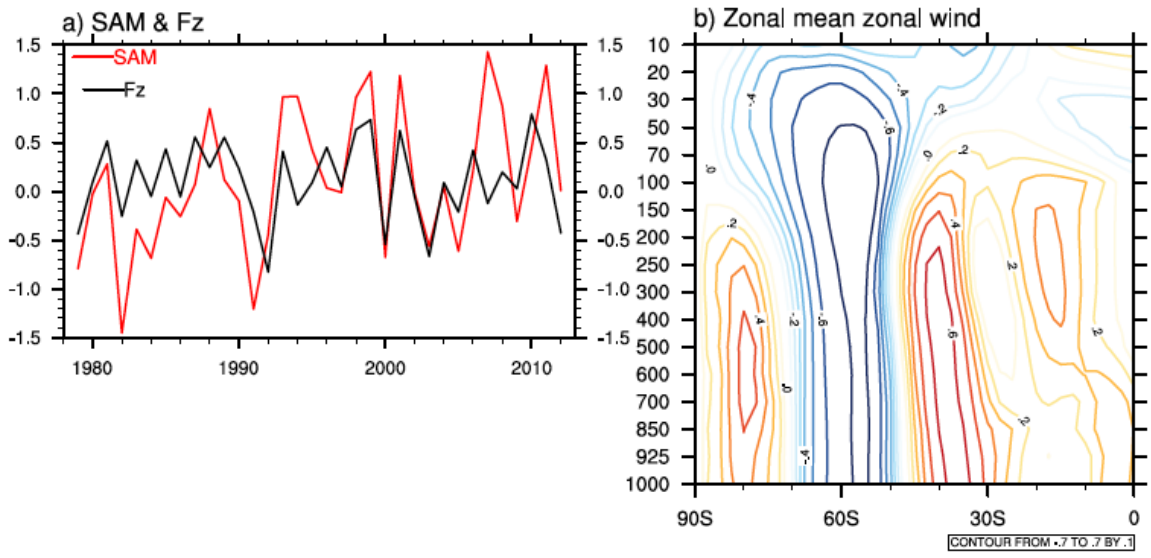

Figure 6.1 (a) December-February Southern Annular Mode index and its component which varies coherently with the anomalous springtime planetary wave forcing as measured by the EP flux at 50mb integrated until mid-October. (b) Latitude-height profile of correlation between anomalous EP Flux at 50mb integrated until mid-October and DJF zonal mean zonal wind (c.i. 0.1).

While during October-November the strongest downward signal from the stratosphere was found to be coincident with the downward wave fluxes (chapter 4), the link between stratosphere and troposphere during summer doesn't necessary imply only persistence of the tropospheric component of the SAM. In the absence of planetary wave forcing, the interannual variability in the state of the easterly stratospheric vortex and the lower stratosphere during summer can be to a large extent set by the spring-time dynamics and other factors, such as sensitivity of wave propagation to the wind shear near the tropopause, might begin to play a role [Chen and Robinson, 1992]. Despite that, as it will be shown below, a large fraction of variability in the SAM during January, at least since 1979 appears to come from the Pacific Ocean.

It is well-established that different types of ENSO represent influential factors regulating the SAM. During late spring-early summer most of tropical connection to the SAM

comes from the Eastern Pacific and Cold-Tongue ENSO, while during austral winter it is associated mostly with the Central Pacific ENSO [L'Heureux and Thompson, 2006; Lim at al., 2013]. Additionally, the Pacific ocean tends to exhibit ENSO-like low-frequency variability in the tropical and in the extratropical regions of the both hemispheres where it is known as the North and South Pacific Decadal Oscillation [Mantua at al., 1997; Shakun and Shaman, 2009]. Both are defined as the first EOF of the monthly Pacific SST fields poleward of 20° S/N. Despite the interconnection between the two enabled through the tropical SST, the southern PDO represents rather a more regional pattern with a more instantaneous response to the equatorial Pacific SST variability compared to the North Pacific PDO. The latter, defined as the leading pattern of the North Pacific SST poleward of 20° N [Mantua at al., 1997], the PDO also tracks significant anomalies in the tropical Pacific SST [Di Lorenzo at al., 2008]. The latter is less localized in its latitudinal extent compared to ENSO-related anomalies and overall resembles residual ENSO variability described by Zhang at al. (1997) which operates on decadal time scales [Liu and Alexander, 2007]. Figure 6.2 shows the signature of the PDO in the December-February SST and compares PDO index with the SST averaged between 30° N-30°S, 90-180W. Defined as the difference between the SST in the K and L shaped tropical Pacific regions of a typical ENSO impact (areas of positive and negative correlation with the ENSO index), the PDO style variability has been shown to correlate well with the variability in the global monsoon system during boreal summer, both in the year-to-year fluctuations and at the decadal time scales [Wang at al., 2013]. The latter suggests that the long-lived ENSO represents a planetary-scale variation in the coupled atmosphere-ocean system affecting macrocirculation processes in the global atmosphere.

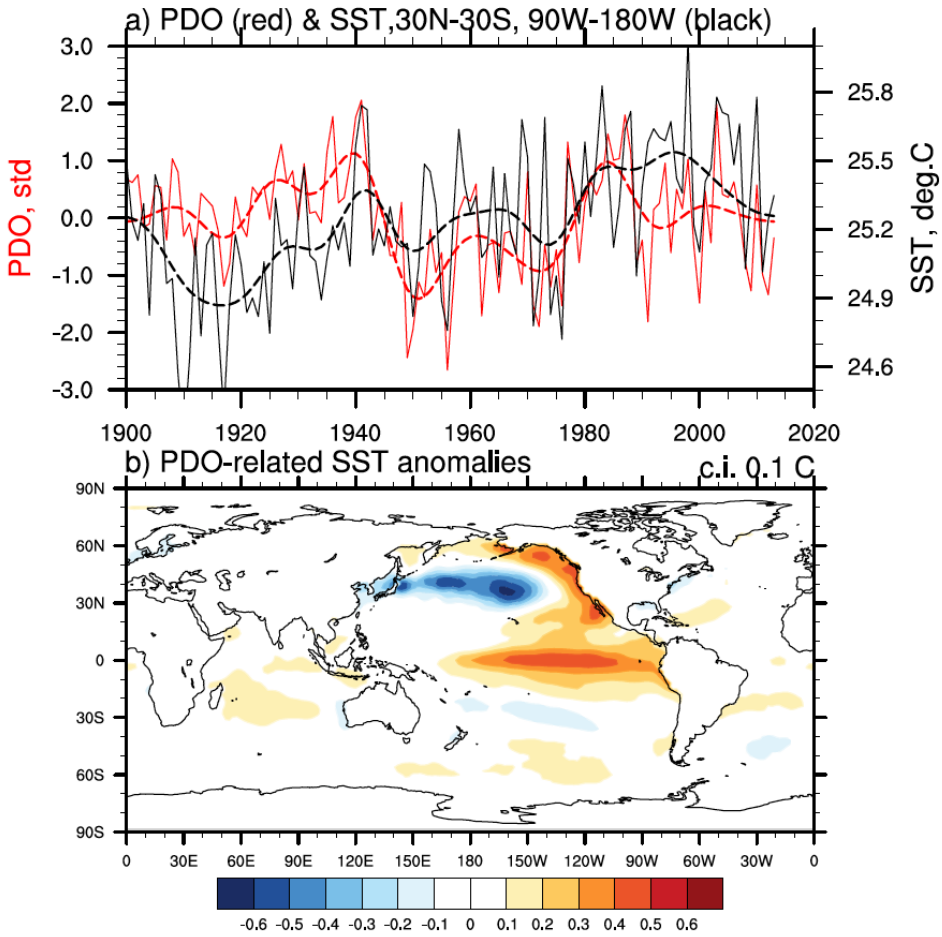

Figure 6.2 (a) Pacific Decadal Oscillation index (red, solid) and SST averaged between 30° N-30°S, 90W-180W (black, solid); dashed curves indicate the time series low-pass filtered to frequencies less than (15 years)$^{-1}$; PDO is defined as the first EOF of the North Pacific monthly SST poleward of 20° N; (b) PDO-related SST anomalies shown as regression map which corresponds to 1 std increase in the PDO index. December-February, 1900-2013.

Indeed, during January and February most of the SAM connection to the Pacific, at least since 1979 appears to be associated with the Pacific Decadal Oscillation whereby the PDO leads the January SAM by 1 month. Figure 6.3 compares SAM index averaged over January and January-February and its component which varies coherently with the November, December and January PDO index. The cross-correlation between the PDO and the SAM is significant at levels greater than 99% assuming a two-tailed test with r = *-0.65/-0.57* for November PDO, r = *-0.69/-0.65* for the December PDO and r = *-0.6/-0.56* for the January PDO before and after removing linear trends respectively. Hence, despite the impact of the ozone depletion on the summer trends simulated by the GCMs, most of the interannual variability in the summer SAM during January and February, at least since 1979, is associated with another mode of tropical variability. The persistence of the PDO and a 1 month lag whereby PDO leads the SAM enables improved seasonal predictions of the SAM.

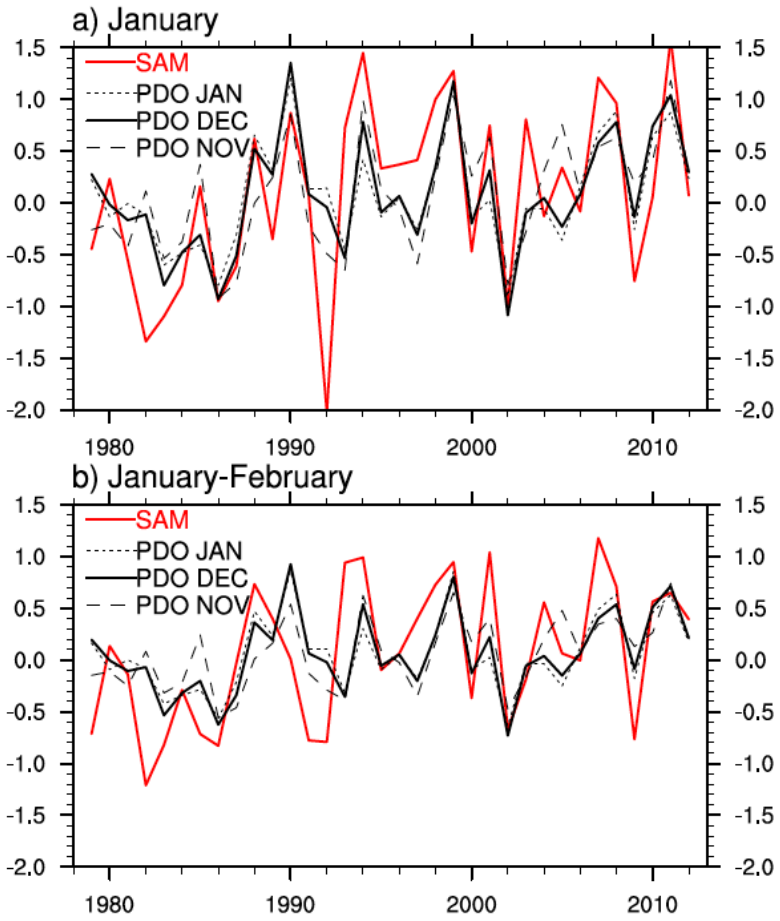

Figure 6.3. January (a) and January-February (b) Southern Annular Mode (red) and its component which varies coherently with the Pacific Decadal Oscillation index during November, December and January (black)

In the next section, I will address the origin of the one month lag between variability captured by the PDO index and the tropically forced anomalies in the midlatitude circulations during summer months

6.2.2 Development of a tropically-forced SAM anomaly following solsticial migration of the circulation poleward

Analogous to its canonical ENSO variability, the PDO index shows a pronounced spatial signal in the variability of the tropical circulations. Essentially, the PDO captures a long-lived anomaly in the tropics, which persists between the seasons and moves together with the seasonal cycle of the equatorial convective systems. Figure 6.4 a-c shows seasonal

drift of correlations between PDO index and zonally averaged geopotential height, zonal wind at 200mb level, lower tropospheric relative humidity (700-850mb) plotted as a function of the latitude. Shown in Figure 6.4d is the serial correlation function of the PDO. A significant correlation value is equal to -/+ 0.34 assuming a two-tailed test and the sample size of 34 years.

Throughout the year, a warm phase of the PDO corresponds to warm anomalies in the tropical geopotential height flanked by cool anomalies that peak in the midlatitudes of both hemispheres. Coherent zonal wind changes suggest simultaneous strengthening of the subtropical jets and the equatorial easterlies. The shape and the magnitude of anomalies in the tropics suggest that PDO index varies coherently with the parameters of both the northern and southern cells of the Hadley circulation. Pronounced subtropical anomalies in the lower tropospheric relative humidity indicate an intensification of the downwelling branches of the Hadley circulation in both hemispheres following a shift towards the negative PDO phase. Though somewhat weaker in magnitude and statistically not significant during winter, an enhanced relative humidity near 5°S, in the vicinity of the thermal equator, suggests an intensification of the upwelling branch of the Hadley circulation.

Essentially, during winter PDO index captures the variability in the Northern Hemisphere Summer Monsoon as described by Wang at al. (2013), however its connection to the tropics is not limited to June-August. Given the high degree of autocorrelation, PDO-related anomalies in the tropics persist on monthly time scales and migrate in latitude following the seasonal cycle of the tropical convection. During the austral winter season, PDO-related variability appears to be limited to the Northern Hemisphere and to the tropics, while during the austral summer season, it does exhibit a hemispherically symmetric signature in the zonally averaged midlatitude circulations. The seasonal transition of the equatorial relative humidity anomalies from 5° N in JJA to 10°S during DJF shows that persistent PDO-related anomaly in the tropics moves in latitude following the seasonal cycle of thermal equator. The poleward migration of the PDO anomalies culminates into a strong interhemispheric signal during DJF and JFM when the thermal equator is located in the Southern Hemisphere and southern subtropical boundary is displaced poleward more than during other seasons. A hemispherically symmetric atmospheric response is present both in the tropical belt and in the extratropics whereby anomalies appear to project on the signature of the annular modes. Indeed, during austral summer the PDO index varies coherently with both the SAM and NAM, which is best seen on time scales greater than several years. Cross-correlation coefficients calculated for

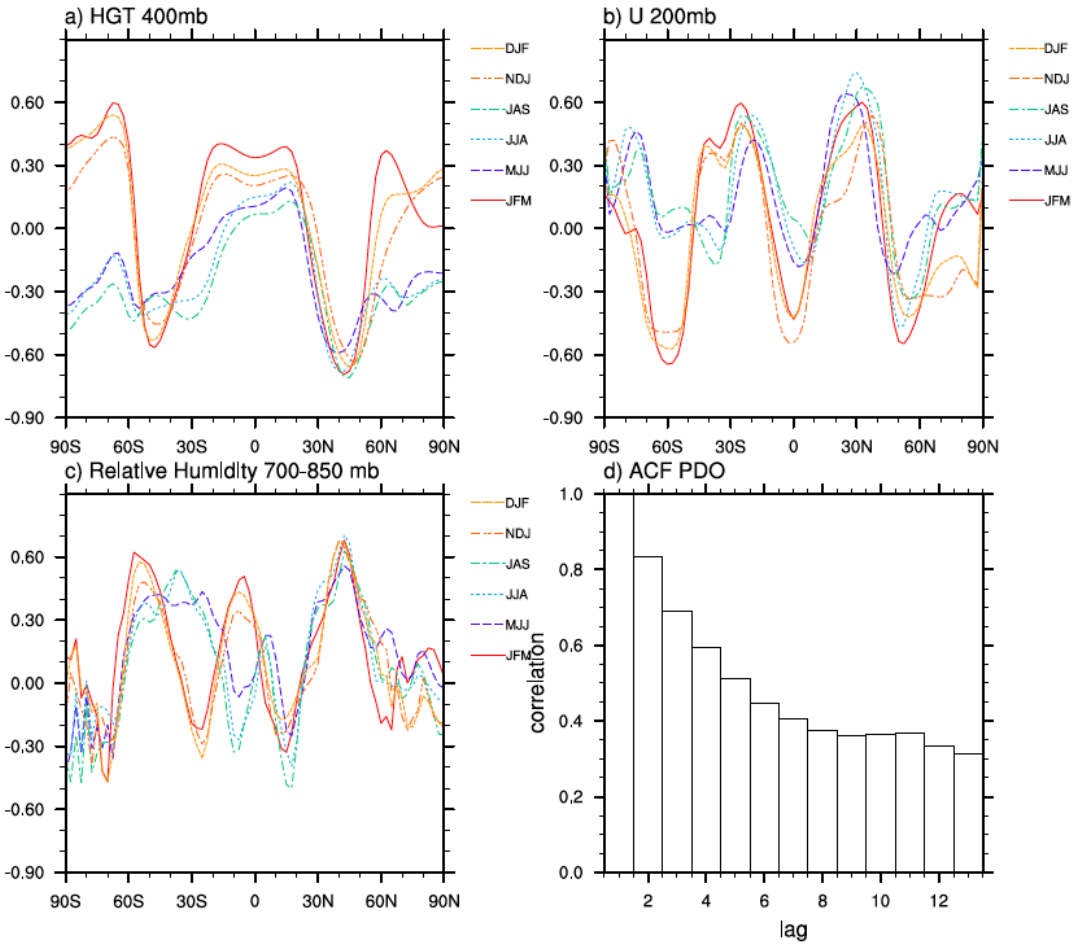

Figure 6.4. (a-c) Correlation between Pacific Decadal Oscillation and zonal mean geopotential height at 400 mb level (a), zonal wind at 200mb (b), relative humidity at 700-850 mb (c). Based of seasonally averaged data covering time period from 1979 to 2013. (d) Auto-correlation function (ACF) of the monthly Pacific Decadal Oscillation index.

unfiltered time series reach -0.51 for the SAM and -0.57 for the NAM (significant at 98 % level) and increase up to -0.6 and -0.78 after applying low-pass filter with cut off frequency equal to $(7 \text{ years})^{-1}$.

Zonally averaged anomalies in the tropics are not very strong since they represent a superposition of opposite signed anomalies in the Eastern Pacific and rest of the tropics which accompany meridional shifts of the Walker circulation. However, they indicate fairly well the seasonal transience of the PDO-related signal in the tropics. The seasonal drift of the PDO-related anomalies in the tropics and a subgrid scale of the processes of interest also explains why the leading EOF of the North Pacific SST, at least under certain conditions, represents a good indirect measure the long-lived ENSO-like tropical variability and captures the link to the SAM. The North Pacific signal does not undergo a seasonal cycle. While the tropical convection is constantly changing, coherent variability in the North Pacific is “fixed” in space and, hence, easily identifiable by EOF analysis of monthly data. In contrast, indices based on

the tropical SST, outgoing long wave radiation and sea level pressure give lower degree of the correlation despite showing significant relationships.

The mechanism which enables a one month lag between PDO-related tropical anomalies and the SAM might then be understood by taking a closer look at the lagged midlatitude circulation response to the PDO-related variability after solstice. Figures 6.5-6.6 illustrates the sequence of events preceding the development of a positive SAM anomaly during January by plotting maps of correlations between the PDO index in November and 3 week averages of sea level pressure, 200 mb geopotential height and 200 mb winds averaged within 3 week window sliding over the calendar year. The first 3 weeks (from 21 December to 10 January) are taken immediately after solstice, the second (31 December-20 January) and the third one (10 January – 30 January) are shifted by 1.5 weeks.

Around the solstice, a cool phase of the PDO corresponds to the deepening of equatorial depressions (low sea level pressure anomalies) and amplification of convection (divergent wind anomalies) over the equatorial South America, Africa and Indonesia. Anomalous patterns of 200mb height anomalies shown in Figure 6.6 indicate a sequence of trough and ridges which extend poleward of convective cells along 30°S. Four anticyclonic anomalies are clearly discernible on the south-eastern flanks of the subtropical highs in the Atlantic, in the Pacific, in the Indian Ocean and poleward of Australia. 1.5 weeks later, the troughs and ridges wrap anticyclonically and extend into the midlatitudes. A positive SAM anomaly with the stronger westerlies along the 60°S and decreased pressure over the polar cap begins to develop reaching its full extent 10 days later, in the middle of January.

The sequence of events which precedes development of the SAM anomaly during January overall resembles an anticyclonic wave-breaking amplified by the poleward migration of the of the subtropical highs after solstice. Indeed, the anticylonic wrapping of the troughs shown in Figure 6.6 takes place in the regions of frequent upper-tropospheric Rossby wave breaking described by Postel and Hitchman (1999) and Berrisford at al. (2007). It was hypothesized in these studies that the episodes of wave breaking in these regions result from the propagation into the subtropics of the Rossby wave trains emanating from the Pacific. As the eddies propagate into the Atlantic sector, they are likely to encounter the poleward side of the subtropical jet and the anticyclonic shear of the subtropical highs. The trajectories of air parcels which precede the wave breaking episodes in the Atlantic are illustrated in Figure 7 in Postel and Hitchmann (1999). The air parcels coming both from the Pacific and from the South America adopt an anticyclonic trajectory upon approaching the eastern flanks of the subtropical highs which results into a wave breaking event. Anticyclonic wave breaking at the decaying stage of the baroclinic lifecycle in turn corresponds to the poleward flux of

momentum in the upper troposphere which would contribute to the positive SAM [Thorncroft at al., 1993].

Preferred propagation pathways of the Rossby waves can be approximated by the E-vectors introduced by Hoskins (1983). The components of the vector are given by:

$$E = (\overline{v'^2 - u'^2}; -\overline{u'v'}) \tag{6.1}$$

where u denotes zonal wind, v denotes meridional wind, a prime denotes deviation from the time mean. Deviations from the time mean have been computed by high pass filtering daily data with a 51-weight Lanczos filter with a cut-off at 15 days.

Figure 6.7 shows PDO-related anomalies and time mean E-vectors of the transient eddies (high pass filtered to frequencies greater than 15 days) during first 3 weeks of January. Under mean conditions E-vectors indicate preference of the transients to propagate into the low latitudes in the vicinity of subtropical highs. Upon approaching the subtropical highs the E-vectors get diverted both northward and eastward assuming an anticyclonic trajectory. Convergence of wave activity is most pronounced on the south-eastern flanks of the subtropical highs in the Pacific and Atlantic, in the regions of frequent subtropical wave breaking events identified in Postel and Hitchman (1999). Deepening of the equatorial depressions contributes to an anticyclonic anomaly on these south eastern flanks of the subtropical highs. The latter is followed by a stronger flux of high pass eddies diverted towards these regions as suggested by anomalous E-vectors in Fig. 6.7a diverted eastward and northward. An equatorward deflection of eddies and an anticyclonic breaking of equatorward propagating Rossby waves is accompanied by a poleward flux of momentum and, hence, is expected to reinforce the westerly winds in the midlatitudes. Indeed stronger westerlies and lower sea level pressure over the polar cap appears to follow the changes in transients.

Upon the solstice the equatorial depressions shift poleward, so do the subtropical jets and the subtropical high-pressure systems. The poleward shift of the circulation after solstice would then increase the probability of the eddies encountering the flanks of subtropical highs and the subtropical wave breaking episodes which would then affect the SAM. Similar processes might be at work in the Northern Hemisphere. For instance, Benedict at al. (2013) considered the synoptic representation of the North Atlantic Oscillation and hypothesized its sensitivity to the location of the subtropical highs in the Northern Hemisphere. A hemispherically symmetric anomaly superimposed on the stationary anticyclones in the subtropics of both hemispheres would then have an impact on both the SAM and the NAM, enabling an interhemispheric connection during austral summer evident in Figure 6.4. The

results are also consistent with the study by Fogt at al (2011). It can be also expected that location of subtropical boundary plays a regulating role in the climate system enabling or prohibiting teleconnections between tropical and midlatitude circulations. In the next section, the sensitivity of the SAM response to the tropical variability in the location of the tropical boundary will be addressed.

6.2.3 Dependence of the tropically-forced variability in the SAM on the location of subtropical boundary during austral summer.

While the PDO influence maximizes in January following the solstitial shift of the circulation, it can also span the entire summer season subject to the mean conditions. The diversion of the transient eddies towards the subtropical highs as they shift poleward in the seasonal cycle and strengthen on the south-eastern flanks in response to a stronger equatorial convection suggests a sensitivity of the annular modes to the changes in the location of subtropical boundary. Since most of the interannual variability in the tropics is associated with ENSO, it is then possible to group the data according to two different mean states of the tropical circulation – the one with strong subtropical jets, contracted and stronger Hadley circulation (El Niño-like conditions) and the opposite (La Niña-like conditions) [Oort and Yienger, 1996; Seager at al., 2003]. Grouping data according to the 1979-2013 DJF Nino 3.4 index would then yield 18 years when the SST in the equatorial Pacific was below its mean (La Niña-like conditions) and 16 years when it was above the mean (El Niño-like conditions). The grouping threshold is based on the climatology of ENSO during the 1979-2013 period.

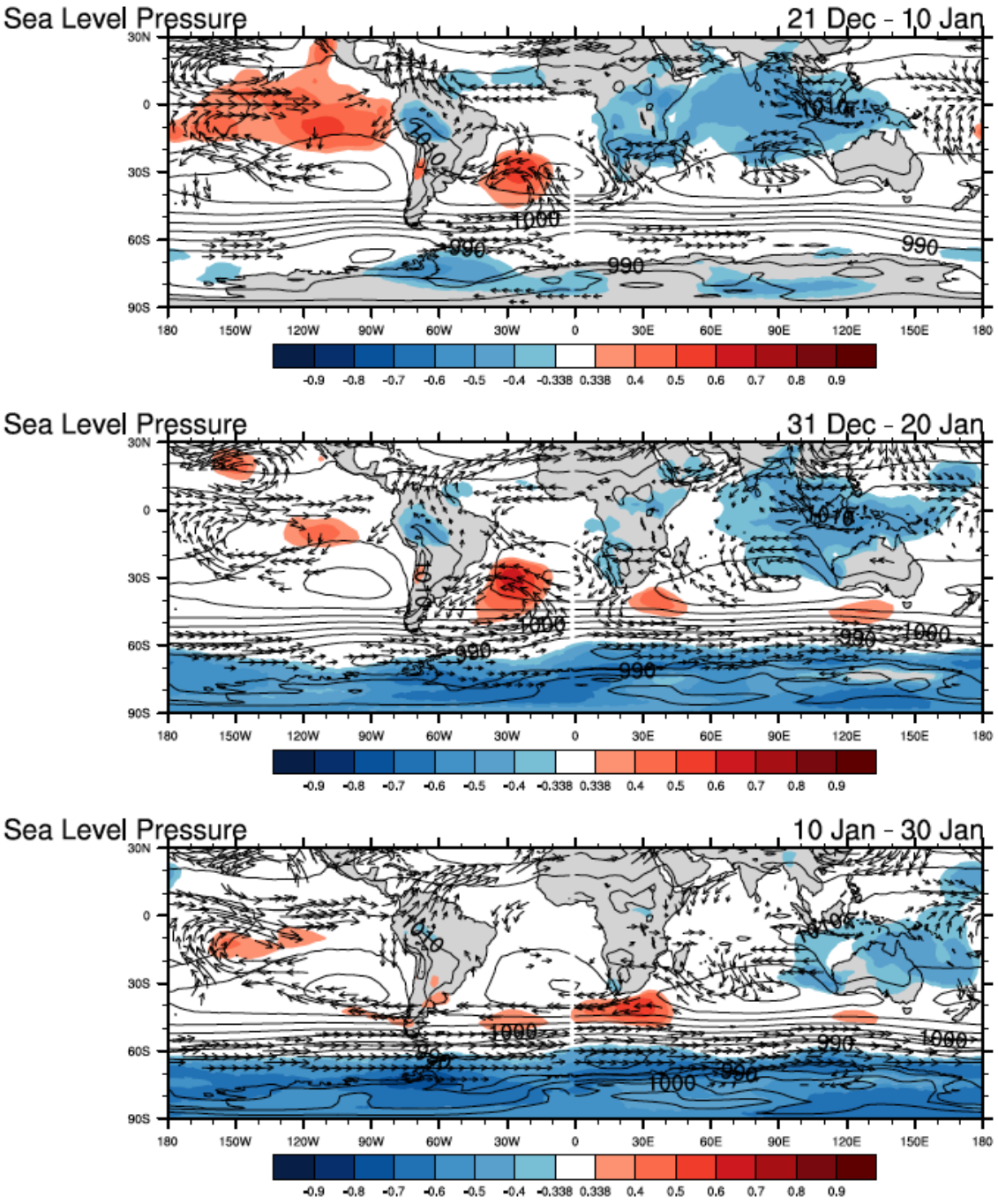

Figure 6.5 Anomalies in 200 mb wind (vectors) and sea level pressure (shading, shown as correlation) related to the Pacific Decadal Oscillation during November. Overlaid is climatology of sea level pressure (black contour, c.i. 5 hPa). PDO index has been inverted so that anomalies are displayed in terms of the cool PDO phase, i.e. La-Nina–like cooling of the equatorial Pacific corresponds to the lower pressure in the equatorial depressions over the South America, Africa and Indonesia right after solstice and to the strengthened of the westerlies along 60°S and low sea level pressure over the polar cap (positive phase of the SAM) during second half of January.

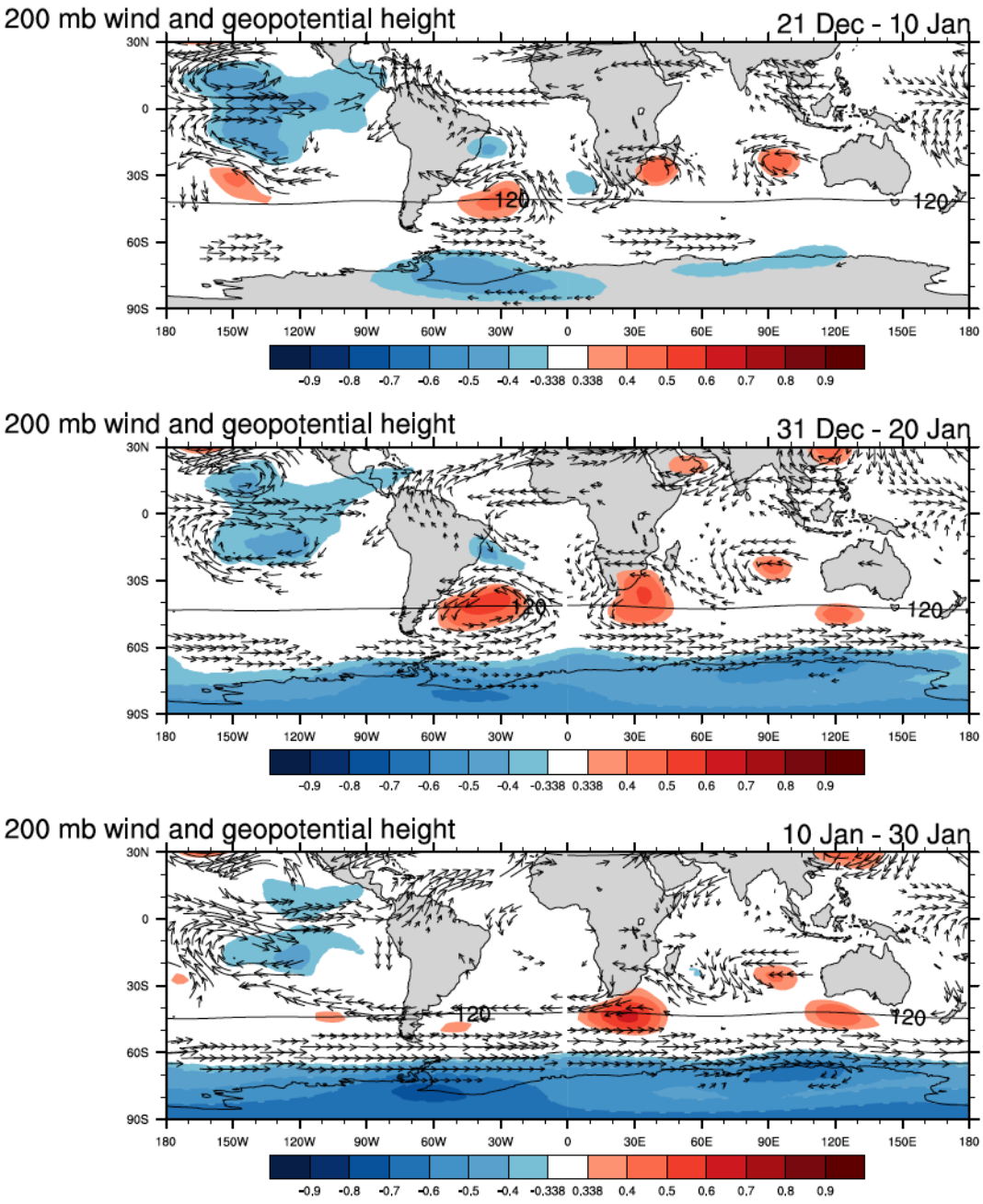

Figure 6.6 Anomalies in 200 mb wind (vectors) and 200 mb geopotential height (shading, shown as correlation) related to the Pacific Decadal Oscillation during November. PDO index has been inverted so that anomalies displayed in terms of the cool PDO phase.

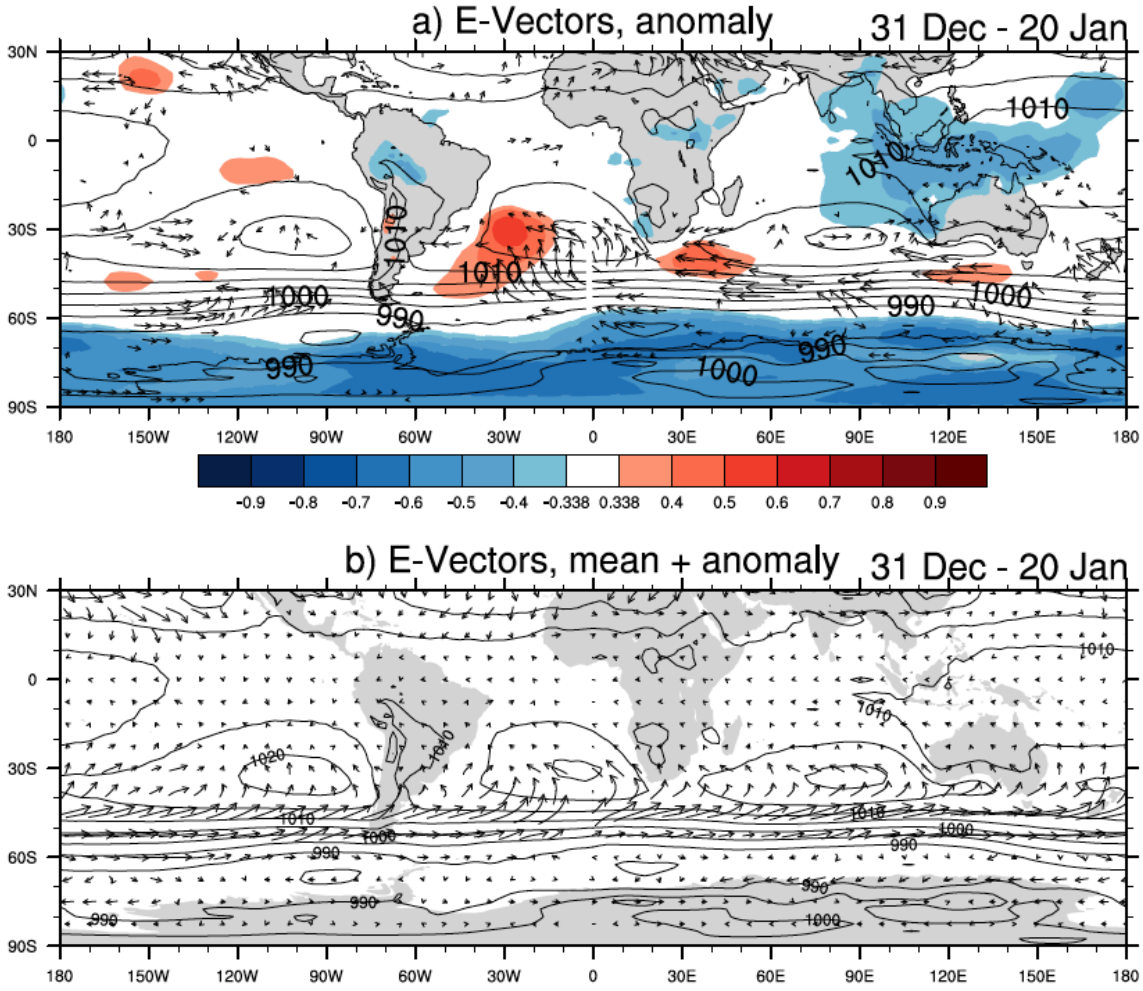

Figure 6.7 (a) Anomalies in 300 mb E-vectors (vectors) and sea level pressure (shading, shown as correlation), (b) sum of the climatology and anomalies in E-vectors related to the Pacific Decadal Oscillation during November. Overlaid is climatology of sea level pressure (black contour, c.i. 5 hPa). PDO index has been inverted so that anomalies displayed in terms of the cool PDO phase.

While grouping the data that way breaks down any low-frequency variability present in the time series, correlations computed based two subsamples show which years tend to amplify coherent high frequency changes between indices and which years tend to break coherency. Table 1 shows correlation between DJF SAM and PDO split according to Nino3.4 index. Additionally, correlation with the Northern Annular Mode index is provided to illustrate existence of hemispherically symmetric variations in response to the tropical variability and with the Nina 3.4 index to illustrate difference between canonical ENSO and its long-lived analogue. The NAM index is defined using the first EOF of the 1000mb geopotential height field poleward of 20° N. Indeed, years that amplify PDO impact on the SAM show existence of coherent changes between the hemispheres. Most of the coupling between PDO and SAM, NAM and SAM appears to come from La Niña years (r = -0.82 and

-0.73 respectively) and is close to absent under El Niño conditions. Interestingly, there is no strong correlation with the ENSO index itself based on grouped data.

Table 1. Correlation between Southern Annular Mode (SAM) and Northern Annular Mode (NAM), Pacific Decadal Oscillation and Nino3.4 under La-Nina- and El Niño-like mean states, December-February, 1979-2013[2]

	Correlation with the Southern Annular Mode, DJF			
	Number of years	NAM	PDO	Nina 3.4
La Niña (Nino3.4 ≤ 26.7)	18	0.73*	-0.82*	-0.34
El Niño (Nino3.4 > 26.7)	16	0.14*	-0.11*	-0.42

The dependence on the ENSO phase further confirms that stronger tropically forced anomalies in the SAM are favoured by conditions accompanying a wider Hadley circulation with subtropical jets and subtropical high-pressure systems shifted poleward. As it will be shown below, there exists a close to linear dependence between strength of connection between SAM, PDO and the NAM on the location of subtropical boundary. During summer the subtropical jet maximum in the Southern Hemisphere appears to be merged with the secondary eddy-driven jet maximum, hence, there is no straightforward way to compute its parameters. Besides, the extent of the tropics can be determined using different measures, such location of trade winds, subtropical tropopause, latitude of transition from Hadley to Ferrel cell or of a subtropical jet. Despite being related, these diagnostics are controlled by different dynamical processes and, hence, a change in one measure doesn't necessary imply a change in the other [Levine and Schneider, 2011]. Plus the relationship between upper and lower, upwelling and downwelling branches in the Hadley circulation is far from linear. The latter contributes to the uncertainty in the estimating the exact location of subtropical boundary. However, the changes in the Hadley cell extent evaluated from the mass stream function in the upper branches (at 600-200mb) which form the subtropical jet should reflect changes in subtropical terminus which can affect the propagation of the extratropical waves through the modification of the subtropical jet. Figure 6.8 shows time series of latitudes of the

[2] Asteriks * denotes significant (at 95% level) differences in ***r*** as estimated using Fishers *r-to-z* transformation

southern boundary of the Hadley circulation averaged between 600 and 200mb. Consistent with the previous studies, the mass stream function based index of the subtropical terminus exhibits much of the ENSO-related variability on a background of a strong trend towards poleward shift of the tropics. It should be noted, however, that, even during satellite era, the reanalysis doesn't capture well the trends in circulation parameters which involve first and higher order derivatives and might exhibit internal drift in such diagnostics [Mitas et al., 2005-2006].

Grouping the SAM, PDO and NAM indices according to the latitudes of the subtropical terminus estimated from the mass stream function yields a close to linear relationship between strength of coupling and latitude of the tropical belt. Figure 6.9 shows the correlation coefficient between PDO/NAM and SAM as a function of the location of the subtropical boundary. By arranging the years within 1.5 degrees bands of subtropical boundary locations, more than 20 different combinations of years can be formed with 3 non-overlapping groups. The correlation coefficient tends to increase following the poleward shift of the tropics reaching its maximum values of ~0.8 when the subtropical boundary is poleward of 35.5°S. Analogous increase in the strength of relationship can be found between NAM and Pacific Decadal Oscillation by shifting the mass stream function based index of northern subtropical boundary (not shown). The relationship does maximise when the Northern Hemisphere subtropical boundary is poleward of 29.5° N.

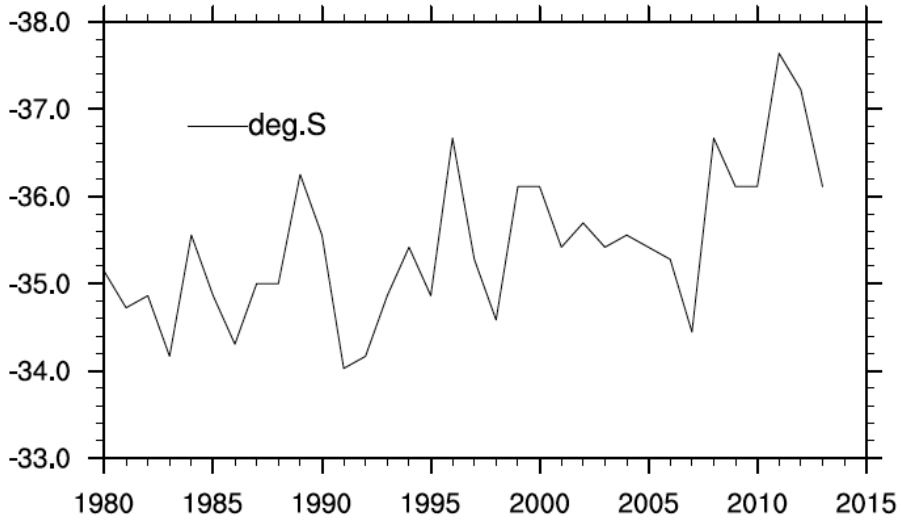

Figure 6.8. Latitude of the southern boundary of the the Hadley circulation, December-February , 1979-2013. The subtropical boundary is defined as the latitude where mass stream function changes sign (averaged between 600 and 200mb).

Contrary, grouping data within 2 degree bands of the equatorial SST measured by Nino3.4 index yields a rather abrupt transition when temperatures drop below 27C. When Nina 3.4 index falls within upper groups of values, the correlation between PDO and annular modes fluctuates around 0.35/0.45 without a pronounced tendency to increase.

It can be then expected that any systematic change in location of subtropical boundary will result not only in the positive SAM trend, but also into a stronger impact of the tropical variability on the midlatitude circulations enabling a stronger interhemispheric connection. In the next section, decadal variability in the impact of the PDO-related variability on the SAM will be addressed.

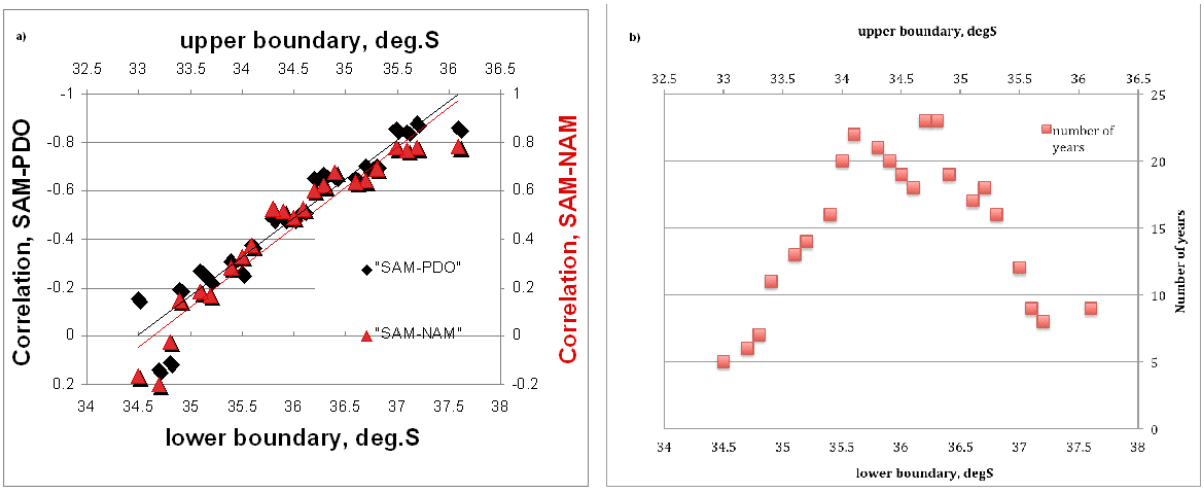

Figure 6.9. (a) Correlation between Southern Annular Mode and Pacific Pecadal Oscillation (blue), Nothern Annular Mode (green) shown as a function of the latitude of subtropical boundary, DJF, 1979-2013. Lower boundary is denoted at the bottom X axis, upper boundary – at the top X axis. (b) Red markers denote number of years within the respective range of subtropical boundary locations. Based on detrended data. December-February, 1979-2013

6.2.4 Tendency towards stronger tropically-forced variability in the SAM and a stronger interhemispheric connection observed over the last 55 years

Figure 6.10 compares December-February PDO, the Northern Annular Mode and an observation-based Marshall's SAM index [Marshall at al., 2003], which covers time period since 1957. Extending record up to 1958 worsens the relationship between SAM and the PDO reducing correlation up to -0.18. Connection appears to be close to absent prior to 1976 and shows a tendency enhance over time becoming pronounced during last 15-17 years (marked in bold). The coherent anomalies between the SAM and the PDO are also congruent with a

link to the Northern Annular Mode with a strong interhemispheric connection prevailing since approximately 1995 (marked in bold).

To track the changing relationship between annular modes and the PDO, the time-evolving Pearson correlation coefficient is plotted. Figure 6.9a shows windowed correlation computed over 15 year sliding time intervals. Each value is centered at the middle of the time window considered. The strength of the connection appears to have been gradually increasing over the past 55 years resulting into a synchronisation of the annular modes reaching its peak during 1995-2008 (r = 0.92). Since approximately 1998 the correlation of the SAM index with PDO

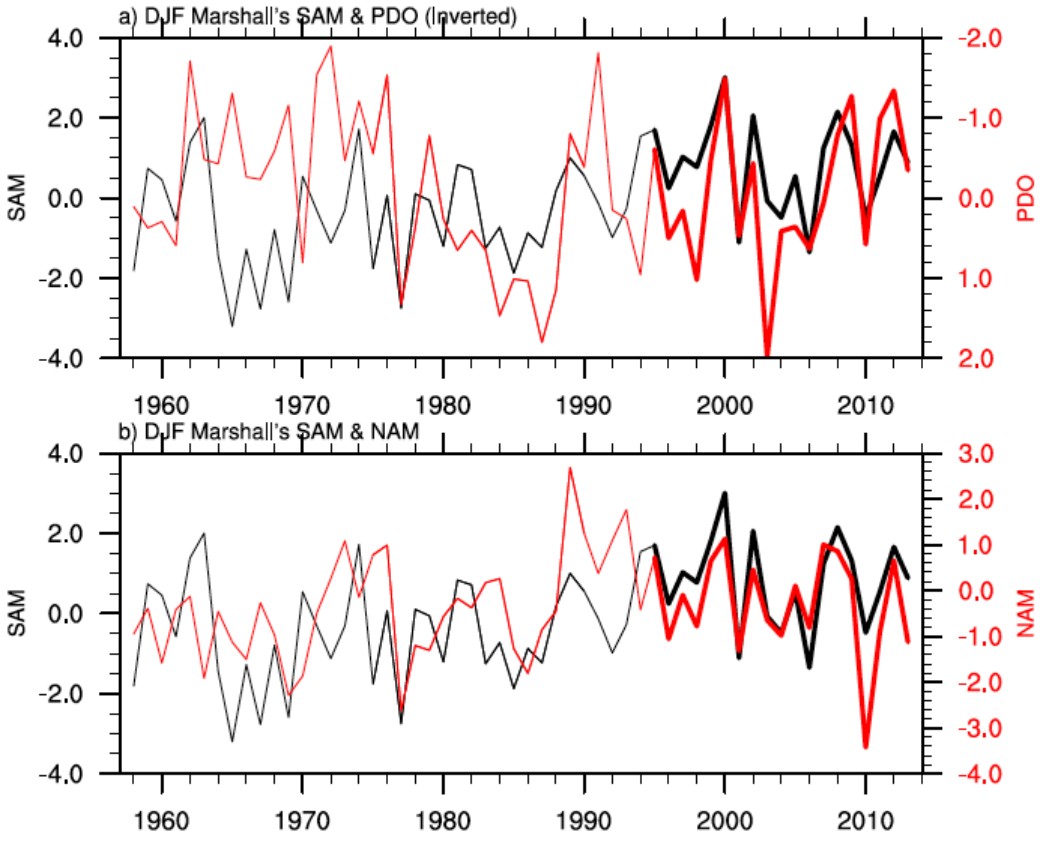

Figure 6.10 Marshall's Southern Annular Mode index and Pacific Decadal Oscillation (a), Northern Annular Mode (b). December-February (c), 1957-2013.

and NAM remains stable at the level of ~0.78. The weakening in the connection during early 90's could be attributed to the impact of the 1991 Pinatubo explosion on the oceans which disrupts the PDO signal. I.e. due to the very long relaxation time of the ocean the radiative cooling of the ocean after an explosion tends to persist over a range of time scales [Stenchikov et al., 2009]. Additional short-live (2-3 years) perturbations in the aerosols emitted by volcanoes make years after strong explosions outliers which can disrupt the relationships observed under normal conditions. Windowed correlations between PDO index

and tropical SST over the last century (not shown) suggest a relationship stable over time except the years directly following the Pinatubo eruption when it was undetectable. Omitting winters of 1992-1994 yields then a nearly steady increase in the strength of climate system coupling (Fig. 6.11b). Using Fisher r-to-z transformation and sample size N =15, it can be estimated that the confidence intervals for r = 0.9/0.8 is equal to {0.72,0.97} and {0.48,0.93} respectively. Hence, despite a short sample size the decadal variations in the correlations appear to be significant. The coupling is more pronounced during January where it started approximately since 1976 and later extended into December and February becoming pronounced at seasonal time scale. It must be noted that the period considered includes 2 cold PDO events and one warm. The strong relationship with the SAM was observed on the background of the cold PDO phase during 2000's, however it was completely absent during cold PDO phase of the 1960's.

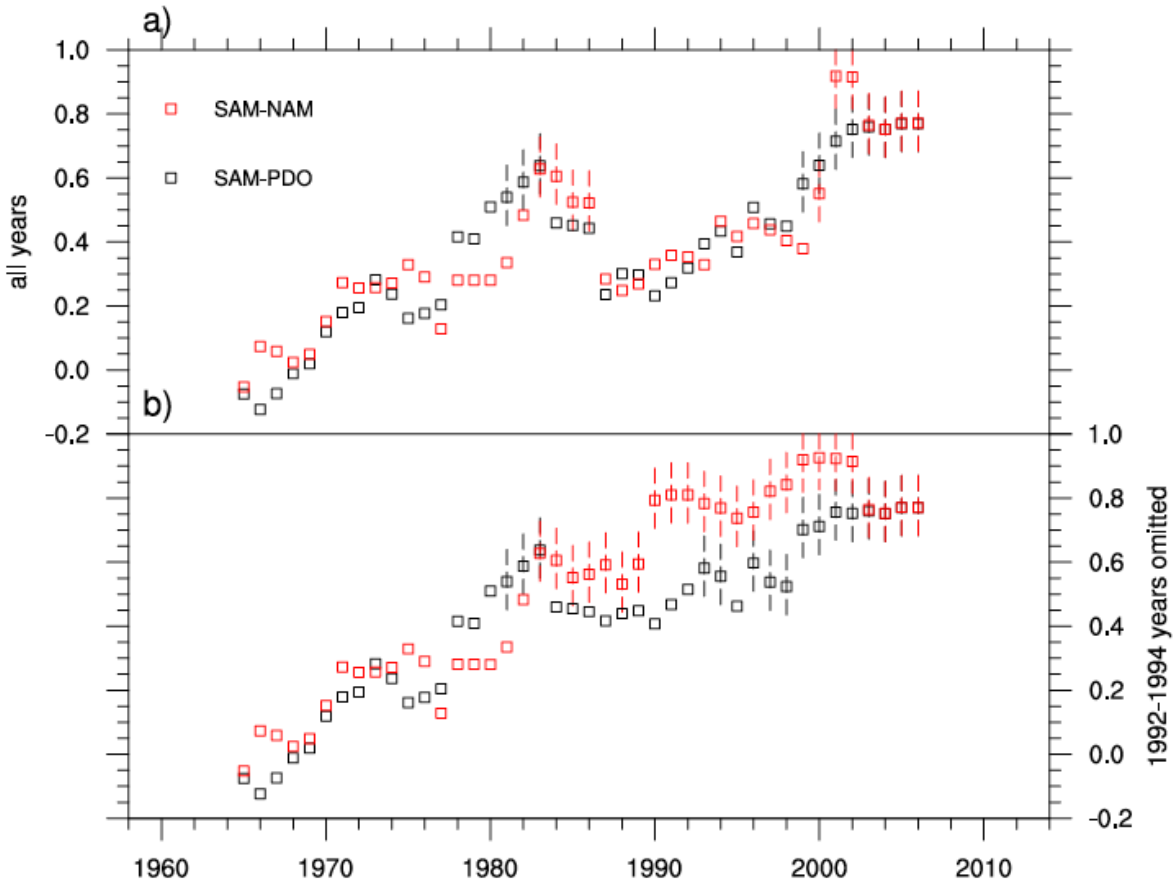

Figure 6.11 Windowed Pearson correlation between the Southern Annular Mode and Pacific Decadal Oscillation (black), Northern Annular Mode (red) computed over 15 year sliding time intervals. Top: all years; Bottom: Pinatubo years (1992-1994) omitted. Each data point is centered at the middle of time window. Based on detrended data. Values significant at 95% level and higher are marked with a vertical bar.

Interestingly, the relationship between NAM and PDO, while more stable over time (due to internal feedbacks between the North Pacific SST, Aleutian Low and the NAM that are independent of tropics), appears to have been slowly increasing as well, overall following the curve in Fig.6.9 (not shown). The latter is in line with the study by Feldstein (2002) which found that the Northern Annular Mode exhibited not only the shift in the mean but also an increase in the variance of its index over the past 60 years.

6.2.5 Influence of tropical belt extent on the wave-mean flow interaction with subtropical jet

The dynamical concepts of the wave-mean flow interaction provide a framework useful in describing the impact of the wind shear in the subtropical highs on the propagation of wave trains. So, the timing anticyclonic Rossby wave breaking corresponds to an absorption of wave activity flux in the upper tropospheric subtropics at the decaying stage of a baroclinic lifecycle (compare Figure 15-16 at days 5-9 in Thorncroft at al. (1993)). At the same time, upward and equatorward Rossby wave propagation is known to be a part of SAM variability [Lorenz and Hartmann, 2000].

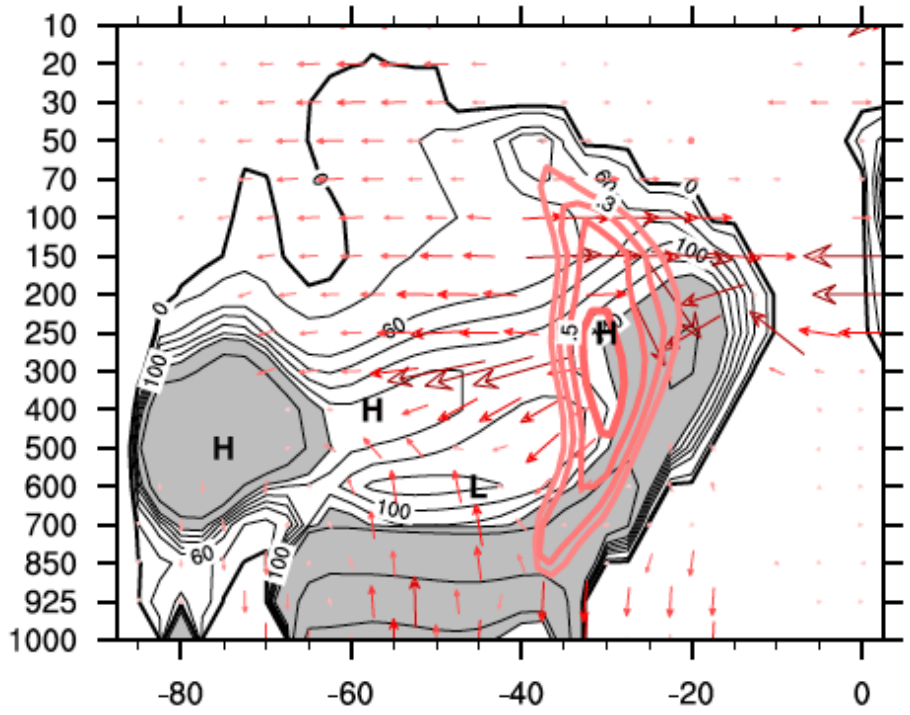

Figure 6.12. SAM-related Eliassen Palm Flux anomaly (vectors, corresponds to the negative SAM phase), climatology of refractive index for stationary wave with zonal wave number 1 (black contour, contours greater than 140 are shaded) and correlation between refractive index and latitude of the SH subtropical boundary (red contour, first contour is equal to 0.3 and then increases by 0.1). December-February, 1979-2013.

In that perspective, the dependence of the tropical influence on the SAM on the extent of the tropics can be understood in terms of subtropical jet influence on the wave propagation discussed in previous chapters. Figure 6.12 plots anomalous EP Flux which corresponds to 1 std decrease in the SAM. Overlaid is the climatology of the refractive index for zonal wave number 1 defined as the median of the daily values during December-February, 1979-2013. As follows from Fig. 6.12, the anomalous propagation of wave activity in the upper troposphere which controls the SAM [Lorenz and Hartmann. 2000] essentially follows the isolines of the refractive index climatology. The latter is characterized by the presence of a belt of high index values which extends from the midlatitude middle troposphere towards the subtropical jet. The waves tend to avoid regions of a negative refractive index and get attracted to the values of a higher refractive index to be absorbed there. Hence, it is the gradient of refractive index which appears to control the direction of anomalous waves fluxes at these levels. In fact, there is a strong correlation (up to 0.7) between SAM index and refractive index of subtropical jet.

The latitude of subtropical boundary computed from mass stream function should reflect changes in the position and meridional profile of subtropical jet and its refractive index. Pink contours in Figure 6.12 indicate the cross-correlation between latitude of subtropical boundaries presented in Fig. 6.8 and the median of refractive index. As the tropics get wider, the refractive index of subtropical jet along 30°S tends to increase as well. Figures 6.13 and 6.14 display the time series of subtropical and midlatitude refractive indices at {500mb, 55°S} and {300mb, 30°S} and the latitude of subtropical boundary. As follows from the graphs, the poleward shift of the circulation has been accompanied by an increase in the meridional gradient of refractive index in the upper troposphere. The subtropical maximum started to exceed the midlatitude one since ~1999. Under such conditions the propagation of atmospheric waves towards higher values of refractive index can be to a greater extent controlled by the variability of subtropical jet than internal feedbacks in the extratropics. Indeed, the time period when the subtropical maximum greatly exceeds the midlatitudes one roughly coincides with the period of enhanced coupling between northern and southern annular modes. It can also be noticed that since the middle 90's the subtropical and midlatitude refractive index maxima appear to vary coherently as well. The correlation coefficient between detrended time series during first half of the record (1980-1993) is equal to 0 and during second half of the record (1994-2103) increases up to 0.7.

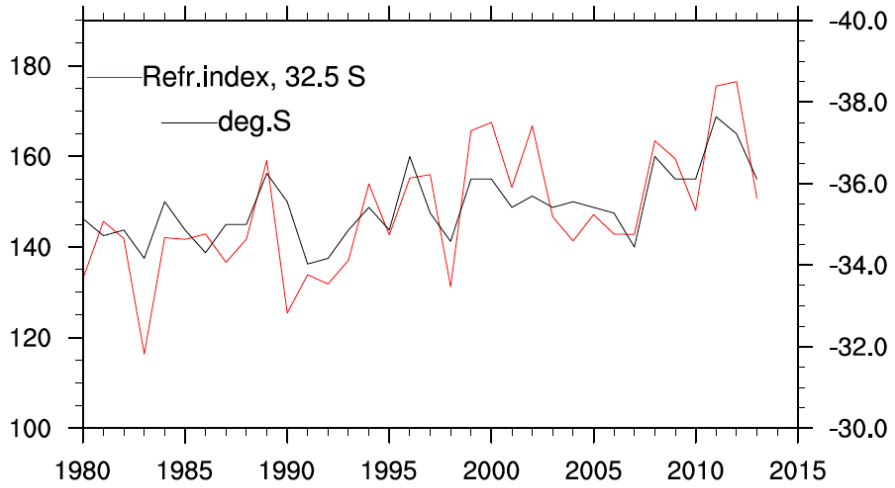

Figure 6.13. Latitude of subtropical boundary and subtropical {250mb,32.5°S} refractive index by stationary zonal wave number 1 during December-February, 1979-2013.

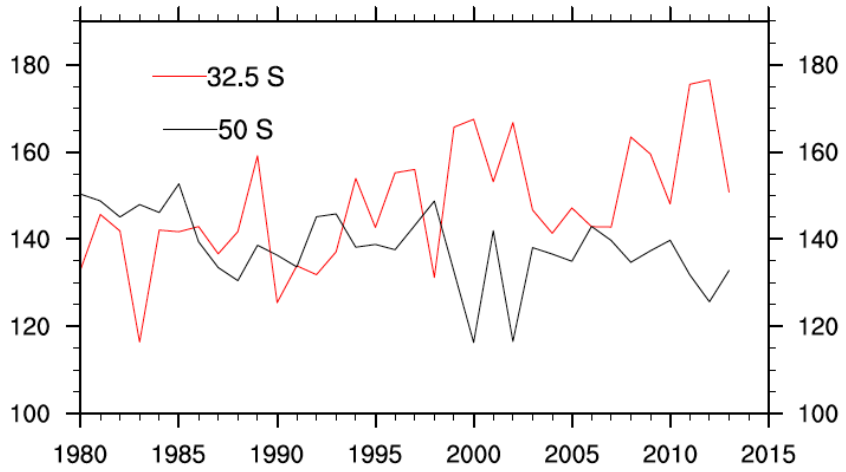

Figure 6.14. Midlatitude {400mb,50°S} and subtropical {250mb,32.5°S} refractive index by stationary zonal wave number 1 during December-February, 1979-2013.

6.2.6 Incorporating stratospheric and tropospheric aspects of the summertime SAM variability

Non-stationarity of the PDO impact introduces the problem similar to that of heteroscedasticity in applying regression analysis to the SAM whereby the variance of the error terms in no longer stationary and depends on some external parameters. Therefore, using linear multiple regression to account for both persistence due to the stratospheric influence and the influence of the tropical ocean requires taking into account the time dependence. The latter implies that both the intercept and the slope vary across ***t*** subject to changes in the mean state:

$$y_t = \alpha_t + \beta_{1t} x_{1t} + \beta_{2t} x_{2t} + e_t \quad (6.2)$$

where y_t denotes SAM, x_{1t} denotes PDO, x_{2t} denotes stratospheric forcing, e_t denotes residuals.

The latter is illustrated in Figure 6.15 which shows squared residuals e_t^2 computed as the difference between observed DJF SAM and its component which varies coherently with the PDO as a function of the latitude of the SH subtropical boundary:

$$e_t^2 = (y_t - \hat{y}_t)^2 \quad (6.3)$$

$$y_t = \hat{\alpha} + \hat{\beta} x_{1t} \quad (6.4)$$

As it follows from Fig. 6.15, residuals squared show an increase in variance as the latitude of subtropical boundary contracts towards the equator. To allow for time-varying linear relationship between the SAM, PDO and stratospheric influence, the sample is split into three subsamples subject to the location of subtropical boundary and ordinary least squares estimates of the slope and the intercept are computed separately for each subsample. It is then assumed that

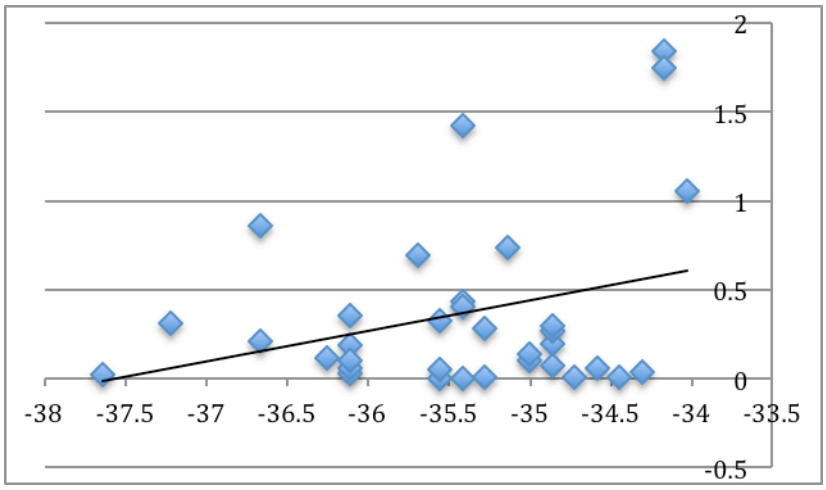

Figure 6.15 Squared residual terms computed as the difference between the observed SAM and its linear fit to the PDO and shown as the function of the SH subtropical boundary

under anomalous mean states either the variability of the SAM is fully decoupled from the PDO or PDO largely dampens other variability, such as the persistence related to the stratosphere. Under such extreme conditions only one explanatory variable in regression is used, that is planetary wave forcing ***Fz*** under narrow tropics or PDO under expanded tropics. Under the intermediate conditions both factors play a role and both Fz and PDO are included

as explanatory variables. Best results are achieved by limiting “extreme” narrow and wide conditions to 5 “outlier” years. Thus, first two subsamples includes 5 “outlier” years when the tropics were exceptionally narrow (<34.5°S) or wide (>36.2S) and the third subsample includes 24 years in between. For the 24 years of data excluding anomalous years, correlation between predicted SAM and the observed one reaches 0.78. Adding 10 years of data with exceptionally narrow or wide tropics improves correlation up to 0.85 (both with and without trends). The predicted SAM is shown in Figure 6.16.

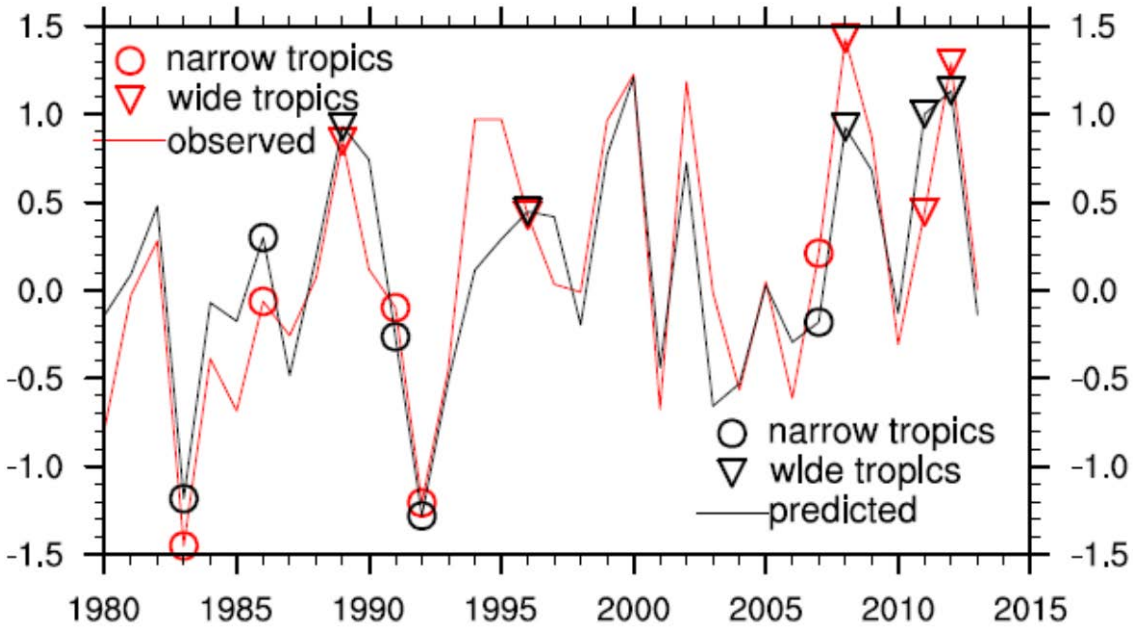

Figure 6.16 Southern Annular Mode: observed (red) and predicted (black) based on linear regression with two explanatory variables: springtime stratospheric planetary wave forcing and the Pacific Decadal Oscillation. Regression coefficients vary subject to the changes extent of tropics (see text for details).

To test the sensitivity of the time-varying regression to the choice of the outlier years as well as to the small 5 year subsample sizes, a set of Monte Carlo experiments is performed. Namely, 10000 random indices are generated of length 34 years and each index (thus SAM, Fz and PDO and randomly permuted) is split into 3 subsamples of length [5, 5, 24] according to the analysis above. The time varying regression is then performed based on the observed time series of the SAM, Fz and PDO and random indices. Histogram of estimated correlations between the observed and predicted SAM is shown in Figure 6.17. Only in 1 (with trends) and 6 (without trends) cases out of 10000 correlation exceeds 0.85. Hence the likelihood of the observed dependence on the mean state being random is less than 0.001%.

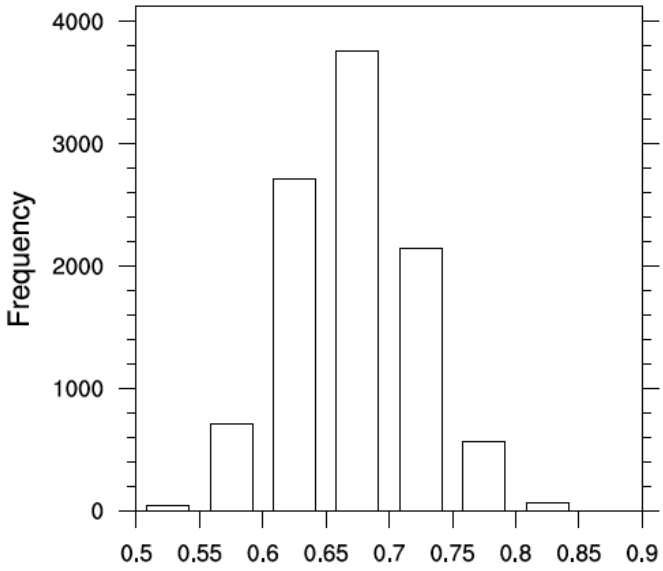

Figure 6.17 Sensitivity of regression parameters to the choice of mean state: distribution of estimates of correlation between the observed SAM and predicted based on multiple regression with two explanatory variables: springtime stratosphere variability and PDO and time-varying regression coefficients. Based on 10000 samples with random indices for mean state (see text for details).

Thus, the strength of coupling between annular modes and PDO enabled through the tropical circulation appears to be regulated by the location of subtropical terminus and associated changes in the mean state. Once the extent of tropics exceeds certain threshold, tropical variability begins to dominate extratropics. While during years with contracted tropics (which include Pinatubo years), in the absence of other factors, stratospheric signal becomes more pronounced and extends into January-February.

6.3 Conclusions

The stratospheric and tropospheric aspects of the summertime variability in the Southern Annular Mode have been examined. It is found that impact of the springtime stratospheric variability extends into the summer circulation and contributes significantly to the persistence of the SAM at a seasonal time scale. The year-to-year variability in this persistence depends on the springtime forcing of the stratosphere by planetary waves. The springtime seasonal maximum of the latter sets up the anomaly in the summertime stratospheric vortex, which prevails during the next several months when the planetary wave forcing is absent. It can be argued that the lower stratosphere acts as persistent upper boundary condition which can influence the circulation through the mechanisms independent of the downward reflection of wave activity described in chapter 4 and unless disrupted, it

will affect the SAM until the next autumn. The degree to which summertime SAM is affected by the stratosphere depends, however, on the mean state of the circulation and in particular, the location of subtropical boundary. Once the subtropical terminus intrudes poleward, the tropically-forced anomalies in the SAM begin to dominate over the stratospheric link.

The tropical influence is most pronounced in January. Upon solstice, as the thermal equator and the tropics migrate toward the South Pole, the influence of the tropical variability becomes the dominant factor in the predictability of the SAM. The anticyclonic wind shear of the poleward intruding subtropical highs begins to affect pathways of the Rossby wave trains propagating into the subtropics. Upon approaching the southern flanks of the subtropical highs, the transient eddies coming both from the Pacific and from the Atlantic adopt an anticyclonic trajectory which results into a wave breaking event and a shift towards positive SAM phase. The zonally symmetric anomalies superimposed on the climatology of subtropical highs and related to the impact of the long-lived ENSO-like variability on the equatorial depressions become then the dominant factor in driving the variability and predictability of the SAM after solstice. This variability is captured by the index of Pacific Decadal Oscillation. Throughout the year it correlates significantly with the different parameters of the tropical circulation. The coherent anomalies migrate in latitude following the seasonal cycle of the equatorial depressions. Once the thermal equator shifts in the Southern Hemisphere, the PDO signal begins to correspond to a hemispherically symmetric signal which has an impact on both the SAM and the NAM.

It is then shown that interannual variability and trends in the mean extent of the tropics play an important role by regulating the relative role of the stratospheric and tropical impact on the SAM. Under conditions typical of La Niña or the subtropical boundary shifted poleward the influence of the PDO begins to dominate, under La Niñas or contracted tropics, the stratospheric signal is more pronounced. A systematic poleward shift of the subtropical boundary increases then the probability of the eddies encountering the flanks of subtropical highs and the subtropical wave breaking episodes which reinforce positive phase of the SAM. Indeed, the expansion of the tropical belt observed during December-February has been accompanied by a tendency towards stronger impact the tropical PDO-related variability on the SAM and has resulted into a synchronization of the northern and southern annular modes since approximately 1997.

Overall, the results suggest that location of subtropical boundary plays a regulating role in the climate system by either enabling of prohibiting the impact of the tropics on the midlatitude circulations, teleconnections between the hemispheres and enabling regime shifts with a change of controlling mechanisms. The results contribute to the growing body of

evidence of nonlinear interactions between tropical and extratropical circulations. So Staten and Reichler (2013) examined the ratio between shifts in the Ferrel cell and boundary of the Hadley circulation in the Southern Hemisphere in GCMs and reanalysis datasets. They found that tropical mean state might govern this ratio on decadal time scales by modulating the year–to–year variability in the impact of midlatitudes eddies on the HC extent and that the latitude of HC is more susceptible to the eddies when it is shifted poleward. Similarly, Kidston et al. (2013) find that correlation between the edge of the HC and the latitude of the eddy-driven jet depends on the time-mean separation between the two. Benedict at al. (2003) hypothesized that a poleward shift of subtropical highs could contribute to the positive trend on the NAO through its impact of propagation of wave trains. The results also hightlight the plausibility of the coherent low frequency variations in the major modes of extratropical ciruclations observed in the recent paleoclimatological studies. So, a low frequency analogue of the current state could be considered the Medieval Warming period when a poleward migration of the subtropical ridge was accompanied by the shift towards the positive SAM phase on a background of a shift towards Central Pacific La Niñas[Goodwin at al., 2013].

The tendency towards enhanced coupling can't be accounted for by the PDO entering its cool phase alone. As shown in Fig. 6.10, the cool PDO phase prevailed in the 60's and 70's, however, unlike during last 15 years the connection between annular modes and PDO is absent. For instance, extending the Marshalls index prior to 1979 shows that the dependence on the ENSO phase analogous to that in Table 1 can be obtained only by setting the Nina 3.4 threshold much lower basically limiting the earlier dataset to the strongest La Niña events (i.e., 1974 &1976). In light of the analysis presented in this chapter, an interhemispheric connection would require a zonally symmetric anomaly in the tropics superimposed on the poleward intruding subtropical highs and jets. To check, whether the observed coupling could result from the internal variability of the present day atmosphere alone, strength of connection between the annular modes has been compared in the 10000 run of Mk3L model (see ch. 2.5 for details). While windowed 15 year correlations tend to fluctuate around zero mean, the Mk3L model exhibits periods of formally significant interhemispheric connections related to the ENSO. However it fails to exhibit any periods of prolonged coupling whereby the strength of the connection between the SAM and the NAM significantly increases over 30 years and reaches the strength comparable to the last 15 years.

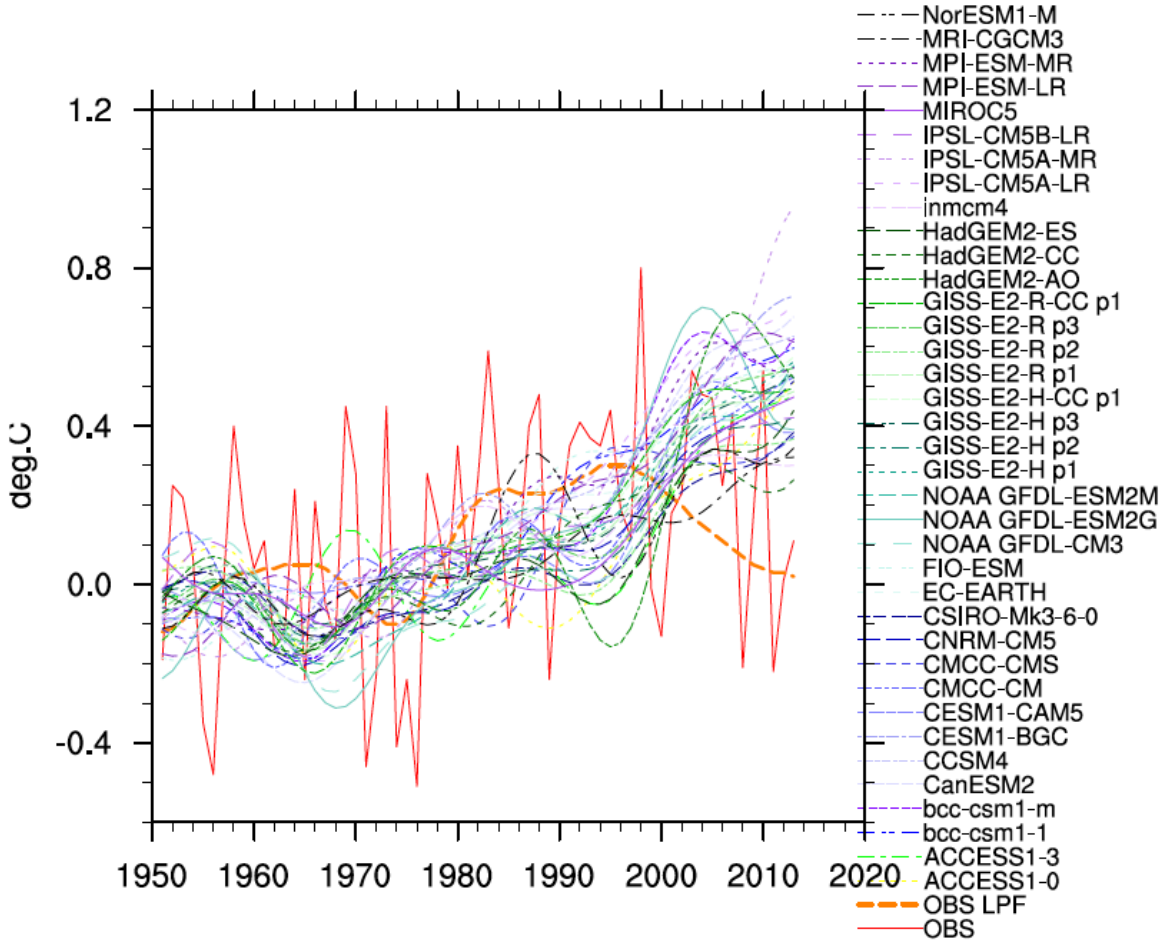

Figure 6.18 SST averaged between 30° N-30°S, 90W-180W, observed and simulated by selected CMIP5 models. The time series have been low-pass filtered to frequencies less than (15 years)$^{-1}$. December-February, 1950-2013.

Hence, it might be argued that recent coupling during the 60's could be an artefact of either an anthropogenic expansion of the tropical belt or changes in the natural variability (poorly represented in the models) which made the PDO signal in the tropics more zonally symmetric. For example, a shift of the Pacific SST variability from the Eastern into the Central Pacific [Ashok at al., 2007; Kao and Yu, 2009; McPhaden at al., 2011] might have played a role in these changes. A comparison of CMIP3/5 models conducted in the studies by [Deser et al., 2011; Furtado et al., 2011; Lienert et al., 2011] has shown that while approximately half of the models exhibit PDO-like variability, generally, they tend to underestimate the tropical-extratropical connection. Hence, understanding the rationale behind recent changes requires improving representation of different types of ENSO-like variability in the simulations.

While the results don’t contradict the role of the stratosphere in driving trends, the relative role of the low-frequency variability in the tropical Pacific on the SAM trends needs better quantification. In particular, the CMIP5 models have been shown to underrepresent the nit only the tropical connection of the Pacific Decadal Variability but also the links of the SAM to the SST [Karpechko at al., 2009]. Most importantly, the majority of CMIP5 models don’t capture the recent cooling phase of the PDO. Figure 6.18 compares the SST averaged over tropical Pacific between 30° N-30°S and 90W-180W, observed and simulated by selected CMIP5 models over historical period (1950-2005) and according to RCP4.5 scenario (2005-2013). Unlike the observations, the models show a pronounced warming trend which, given the relationships described in this chapter, can’t contribute to the positive SAM phase. At the same time, as shown in chapter 1, the downward descent of polar vortex anomalies in the CMIP5 models is shifted later into the season compared to the observations. Hence, a better representation of the summertime SAM trends and better seasonal predictions require both a realistic stratospheric seasonal cycle and better representation of a long-lived ENSO-like variability in the tropics.

Chapter 7: Conclusions

The thesis has addressed the evolution of the stratospheric polar vortex over the extended spring season and its relationship with the tropospheric component of the Southern Annular Mode. The main objective of this analysis has been to improve our understanding of the mechanisms which enable seasonal predictions of the springtime stratosphere and its impact on the surface climate. In that respect, the focus has been on dynamical processes which give rise to the low-frequency evolution of the stratospheric polar vortex which is closely locked to the annual cycle. Using dynamical concepts of wave-mean flow interaction, an observational analysis of the role of upward wave propagation and refractive properties of the stratospheric flow, as well as of the tropospheric dynamics, in driving poleward and downward descent of vortex anomalies has been performed.

It has been shown that low frequency variability in the vortex is largely driven by its relatively slow response to the randomly distributed stresses of upward propagating waves and by the back-effect of the vortex on the propagation of wave activity. Following the seasonal cycle of radiative heating in the stratosphere, this variability descends to the surface during late spring and early summer and accounts for most of the coupling observed between troposphere and stratosphere at a seasonal scale. The pre-conditioned nature of this variability enables then improved seasonal predictions not only of the springtime stratosphere but also of tropospheric weather. Furthermore, different aspects of the dynamical stratosphere-troposphere coupling have been addressed, including the factors which set up its winter and spring stratospheric dynamics, dynamical mechanisms and lifecycle of the downward coupling with the Southern Annular Mode, its seasonal timing.

The main aspects of wave-driven evolution of the polar vortex revealed in the thesis can be summarized as follows:

1) The daily evolution of the polar vortex can be represented as an integrated response to the stochastic fluctuations in upward propagating wave activity. Under conditions which permit the upward penetration of planetary waves such as the westerly mean zonal flow and wind speeds below critical thresholds, the vortex integrates the stresses of the waves with an approximately $(60\ \text{day})^{-1}$ relaxation time. The wave forcing of the polar vortex as measured by the zonal mean zonal wind averaged between 30 and 90° S is fairly well approximated by the vertical component of the Eliassen-Palm Flux averaged at the appropriate lower-stratospheric boundary.

2) The ~$(60\ day)^{-1}$ relaxation time of the stratospheric jet to the perturbation by a wave disturbance determines the lagged covariance structure observed in the monthly and seasonal mean fields between upward propagating waves and the strength of the jet. It implies a one month delay in zonal wind variability relative to variability in the seasonal cycle of its dynamical forcing as is the case in the observed seasonal cycle.

3) At the same time, the polar vortex regulates the amount of wave activity to be absorbed by setting two properties – the latitude of the poleward turning level (in the time mean, it is located poleward of 60° S and undergoes a seasonal cycle) and maximum value of refractive index. The refractive index captivity develops in the lower stratosphere during September coincident with the observed narrow seasonal peak in the upward propagating wave activity.

4) This wave driven evolution is superimposed on a strong seasonal cycle which generally tends to inhibit propagation of wave activity during the middle winter whereby the penetrating waves are being refracted either downward or towards the equator escaping the polar vortex. The anomalous winter and spring dynamics is then to some extent set by the perturbations of the vortex during late autumn and early winter when its background state is weak enough to absorb the wave activity. The perturbations are influenced by the phase of the Southern Annular Mode at the surface. The latter diverts the upfloating wave activity either towards equator (under positive SAM) or poleward (under negative SAM) allowing it to float up into the stratosphere. As a consequence, the phase of the SAM during May-June correlates well with the spring-time planetary wave forcing and captures the “downward” descent of zonal wind anomalies along 55° S.

5) This lagged response of the polar vortex under the $(60\ day)^{-1}$ relaxation time and the pre-conditioning of its spring-time planetary wave forcing implies a downward nature of the observed coupling between the SAM and the stratospheric vortex observed during October-December. The coupling follows the narrow peak in the seasonal cycle of upward propagating waves and can be predicted from the planetary wave forcing integrated over previous winter-spring months.

6) The downward coupling between polar vortex and the SAM maximizes during middle October directly following the narrow seasonal peak in the upward propagating wave activity. A lifecycle of a single upward propagating disturbance has shown that the timing of the downward signal coincides with the downward wave fluxes emanating

from the stratosphere. The latter, being a result of either a reflection of an upward propagating wave or emission of wave activity by the polar vortex, is followed by interaction with the tropospheric waves whereby they get diverted towards the pole and weaken the westerlies in the midlatitudes.

7) The springtime impact of the stratosphere on the SAM extends through the summer season well into the early autumn and represents an influential factor contributing to the persistence of the SAM from October till February. However, during January and February the variability of the SAM is dominated by the impact of tropical variability. Subject to the mean state, tropical influence can span the entire season disrupting stratosphere-related persistent anomalies.

The thesis also revealed coherent changes between the SAM, the Brewer Dobson circulation and the tropical Hadley circulation through the upward propagating wave activity. For instance, during early winter, when tropospheric dynamics sets up the polar vortex, the SAM is strongly coupled to the tropical Hadley circulation. It appears that the strong thermally-driven subtropical jet which bounds the cross-equatorial cell of the Hadley circulation modulates the propagation of wave activity. A composite analysis has shown that latitudinal shifts of this jet are followed by a change of the SAM phase with a poleward intruding subtropical jet contributing to the positive SAM phase and reduced wave flux into the stratosphere. In particular, a strong latitudinal shift of the subtropical jet during 2002 was one of the factors which contributed to the early close-down of the ozone hole. Similarly, during austral summer, location of the subtropical boundary appears to play a regulating role in the climate system by either permitting or prohibiting the impact of tropical variability on the SAM. On the other hand, under the negative SAM the fluxes of upward propagating wave activity are more likely to reach the deep tropics driving the stronger upwelling branch of the Hadley circulation. Seasonal maximum of the upward propagating wave activity during austral spring as well as presence of the westerly duct over the equatorial Pacific during these seasons explains the springtime coupling between Brewer-Dobson circulation, upwelling branch of the Hadley circulation and the SAM which was first observed in the studies by Salby and Callaghan (2004-2005).

Proper representation of stratospheric climate variability in global circulation models is thus essential not only for improved future projections of the ozone hole but also for surface climate. Comparison of CMIP5 models has shown global circulation models exhibit a delay in the break-down of the polar vortex [Eyring at al., 2006]. The latter affects not only

the ability of current general circulation models with interactive chemistry to reproduce the distribution of trace gases and stratospheric climate as reported in [Hurwitz at al., 2010], but also results into a delayed seasonality of the downward coupling between the polar vortex and the SAM. Namely, these model biases result in no stratospheric impact when it is the strongest in the observations and contribute to a far too persistent SAM during the summer [Simpson at al., 2011]. Although the latter has implications for improved seasonal predictions of the SAM, it does not, however, affect the reproducibility of the SAM trends [Charlton at al., 2013]. Attempts to improve the seasonal cycle of the vortex break down involved increasing the surface roughness [Garfinkel at al, 2013]. The latter resulted in a better representation of a tropospheric stationary wave pattern and helped to improve shift the breakdown of the vortex earlier into the season, however the seasonal cycle of variability in the planetary wave forcing which is essential for predicting the SAM still exhibited a delay. The results in this thesis, highlight the importance of the coupling between the SAM and the Hadley circulation during the autumn months which affects and sets up the stratospheric vortex and its springtime variability.

At the same time, the study by Simpson at al. (2011) suggests that applying correcting procedures to eliminate models biases related to the both of the vortex break-down in the models and deficiencies in the climatology of the midlatitude jet, i.e. its equatorward bias, still do not help to improve the simulated variability of the SAM during the summer. The analysis presented here suggests, however, that improved variability of the summer SAM can be achieved by a proper representation of ENSO variability in the tropical equatorial depressions and its impact on the midlatitude circulations on the summer SAM. The persistence of such variability during the previous spring season also enables improved seasonal prediction of the SAM during January-February.

The results presented in the thesis highlight the processes relevant for improved seasonal predictions of the SAM during austral spring and summer and underscore the importance of the stratospheric climate for understanding dynamical processes at the surface. The Southern Hemisphere example is illustrative of the stratospheric role in driving surface weather patterns since the downward signal peaks during same time each season and, therefore, it is simpler to isolate on the background of daily noise. It might be expected that results presented here are also relevant for the Northern Hemisphere where the stratospheric impact can be much stronger due to a stronger dynamical activity.

References

1. Aleksandrov A.L., U. A. Israel, I. L. Karol and A. H. Hrgian, 1992: A ozone protection of the Earth and its change, Gidrometeoisdat, St-Petersburg. (In Russian).
2. Ambaum, M. H. P., B. J. Hoskins, 2002: The NAO Troposphere–Stratosphere Connection. J. Climate, 15, 1969–1978.
3. Andrews, D. G., 1983: A Finite-Amplitude Eliassen-Palm Theorem in Isentropic Coordinates. J. Atmos. Sci., 40, 1877–1883.
4. Andrews, D. G., J. R. Holton, and C. B. Leovy, 1987: Middle Atmospheric Dynamics. Academic Press, 489 pp.
5. Anstey, J. A., P. Davini, L. J. Gray, T. J. Woollings, N. Butchart, C. Cagnazzo, B. Christiansen, S. C. Hardiman, S. M. Osprey, and S. Yang , 2013: Multi-model analysis of Northern Hemisphere winter blocking: Model biases and the role of resolution, J. Geophys. Res. Atmos., 118, 3956–3971, doi:10.1002/jgrd.50231.
6. Ashok, K., S. K. Behera, S. A. Rao, H. Weng, and T. Yamagata, 2007: El Niño Modoki and its possible teleconnection, J. Geophys. Res., 112, C11007, doi:10.1029/2006JC003798.
7. Baldwin, M. P., and T. J. Dunkerton (1999), Propagation of the Arctic Oscillation from the stratosphere to the troposphere, J. Geophys. Res., 104(D24), 30937–30946.
8. Baldwin, M.P. and T.J. Dunkerton, 2001: Stratospheric harbingers of anomalous weather regimes, Science, 244, 581-584.
9. Baldwin, M.P, Stephenson D.B, Thompson D.W.J., Dunkerton T.J., Charlton A.J and A.O'Neill, 2003: Stratospheric Memory and Skill of Extended-Range Weather Forecasts, Science, 301, 636-640.
10. Barnes E.A., N.W. Barnes and L.M. Polvani, 2013: Delayed Southern Hemisphere climate change induced by stratospheric ozone recovery, as projected by the CMIP5 models, J. Climate, (in press).
11. Barnes, E.A. and D.L. Hartmann, 2010: Dynamical feedbacks of the Southern Annular Mode in winter and summer. Journal of the Atmospheric Sciences, 67, 2320-2330.
12. Barnes, E.A. and D.W.J. Thompson, 2013: Comparing the roles of barotropic versus baroclinic feedbacks in the atmosphere's response to mechanical forcing. Journal of the Atmospheric Sciences, submitted Feb. 24.
13. Bates, J. R., 1977: Dynamics of stationary ultra-long waves in middle latitudes. Q.J.R. Meteorol. Soc., 103: 397–430. doi: 10.1002/qj.49710343703.

14. Bell, C. J., L. J. Gray, A. J. Charlton-Perez, M. M. Joshi, A. A. Scaife, 2009: Stratospheric Communication of El Niño Teleconnections to European Winter. J. Climate, 22, 4083–4096.doi: http://dx.doi.org/10.1175/2009JCLI2717.1.
15. Benedict, J. J., S. Lee, S. B. Feldstein, 2004: Synoptic View of the North Atlantic Oscillation. J. Atmos. Sci., 61, 121–144.
16. Berrisford, P., B. J. Hoskins, E. Tyrlis, 2007: Blocking and Rossby Wave Breaking on the Dynamical Tropopause in the Southern Hemisphere. J. Atmos. Sci., 64, 2881–2898.
17. Black, Robert X., 2002: Stratospheric Forcing of Surface Climate in the Arctic Oscillation. J. Climate, 15, 268–277.
18. Butler, A.H., D.W.J. Thompson, and K.R. Gurney, 2007: Observed Relationships between the Southern Annular Mode and Atmpospheric Carbon Dioxide.Glob. Bio. Cycles, 21, GB4014, doi:10.1029/2006GB002796.
19. Butler, A.H., D.W.J. Thompson, and R. Heikes, 2010: The Steady-State Atmospheric Circulation Response to Climate Change-Like Thermal Forcings in a Simple General Circulation Model. J. Climate, 23, 3474-3496.
20. Caballero, R. , 2007: Role of eddies in the interannual variability of Hadley cell strength, Geophys. Res. Lett., 34, L22705, doi:10.1029/2007GL030971.
21. Cai, W., and T. Cowan, 2007: Trends in Southern Hemisphere circulation in IPCC AR4 models over 1950–99: Ozone depletion versus greenhouse forcing, J. Clim., 20 (4), 681-693, doi: 10.1175/JCLI4028.1.
22. Ceppi, P, Y.T. Hwang, X. Liu, D.M.W. Frierson and D.L. Hartmann, 2013: The relationship between the ITCZ and the Southern Hemisphere eddy-driven jet. JGR-Atmospheres, J. Geophys. Res. Atmos. , 118, 5136-5146, doi:10.1002/jgrd.50461.
23. Ceppi, P., and D.L. Hartmann, 2013: On the Speed of the Eddy-Driven Jet and the Width of the Hadley Cell. J. Climate, 26, 3450–3465.
24. Charlton, A. J., O'Neill, A., Stephenson, D. B., Lahoz, W. A. and Baldwin, M. P., 2003: Can knowledge of the state of the stratosphere be used to improve statistical forecasts of the troposphere? Q.J.R. Meteorol. Soc., 129: 3205–3224. doi: 10.1256/qj.02.232.
25. Charlton-Perez, A. J., et al., 2013: On the lack of stratospheric dynamical variability in low-top versions of the CMIP5 models, J. Geophys. Res. Atmos., 118, 2494–2505, doi:10.1002/jgrd.50125.

26. Charney, J. G., and P. G. Drazin, 1961: Propagation of planetary-scale disturbances from the lower into the upper atmosphere, J. Geophys. Res., 66(1), 83–109, doi:10.1029/JZ066i001p00083.
27. Chen, P., W. A. Robinson, 1992: Propagation of Planetary Waves between the Troposphere and Stratosphere. J. Atmos. Sci., 49, 2533–2545.
28. Chen, G., and I. M. Held, 2007: Phase speed spectra and the recent poleward shift of Southern Hemisphere surface westerlies. Geophys. Res. Lett., 34, L21805. doi:10.1029/2007GL031200.
29. Christiansen, B., 2001: Downward propagation of zonal mean zonal wind anomalies from the stratosphere to the troposphere: Model and reanalysis, J. Geophys. Res., 106(D21), 27307–27322, doi:10.1029/2000JD000214.
30. Christiansen, B., 2005: Downward propagation and statistical forecast of the near-surface weather,J. Geophys. Res., 110, D14104, doi:10.1029/2004JD005431.
31. Chylek, P., C. K. Folland, G. Lesins, and M. K. Dubey, 2010: Twentieth century bipolar seesaw of the Arctic and Antarctic surface air temperatures, Geophys. Res. Lett., 37, L08703.
32. Ciasto, L.M., and D.W.J. Thompson, 2008: Observations of large-scale ocean-atmosphere interaction in the Southern Hemisphere. J. Climate, 21(6), 1244-1259.
33. Deser, C., A. S. Phillips, V. Bourdette, and H. Teng, 2011: Uncertainty in climate change projections: The role of internal variability. Climate Dynamics, 38, 527-546.
34. Di Lorenzo E., N. Schneider, K. M. Cobb, K. Chhak, P. J. S. Franks, A. J. Miller, J. C. McWilliams, S. J. Bograd, H. Arango, E. Curchister, T. M. Powell and P. Rivere, 2008: North Pacific Gyre Oscillation links ocean climate and ecosystem change. Geophys. Res. Lett., 35, L08607, doi:10.1029/2007GL032838.
35. Dima, I. M., J. M. Wallace, 2003: On the Seasonality of the Hadley Cell. J. Atmos. Sci., 60, 1522–1527.
36. Ding, Q., E.J. Steig, D.S. Battisti, J.M. Wallace, 2012: Influence of the Tropics on the Southern Annular Mode. J. Climate, 25, 6330–6348.
37. Dunkerton, T., 1978: On the Mean Meridional Mass Motions of the Stratosphere and Mesosphere. J. Atmos. Sci., 35, 2325–2333.
38. Edmon, H. J., B. J. Hoskins, M. E. McIntyre, 1980: Eliassen-Palm Cross Sections for the Troposphere. J. Atmos. Sci., 37, 2600–2616.
39. Egger, J., 1996: Comments on “On the ‘Downward Control’ of Extratropical Diabatic Circulations by Eddy-Induced Mean Zonal Forces”. J. Atmos. Sci., 53, 2103–2104.

40. Egger, J., K.-P. Hoinka, 2005: Downward Control from the Lower Stratosphere?. J. Atmos. Sci., 62, 3808–3817.
41. Eichelberger, S. J., and D. L. Hartmann, 2005: Changes in the strength of the Brewer-Dobson circulation in a simple AGCM.Geophys. Res. Lett., 32, L15807, doi:10.1029/2005GL022924.
42. Eliassen A. and Palm E.. On the transfer of energy in stationary mountain waves.
43. Enger, I., 1957: Some attempts at predicting a meteorological time series from its past history. Unpubl. M.S. thesis Dept. Meteor., Mass. Inst. Tech., 34 pp.
44. Feldstein, S., S. Lee, 1998: Is the Atmospheric Zonal Index Driven by an Eddy Feedback?. J. Atmos. Sci., 55, 3077–3086.
45. Ferreira R.N, M. J. Suarez, and S. Nigam, 2001: Idealized Simulations of the Effects of Amazon Convection and Baroclinic Waves on the South Atlantic Convergence Zone, NASA, 20010026442.
46. Fogt, Ryan L., David H. Bromwich, 2006: Decadal Variability of the ENSO Teleconnection to the High-Latitude South Pacific Governed by Coupling with the Southern Annular Mode*. J. Climate, 19, 979–997.
47. Fog, R.L., D.H. Bromwich, and K.M.Hines, 2011: Erratum to: Understanding rge SAM influence on the South Pacific ENSO teleconnections. Clim.Dyn., 37, 2127-2128, doi.10.1007/s00382-011-1201-3.
48. Frankignoul, C. and Hasselmann, K., 1977: Stochastic climate models, Part II Application to sea-surface temperature anomalies and thermocline variability. Tellus, 29: 289–305. doi: 10.1111/j.2153-3490.1977.tb00740.x
49. Frierson, D. M. W., J. Lu, and G. Chen, 2007: Width of the Hadley cell in simple and comprehensive general circulation models. Geophys. Res. Lett., 34, L18804. doi:10.1029/2007GL031115.
50. Furtado, J., E. Di Lorenzo, N. Schneider, and N. A. Bond, 2011: North Pacific Decadal Variability and Climate Change in the IPCC AR4 Models. Journal of Climate, 24, 3049-3067 .
51. Fusco, A. C., M.L. Salby, 1999: Interannual Variations of Total Ozone and Their Relationship to Variations of Planetary Wave Activity. J. Climate, 12, 1619–1629.
52. Fyfe, J.C., O.A. Saenko, K. Zickfeld, M. Eby, and A.J. Weaver, 2007: The role of poleward-intensifying winds on Southern Ocean warming, J. Clim., 20 (21), 5391-5400, doi: 10.1175/2007JCLI1764.1.

53. Gerber, E. P. and G. K. Vallis. 2007: Eddy-Zonal Flow Interactions and the Persistence of the Zonal Index. Journal of the Atmospheric Sciences, 64, 3296-3311.
54. Gillett, N. P. & Thompson, D. W. J., 2003: Simulation of recent Southern Hemisphere climate change. Science 302, 273–275.
55. Gong, D., and S. Wang, 1999: Definition of Antarctic oscillation index. Geophys. Res. Lett., 26, 459–462.
56. Goodwin I.D., S. Browning, A.M. Lorrey, P.A.Mayewski, S.J. Phipps, N.A.N Bertler, R.P. Edwards, T.J. Cohen, T. van Ommen, M. Curran, C. Barr, J.C. Stager, 2013: A reconstruction of extratropical Indo-Pacific sea –level pressure patterns during the Medieval Climaet Anomaly. Climate Dynamics, doi: 10.1007/s00382-013-1899-1.
57. Goosse, H., W. Lefebvre, A. de Montety, E. Crespin, and A.H. Orsi, 2009: Consistent past half-century trends in the atmosphere, the sea ice, and the ocean at high southern latitudes, Clim. Dyn., 33 (7-8), doi: 10.1007/s00382-008-0500-9.
58. Graversen, R. G., and B. Christiansen, 2003: Downward propagation from the stratosphere to the troposphere: A comparison of the two hemispheres, J. Geophys. Res., 108, 4780, doi:10.1029/2003JD004077, D24.
59. Grise K.M., L.M. Polvani, G. Tselioudis, Y. Wu and M.D. Zelinka: The ozone hole indirect effect, 2013: Cloud-radiative anomalies accompanying the poleward shift of the eddy-driven jet in the Southern Hemisphere, Geophys. Res. Lett., 40, 1-5, doi:10.1002/grl.50675.
60. Grise K.M., S.-W. Son, G.P.J. Correa and L.M. Polvani, 2013: The response of mid-latitude storms in the Southern Hemisphere to stratospheric ozone depletion in the 20th Century, Atmos. Sci. Lett., in press.
61. Grise, K. M., D.W.J. Thompson, Piers M. Forster, 2009: On the Role of Radiative Processes in Stratosphere–Troposphere Coupling. J. Climate, 22, 4154–4161.
62. Hardiman, S. C., N. Butchart, T. J. Hinton, S. M. Osprey, L. J. Gray, 2012: The Effect of a Well-Resolved Stratosphere on Surface Climate: Differences between CMIP5 Simulations with High and Low Top Versions of the Met Office Climate Model. J. Climate, 25, 7083–7099.doi: http://dx.doi.org/10.1175/JCLI-D-11-00579.1
63. Harnik, N. and R.S. Lindzen (2001) The effect of reflecting surfaces on the vertical structure and variability of stratospheric planetary waves. J. Atmos. Sci., 58, 2872-2894.

64. Harnik, N., 2009: Observed stratospheric downward reflection and its relation to upward pulses of wave activity, J. Geophys. Res., 114, D08120, doi:10.1029/2008JD010493.
65. Hartmann, D. L., J. M. Wallace, V. Limpasuvan, D. W. J. Thompson, J. R. Holton, 2000: Can ozone depletion and global warming interact to produce rapid climate change?, Proc. Natl. Acad. Sci., 97(4), 1412–1417.
66. Hartmann, Dennis L., Fiona Lo, 1998: Wave-Driven Zonal Flow Vacillation in the Southern Hemisphere. J. Atmos. Sci., 55, 1303–1315.
67. Hasselmann, K., 1976: Stochastic climate models Part I. Theory. Tellus, 28: 473–485. doi: 10.1111/j.2153-3490.1976.tb00696.x
68. Haynes, P. H. and Shepherd, T. G., 1989: The importance of surface pressure changes in the response of the atmosphere to zonally-symmetric thermal and mechanical forcing. Q.J.R. Meteorol. Soc., 115: 1181–1208. doi: 10.1002/qj.49711549002.
69. Haynes, P. H., M. E. McIntyre, T. G. Shepherd, C. J. Marks, K. P. Shine, 1991: On the "Downward Control" of Extratropical Diabatic Circulations by Eddy-Induced Mean Zonal Forces. J. Atmos. Sci., 48, 651–678.
70. Held, I.M., A.Y. Hou, 1980: Nonlinear Axially Symmetric Circulations in a Nearly Inviscid Atmosphere. J. Atmos. Sci., 37, 515–533.
71. Held, I. M., 2000: The general circulation of the atmosphere. Geophysical Fluid Dynamics Program, Woods Hole Oceanographic Institute, 70pp.
72. Hendon, H. H., D. W. J. Thompson, M.C. Wheeler, 2007: Australian Rainfall and Surface Temperature Variations Associated with the Southern Hemisphere Annular Mode. J. Climate, 20, 2452–2467.
73. Hide, R., 1953: Some experiments on thermal convection in a rotating liquid. Q.J.R. Meteorol. Soc., 79: 161. doi: 10.1002/qj.49707933916
74. Holton, J. R., and C. Mass, 1976: Stratospheric vacillation cycles. J. Atmos. Sci., 33, 2218-2225.
75. Hoskins, B. J., I. N. James, G. H. White, 1983: The Shape, Propagation and Mean-Flow Interaction of Large-Scale Weather Systems. J. Atmos. Sci., 40, 1595–1612.
76. Ineson, S., Scaife, A.A., Knight, J.R., Manners, J.C., Dunstone, N.J., Gray, L.J. and Haigh, J.D. 2011: Solar forcing of winter climate variability in the Northern Hemisphere. Nature Geoscience 4: 753-757.
77. Ineson, S., and A. A. Scaife, 2009: The role of the stratosphere in the European climate response to El Niño. Nature Geosci., 2, 32–36. doi:10.1038/ngeo381.

78. James, I.N., 1995: Introduction to Circulating Atmospheres. Cambridge Atmospheric and Space Science Series.
79. Jenkins G. M., Watts D. G., 1968: Spectral Analysis and its applications. San Francisco: Holden-Day.
80. Johanson, C.M., Q. Fu, 2009: Hadley Cell Widening: Model Simulations versus Observations. J. Climate, 22, 2713–2725.
81. K.M. Smith, L.M. Polvani and D.R. Marsh, 2012: Mitigation of 21st century Antarctic sea ice loss by stratospheric ozone recovery, Geophys. Res. Lett., 39, L20701, doi:10.1029/2012GL053325.
82. Kalnay et al.,The NCEP/NCAR 40-year reanalysis project, Bull. Amer. Meteor. Soc., 77, 437-470, 1996.
83. Kang S., L.M. Polvani, J. C. Fyfe and M. Sigmond, 2011: Impact of polar ozone depletion on subtropical precipitation, Science, 332, 951-954.
84. Kang S.M. and L.M. Polvani, 2011: The interannual relationship between the eddy-driven jet and the edge of the Hadley cell, J. Climate, 24, 563-568, doi:10.1175/2010JCLI4077.1.
85. Kang S.M., C. Deser and L.M. Polvani: Uncertainty in climate change projections of the Hadley circulation: the role of internal variability, J. Climate, to appear
86. Kang, S. M., L. M. Polvani, 2011: The interannual relationship between the latitude of the eddy-driven jet and the edge of the Hadley cell. J. Climate, 24, 563–568.
87. Kang, Sarah M., Jian Lu, 2012: Expansion of the Hadley Cell under Global Warming: Winter versus Summer. J. Climate, 25, 8387–8393.
88. Kao, H.-Y., and J.-Y. Yu, 2009: Contrasting eastern-Pacific and central-Pacific types of ENSO, J. Clim., 22, 615–632, doi:10.1175/2008JCLI2309.1.
89. Karoly, D. J., 1990: The role of transient eddies in low-frequency zonal variations in the Southern Hemisphere circulation. Tellus,42A, 41–50.
90. Karpechko, A.Y., N.P. Gillett, G.J. Marshall, J.A. Screen, 2009: Climate Impacts of the Southern Annular Mode Simulated by the CMIP3 Models. J. Climate, 22, 3751–3768. doi: http://dx.doi.org/10.1175/2009JCLI2788.1
91. Kidson, J. W., 1999: Principal Modes of Southern Hemisphere Low-Frequency Variability Obtained from NCEP–NCAR Reanalyses. J. Climate,12, 2808–2830.
92. Kidson, J.W., 1975: Eigenvector Analysis of Monthly Mean Surface Data. Mon. Wea. Rev., 103, 177–186.
93. Kidson, J.W., 1988: Interannual Variations in the Southern Hemisphere Circulation. J. Climate, 1, 1177–1198.

94. Kidson, J.W., and M.R. Sinclair, 1996: The influence of persistent anomalies on Southern Hemisphere storm tracks. Journal of Climate, 8, 1938-1950.
95. Kidston, J., A. S. Taschetto, D. W. J. Thompson, and M. H. England, 2011: The influence of Southern Hemisphere sea-ice extent on the latitude of the mid-latitude jet stream, Geophys. Res. Lett., 38, L15804.
96. Kidston, J., C. W. Cairns, and P. Paga, 2013: Variability in the width of the tropics and the annular modes, Geophys. Res. Lett., 40, 2328–2332, doi:10.1029/2012GL054165.
97. Kirchner, I., G. L. Stenchikov, H.-F. Graf, A. Robock, and J. C. Antuña, 1999: Climate model simulation of winter warming and summer cooling following the 1991 Mount Pinatubo volcanic eruption, J. Geophys. Res., 104(D16), 19039–19055, doi:10.1029/1999JD900213.
98. Kodera, K., 1994: Influence of volcanic eruptions on the troposphere through stratospheric dynamical processes in the northern hemisphere winter, J. Geophys. Res., 99(D1), 1273–1282, doi:10.1029/93JD02731.
99. Kuroda, Y. and K. Kodera, 2001: Variability of the polar-night jet in the northern and southern hemispheres, J. Geophys. Res. 106, D18, 20,703-20,713
100. Kuroda, Y., 2002: Relationship between the polar-night jet oscillation and the annular mode, Geophys. Res. Lett. 29(8), 1240, 10.1029/2001GL013933. click here
101. Kuroda, Y., and K. Kodera, 1998: Interannual variability in the troposphere and stratosphere of the southern hemisphere winter, J. Geophys. Res., 103(D12), 13787–13799, doi:10.1029/98JD01042.
102. Kushnir, Y., W. A. Robinson, I. Blade, N. M. J. Hall, S. Peng, and R. Sutton, 2002: Atmospheric GCM response to extratropical SST anomalies: Synthesis and evaluation, J. Clim., 15(16), 2233–2256.
103. L'Heureux, M. L., D.W. J. Thompson, 2006: Observed Relationships between the El Niño–Southern Oscillation and the Extratropical Zonal-Mean Circulation. J. Climate, 19, 276–287.
104. Lau, K-M., P-J. Sheu, I-S. Kang, 1994: Multiscale Low-Frequency Circulation Modes in the Global Atmosphere. J. Atmos. Sci., 51, 1169–1193.
105. Lee, S., H.-K. Kim, 2003: The Dynamical Relationship between Subtropical and Eddy-Driven Jets. J. Atmos. Sci., 60, 1490–1503.
106. Lefebvre, W., H. Goosse, R. Timmermann, and T. Fichefet, 2004: Influence of the Southern Annular Mode on the sea ice–ocean system, J. Geophys. Res., 109, C09005, doi:10.1029/2004JC002403.

107. Levine, X. J., T. Schneider, 2011: Response of the Hadley Circulation to Climate Change in an Aquaplanet GCM Coupled to a Simple Representation of Ocean Heat Transport. J. Atmos. Sci., 68, 769–783.

108. Li, Y., and D. W. J. Thompson, 2013: The signature of the Brewer-Dobson circulation in tropospheric clouds. J. Geophys. Res. 118, 3486-3494.

109. Li, Q., Graf, H.-F., and Giorgetta, M. A., 2007: Stationary planetary wave propagation in Northern Hemisphere winter – climatological analysis of the refractive index, Atmos. Chem. Phys., 7, 183-200, doi:10.5194/acp-7-183-2007.

110. Lienert, f., J. C. Fyfe, and W. J. Merryfield, 2011: Do Climate Models Capture the Tropical Influences on North Pacific sea surface temperature variability? Journal of Climate, 24, 6203–6209.

111. Lim, E.-P., and I. Simmonds, 2008: Effect of tropospheric temperature change on the zonal mean circulation and SH winter extratropical cyclones. Climate Dyn., 33, 19–32, doi:10.1007/s00382-008-0444-0.

112. Lim, E.-P., Harry H. Hendon, Harun Rashid, 2013: Seasonal Predictability of the Southern Annular Mode due to Its Association with ENSO. J. Climate, 26, 8037–8054.doi: http://dx.doi.org/10.1175/JCLI-D-13-00006.1

113. Limpasuvan, V., D. L. Hartmann, 2000: Wave-Maintained Annular Modes of Climate Variability. J. Climate, 13, 4414–4429.

114. Limpasuvan, V., D.W.J. Thompson, and D.L. Hartmann, 2004: On the Life Cycle of sudden stratospheric warmings.J. Climate, 17(13), 2584-2596.

115. Lindzen R.S. and A.Y. Hou, 1988: Hadley circulations for zonally averaged heating centered off the equator. J. Atmos. Sci., 45, 2416-2427.

116. Liu, J., J. A. Curry, and D. G. Martinson, 2004: Interpretation of recent Antarctic sea ice variability,Geophys. Res. Lett., 31, L02205, doi:10.1029/2003GL018732.

117. Liu, Z., and M. Alexander, 2007: Atmospheric bridge, oceanic tunnel, and global climatic teleconnections, Rev. Geophys., 45, RG2005.

118. Lorenz E.N. 1986: The index cycle is alive and well. In Namias Symposium, Roads, J. O., ed. California Univ., Scripps Institution of Oceanography, La Jolla, California, SIO Reference 86-17, Aug., 1986. pp. 188-196.

119. Lorenz, D. J., D.L. Hartmann, 2001: Eddy–Zonal Flow Feedback in the Southern Hemisphere. J. Atmos. Sci., 58, 3312–3327.

120. Lorenz, D. J., D.L. Hartmann, 2003: Eddy–Zonal Flow Feedback in the Northern Hemisphere Winter. J. Climate, 16, 1212–1227.

121. Lorenz, E. N., 1952: Flow of angular momentum as a predictor for the zonal westerlies. J. Meteor., 9, 152-157.

122. Lorenz, E. N., 1964: The problem of deducing the climate from the governing equations. Tellus, 16: 1–11. doi: 10.1111/j.2153-3490.1964.tb00136.x

123. Lorenz, E. N., 1986: The index cycle is alive and well. In Namias Symposium, Roads, J. O., ed. California. Univ., Scripps Institution of Oceanography, La Jolla, SIO Reference 86-17, Aug., 1986. pp. 188-196.

124. Lorenz, E. N., 1970: The nature of the global circulation of the atmosphere: A present view, The Global Circulation of the Atmosphere G. A. Corby, 3–23, Royal Meteorological Society, London.

125. Lu, J., C. Deser, and T. Reichler, 2009: Cause of the widening of the tropical belt since 1958, Geophys. Res. Lett., 36, L03803; doi:10.1029/2008GL036076.

126. Lu, J., G. Chen, D.M. W. Frierson, 2008: Response of the Zonal Mean Atmospheric Circulation to El Niño versus Global Warming. J. Climate, 21, 5835–5851.

127. Lu, J., G. A. Vecchi, and T. Reichler, 2007: Expansion of the Hadley cell under global warming, Geophys. Res. Lett., 34, L06805, doi:10.1029/2006GL028443.

128. Mantua, N. J., S.R. Hare, Y. Zhang, J. M. Wallace, R. C. Francis, 1997: A Pacific Interdecadal Climate Oscillation with Impacts on Salmon Production. Bull. Amer. Meteor. Soc., 78, 1069–1079.

129. Marshall, G. J., 2003: Trends in the Southern Annular Mode from observations and reanalyses. J. Clim., 16, 4134-4143.

130. Marshall, G. J., A. Orr, N. P. M. van Lipzig, J. C. King, 2006: The Impact of a Changing Southern Hemisphere Annular Mode on Antarctic Peninsula Summer Temperatures. J. Climate, 19, 5388–5404.

131. Matsuno, T., 1970: Vertical propagation of stationary planetary waves in the winter Northern Hemisphere, J. Atmos. Sci., 27, 871–883,1970.

132. McPhaden, M. J., T. Lee, and D. McClurg, 2011: El Niño and its relationship to changing background conditions in the tropical Pacific Ocean, Geophys. Res. Lett., 38, L15709, doi:10.1029/2011GL048275.

133. Mitas, C. M., and A. Clement, 2005: Has the Hadley cell been strengthening in recent decades?Geophys. Res. Lett., 32, L03809, doi:10.1029/2004GL021765.

134. Mitas, C. M., and A. Clement, 2006: Recent behavior of the Hadley cell and tropical thermodynamics in climate models and reanalyses, Geophys. Res. Lett., 33, L01810, doi:10.1029/2005GL024406.

135. Mudryk, L.R. and P.J.Kushner, 2011: A method to diagnose sources of annular mode time scales. J.Geophys.Res. – Atmos., 116, D14114, DOI:10.1029/2010JD015291.
136. Munk, Walter H., 1960: Smoothing and Persistence. J. Meteor., 17, 92–93.
137. Nakamura, H., T. Sampe, A. Goto, W. Ohfuchi, and S.P. Xie, 2008: On the importance of midlatitude oceanic frontal zones for the mean state and dominant variability in the tropospheric circulation, Geophys. Res. Lett., 35, L15709, doi:10.1029/2008GL034010.
138. Namias, J., 1950: The index cycle and its role in the general circulation. J. Meteor., 7, 130–139.
139. Newman, P.A. and Nash, E.P., 2005: The unusual Southern Hemisphere stratosphere winter of 2002, J. Atmos. Sci., 62, 614–628.
140. Nigam S. and R.S. Lindzen, 1989: The Sensitivity of stationary waves to variations in the basic state zonal flow. J. Atmos. Sci., 46, 1746-1768.
141. Nigam, S., 1990: On the structure of variability of the observed tropospheric and stratospheric zonal-mean wind. J. Atmos. Sci.,47, 1799–1813.
142. Nishii, K., H. Nakamura, Y.J. Orsolini, 2011: Geographical Dependence Observed in Blocking High Influence on the Stratospheric Variability through Enhancement and Suppression of Upward Planetary-Wave Propagation. J. Climate, 24, 6408–6423.
143. Oke, P.R., and M.H. England, Oceanic response to changes in the latitude of the Southern Hemisphere subpolar westerly winds, J. Clim., 17 (5), 1040-1054, 2004.
144. Oort, A.H., J. J. Yienger, 1996: Observed Interannual Variability in the Hadley Circulation and Its Connection to ENSO. J. Climate, 9, 2751–2767.
145. Orsolini, Y.J., R.Senan, R. Benestad and A. Melsom, 2011: Autumn atmospheric response to the 2007 low Arctic sea ice extent in coupled ocean-atmosphere hindcasts, Climate Dynamics, (DOI) 10.1007/s00382-011-1169-z.
146. Osprey, S.M., L. J. Gray, S.C. Hardiman, N. Butchart, T.J. Hinton, 2013: Stratospheric Variability in Twentieth-Century CMIP5 Simulations of the Met Office Climate Model: High Top versus Low Top. J. Climate, 26, 1595–1606.doi: http://dx.doi.org/10.1175/JCLI-D-12-00147.1
147. P.L.M. Gonzalez, L.M. Polvani, R. Seager and G.J.P Correa, 2013: Stratospheric ozone depletion: a key driver of recent precipitation trends in South Eastern South America, Clim. Dyn., doi:10.1007/s00382-013-1777-x.
148. Panetta, R. L., I. M. Held, 1988: Baroclinic Eddy Fluxes in a One-Dimensional Model of Quasi-geostrophic Turbulence. J. Atmos. Sci., 45, 3354–3365.

149. Panteleeva E.A, 2009: Springtime changes of the stratospheric circulation and their impact on the tropospheric dynamics and weather patterns, RosHydromet, phd thesis (in russian)

150. Petoukhov, V., and V. A. Semenov, 2010: A link between reduced Barents-Kara sea ice and cold winter extremes over northern continents, J. Geophys. Res., 115, D21111.

151. Pezza, Alexandre Bernardes, Tom Durrant, Ian Simmonds, Ian Smith, 2008: Southern Hemisphere Synoptic Behavior in Extreme Phases of SAM, ENSO, Sea Ice Extent, and Southern Australia Rainfall. J. Climate, 21, 5566–5584.

152. Polvani, L. M., D. W. Waugh, 2004: Upward Wave Activity Flux as a Precursor to Extreme Stratospheric Events and Subsequent Anomalous Surface Weather Regimes. J. Climate, 17, 3548–3554.

153. Polvani, L. M., and P. J. Kushner, 2002: Tropospheric response to stratospheric perturbations in a relatively simple general circulation model.Geophys. Res. Lett., 29, 1114. doi:10.1029/2001GL014284.

154. Postel, G. A., M. H. Hitchman, 1999: A Climatology of Rossby Wave Breaking along the Subtropical Tropopause. J. Atmos. Sci., 56, 359–373.

155. Randel, W. J., J. L. Stanford, 1985: An Observational Study of Medium-Scale Wave Dynamics in the Southern Hemisphere Summer. Part I: Wave Structure and Energetics. J. Atmos. Sci., 42, 1172–1188.

156. Randel, W. J., J.L. Stanford, 1985: An Observational Study of Medium-Scale Wave Dynamics in the Southern Hemisphere Summer. Part II: Stationary-Transient Wave Interference. J. Atmos. Sci., 42, 1189–1197.

157. Robinson, W. A., 2002: On the midlatitude thermal response to tropical warmth, Geophys. Res. Lett., 29(8), doi:10.1029/2001GL014158.

158. Robinson, W., 1991: The dynamics of the zonal index in a simple model of the atmosphere. Tellus, 43A, 295–305.

159. Robinson, W.A., 2006: On the Self-Maintenance of Midlatitude Jets. J. Atmos. Sci., 63, 2109–2122.

160. Rogers, J.C., H. van Loon, 1982: Spatial Variability of Sea Level Pressure and 500 mb Height Anomalies over the Southern Hemisphere.Mon. Wea. Rev., 110, 1375–1392.

161. Rosanova I.V., 2006: Cyclonic centers of action, circulation and climate of the Southern Hemisphere during the second half of 20th century, Ros.Hydromet, phd thesis (in Russian).

162. Rosenlof, K. H., and J. R. Holton, 1993: Estimates of the stratospheric residual circulation using the downward control principle, J. Geophys. Res., 98(D6), 10465–10479, doi:10.1029/93JD00392

163. Rossby, C. G., and collaborators, 1939: Relation between variations in the intensity of the zonal circulation of the atmosphere and the displacements of the semi-permanent centers of action. Jour. Marine Research 2, 38–55.

164. Salby, M.L., 2008: Involvement of the Brewer–Dobson circulation in changes of stratospheric temperature and ozone. Dynamics of Atmospheres and Oceans 44:3-4, 143-164.

165. Salby, M.L., and P. F. Callaghan, 2006: Influence of the Brewer-Dobson circulation on stratosphere-troposphere exchange, J. Geophys. Res., 111, D21106, doi:10.1029/2006JD007051.

166. Salby, M.L., and P. F. Callaghan, 2006: Residual mean transport in the stratosphere: Contributions from wave driving and seasonal transience, J. Geophys. Res., 111, D22304, doi:10.1029/2005JD006767.

167. Salby, M.L., E. Titova, and L. Deschamps, 2012: Changes of the Antarctic ozone hole: Controlling mechanisms, seasonal predictability, and evolution, J. Geophys. Res., doi:10.1029/2011JD016285.

168. Salby, M.L., P. F. Callaghan, 2004: Control of the Tropical Tropopause and Vertical Transport across It. J. Climate, 17, 965–985.

169. Salby, M.L., P. F. Callaghan, 2005: Interaction between the Brewer–Dobson Circulation and the Hadley Circulation. J. Climate, 18, 4303–4316.

170. Salby, M.L., P.F. Callaghan, 2004: Interannual Changes of the Stratospheric Circulation: Influence on the Tropics and Southern Hemisphere. J. Climate, 17, 952–964.

171. Scaife, A. A., J. R. Knight, G. K. Vallis, and C. K. Folland, 2005: A stratospheric influence on the winter NAO and North Atlantic surface climate, Geophys. Res. Lett., 32, L18715, doi:10.1029/2005GL023226.

172. Schmitz, G. and Grieger, N., 1980: Model calculations on the structure of planetary waves in the upper troposphere and lower stratosphere as a function of the wind field in the upper stratosphere. Tellus, 32: 207–214. doi: 10.1111/j.2153-3490.1980.tb00948.x

173. Schneider, E.K., 1977: Axially Symmetric Steady-State Models of the Basic State for Instability and Climate Studies. Part II. Nonlinear Calculations. J. Atmos. Sci., 34, 280–296.

174. Schneider, T., 2006: The general circulation of the atmosphere. Annual Review of Earth and Planetary Sciences, 34 . pp. 655-688.

175. Schneider, T., S. Bordoni, 2008: Eddy-Mediated Regime Transitions in the Seasonal Cycle of a Hadley Circulation and Implications for Monsoon Dynamics. J. Atmos. Sci., 65, 915–934.

176. Seager, R., N. Harnik, Y.Kushnir, W. Robinson, J. Miller, 2003: Mechanisms of Hemispherically Symmetric Climate Variability*. J. Climate, 16, 2960–2978.

177. Seidel, D. J., Q. Fu, W.J. Randel and T. Reichler, 2008: Widening of the tropical belt in a changing climate. Nature Geoscience, 1, 21-24.

178. Shakun, J. D., and J. Shaman, 2009: Tropical origins of North and South Pacific decadal variability,Geophys. Res. Lett., 36, L19711, doi:10.1029/2009GL040313.

179. Shaw, T. A. and J. Perlwitz, 2013: The life cycle of Northern Hemisphere downward wave coupling, J. Climate, 26,1745-1763.

180. Shepherd, T., and T. Shaw, 2004: The angular momentum constraint on climate sensitivity and downward control in the middle atmosphere. J. Atmos. Sci., 61, 2899–2908.

181. Simmonds, I., and W. F. Budd, 1991. Sensitivity of the southern hemisphere circulation to leads in the Antarctic pack ice. QJR Met Soc 117:1003–24.

182. Simpson, I. R., P. Hitchcock, T. G. Shepherd, J. F. Scinocca, 2013: Southern Annular Mode Dynamics in Observations and Models. Part I: The Influence of Climatological Zonal Wind Biases in a Comprehensive GCM. J. Climate, 26, 3953–3967.

183. Simpson, I. R., T. G. Shepherd, P. Hitchcock, J. F. Scinocca, 2013: Southern Annular Mode Dynamics in Observations and Models. Part II: Eddy Feedbacks. J. Climate, 26, 5220–5241.

184. Simpson, I. R., P. Hitchcock, T. G. Shepherd, and J. F. Scinocca, 2011: Stratospheric variability and tropospheric annular-mode timescales, Geophys. Res. Lett., 38, L20806, doi:10.1029/2011GL049304.

185. Smith K.L., M. Previdi and L.M. Polvani, 2013: The Antarctic atmospheric energy budget. Part II: The Effect of Ozone Depletion and its Projected Recovery, J. Climate, in press.

186. Smith, T.M., R.W. Reynolds, T.C. Peterson, J.Lawrimore, 2008: Improvements to NOAA's Historical Merged Land–Ocean Surface Temperature Analysis (1880–2006). J. Climate, 21, 2283–2296.

187. Son S.W., A. Purich, H.H. Hendon, B.M. Kim and L.M. Polvani, 2013: Improved seasonal forecast using ozone hole variability?, Geophys. Res. Lett., 40, 6231-6235, doi:10.1002/2013GL057731.

188. Son, S., and S. Lee, 2005: The response of westerly jets to thermal driving in a primitive equation model. J. Atmos. Sci., 62, 3741–3757.

189. Son, S.-W., et al., 2010: Impact of stratospheric ozone on Southern Hemisphere circulation change: A multimodel assessment, J. Geophys. Res., 115, D00M07, doi:10.1029/2010JD014271.

190. Song, Y., and W. Robinson, 2004: Dynamical mechanisms for stratospheric influences on the troposphere. J. Atmos. Sci.,61, 1711–1725.

191. Staten, P. W., and T. Reichler, 2013: On the ratio between shifts in the eddy-driven jet and the Hadley cell edge, Climate Dynamics, in press.

192. Staten, P. W., and T. Reichler, 2013: On the ratio between shifts in the eddy-driven jet and the Hadley cell edge Clim. Dyn., (accepted).

193. Stenchikov, G., A. Robock, V. Ramaswamy, M. D. Schwarzkopf, K. Hamilton, and S. Ramachandran, 2002: Arctic Oscillation response to the 1991 Mount Pinatubo eruption: Effects of volcanic aerosols and ozone depletion, J. Geophys. Res., 107(D24), 4803, doi:10.1029/2002JD002090.

194. Stenchikov, G., T. L. Delworth, V. Ramaswamy, R. J. Stouffer, A. Wittenberg, and F. Zeng, 2009: Volcanic signals in oceans, J. Geophys. Res., 114, D16104, doi:10.1029/2008JD011673.

195. Sun, D.-Z. and R.S. Lindzen, 1994: A PV view of the zonal mean distribution of temperature and wind in the extra-tropical troposphere. J. Atmos. Sci., 51, 757-772.

196. Tandon N.F., E.P. Gerber, A.H. Sobel and L.M. Polvani, 2013: Understanding Hadley cell expansion vs. contraction: Insights from simplified models and implications for recent observations, J. Climate, 26, 4304-4321.

197. Taylor, K. E., R. J. Stouffer, and G. A. Meehl (2012), An Overview of CMIP5 and the Experimental Design, Bull. Am. Met. Soc., 93, 485–498, doi: http://dx.doi.org/10.1175/BAMS-D-11-00094.1

198. Thompson, D. W. J, and J. M. Wallace, 1998: The Arctic Oscillation signature in the wintertime geopotential height and temperature fields.Geophysical Research Letters, 25, 1297-1300.

199. Thompson, D. W. J., and J. M. Wallace, 2000: Annular modes in the extratropical circulation. Part I: Month-to-month variability. J. Climate, 13, 1000-1016.

200. Thompson, D. W. J., D. J. Lorenz, 2004: The Signature of the Annular Modes in the Tropical Troposphere. J. Climate, 17, 4330–4342.

201. Thompson, D. W. J., J. M. Wallace, and G. C. Hegerl, 2000: Annular modes in the extratropical circulation. Part II: Trends. J. Climate, 13, 1018-1036.

202. Thompson, D. W. J., M.P. Baldwin, S. Solomon, 2005: Stratosphere–Troposphere Coupling in the Southern Hemisphere. J. Atmos. Sci.,62, 708–715.

203. Thompson, D. W. J., S. Solomon, P. J. Kushner, M. H. England, K. M. Grise, and D. J. Karoly (2011), Signatures of the Antarctic ozone hole in Southern Hemisphere surface climate change, Nat. Geosci., 4, 741–749.

204. Thompson, D.W.J., and S. Solomon, 2002: Interpretation of recent Southern Hemisphere climate change.Science, 296, 895-899.

205. Thompson, D.W.J., M.P. Baldwin, and S. Solomon, 2005: Stratosphere-troposphere coupling in the Southern Hemisphere.J. Atmos. Sci., 62(3), 708-715.

206. Thompson, D.W.J., S. Solomon, P.J. Kushner, M.H. England, K.M. Grise and D.J. Karoly, 2011: Signatures of the Antarctic ozone hole in Southern Hemisphere surface climate change. Nature Geoscience. doi:10.1038/ngeo1296.

207. Thompson, D. W. J., and S. Solomon, 2002: Interpretation of recent Southern Hemisphere climate change. Science, 296, 895–899.

208. Thorncroft, C. D., Hoskins, B. J. and McIntyre, M. E. , 1993: Two paradigms of baroclinic-wave life-cycle behaviour. Q.J.R. Meteorol. Soc., 119: 17–55. doi: 10.1002/qj.49711950903.

209. Ventsel E.S., 1958: Probability Theory [in Russian], GIFML, Moscow.

210. Von Storch H., Zwiers F.W., 1999: Statistical Analysis in Climate Research, Cambridge University Press, 1998 - 499 pages.

211. Walker, C. C., T. Schneider, 2006: Eddy Influences on Hadley Circulations: Simulations with an Idealized GCM. J. Atmos. Sci., 63, 3333–3350.

212. Wang B., Liu J., Kim H.-J., Webster P.J., Yim S.-Y. and Xian B., 2013: Northern Hemisphere summer monsoon intensified by mega-El Niño/southern oscillation and Atlantic multidecadal oscillation. PNAS 2013, doi:10.1073/pnas.1219405110.

213. Weber, M. and Dhomse, S. and Wittrock, F. and Richter, A. and Sinnhuber, B. M. and Burrows, J. P. , 2003: Dynamical control of NH and SH winter/spring total ozone from GOME observations in 1995 - 2002. Geophysical Research Letter, 30 (11). p. 1583.

214. Webster, P. J., and J. R. Holton, 1982: Cross equatorial response to middle-latitude forcing in a zonally varying basic state. J. Atmos. Sci., 39, 722-733.

215. WMO (World Meteorological Organization), 1987: Atmospheric ozone: Assessment of our understanding of the processes controlling its present distribution and change, Rep. 16, Geneva, Switzerland.

216. WMO (World Meteorological Organization), 2003: Scientific Assessment of Ozone Depletion: 2002, Global Ozone Research and Monitoring Project – Report No. 47, Geneva, Switzerland.

217. WMO (World Meteorological Organization), 2007: Scientific Assessment of Ozone Depletion: 2006, Global Ozone Research and Monitoring Project – Report No. 50, Geneva, Switzerland.

218. WMO (World Meteorological Organization), 2011: Scientific Assessment of Ozone Depletion: 2010, Global Ozone Research and Monitoring Project-Report No. 52, 516 pp., Geneva, Switzerland.

219. Woollings, T., A. Charlton-Perez, S. Ineson, A. G. Marshall, and G. Masato , 2010: Associations between stratospheric variability and tropospheric blocking, J. Geophys. Res., 115, D06108, doi:10.1029/2009JD012742.

220. Yu, J. Y., and D. L. Hartmann, 1993: Zonal flow vacillation and eddy forcing in a simple GCM of the atmosphere. J. Atmos. Sci., 50, 3244–3259.

221. Yuan, X., and C. Li , 2008: Climate modes in southern high latitudes and their impacts on Antarctic sea ice, J. Geophys. Res., 113, C06S91, doi:10.1029/2006JC004067.

222. Zhang, Y., J. M. Wallace, and D. S. Battisti (1997), ENSO-like interdecadal variability: 1900–1993, J. Clim., 10, 1004–1020.

223. Zhou, T., and R. Yu (2004), Sea-surface temperature induced variability of the Southern Annular Mode in an atmospheric general circulation model, Geophys. Res. Lett., 31, L24206, doi:10.1029/2004GL021473.